AN ANALYTICAL PARAMETER STUDY ON THE EROSION OF TURBINE BLADES SUBJECTED TO FLOW CONTAINING PARTICULATES

by

Dennis John Dubberley

Thesis submitted to the Graduate Faculty of the
Virginia Polytechnic Institute and State University
in partial fulfillment of the requirements of the degree of

MASTER OF SCIENCE

in

Mechanical Engineering

APPROVED:

W. F. O'Brien, Jr.

H. L. Moses

N. S. Eiss

July, 1977

Blacksburg, Virginia 24061

II. ACKNOWLEDGEMENTS

The author expresses appreciation to the members of his graduate advisory committee: Professors N. S. Eiss, H. L. Moses and W. F. O'Brien, Jr., Chairman.

The support received as a Domestic Mining and Mineral and Fuel Conservation Fellow from the U. S. Department of Health, Education and Welfare, which made the author's graduate study possible, is gratefully acknowledged.

The author extends thanks to Professor S. W. Conley for his assistance in debugging the computer programs.

The author also wishes to extend special thanks to the Westinghouse Electric Corporation, whose computer programs and facilities were extremely helpful.

III. TABLE OF CONTENTS

III. TABLE OF CONTENTS (Continued)

III. TABLE OF CONTENTS (Continued)

IV. LIST OF FIGURES

IV. LIST OF FIGURES (Continued)

IV. LIST OF FIGURES (Continued)

IV. LIST OF FIGURES (Continued)

V. LIST OF TABLES

V. LIST OF TABLES (Continued)

VI. LIST OF SYMBOLS

Ca_3 = axial absolute velocity

Cd = drag coefficient

Cp = specific heat of gas at constant pressure

d_p = diameter of particle

E = specific erosion rate defined by Equation (15)

$\vec{F}$ = drag force vector

h = stream channel thickness

K_1, K_2 = amplitudes of erosion for brittle and ductile modes

M = mass of impacting particle

m = meridional streamline distance

m_1, m_2 = velocity exponents of erosion for brittle and ductile modes

r = radial coordinate

Re = Reynolds number

S = volume of material eroded per particle impact

T = gas temperature

T_{o_3} = inlet gas stagnation temperature

U_T = tangential rotational velocity

$\vec{V}_G$ = gas velocity vector

$\vec{V}_P$ = particle velocity vector

$\vec{V}_{P_1}$, $\vec{V}_{P_2}$ = particle velocity vector before and after impact

$V_{p_{el}}$ = impact velocity associated with limiting elastic deformation

$V_{p_{n1}}$, $V_{p_{n2}}$ = particle velocity component in the direction normal to the surface before and after impact

VI. LIST OF SYMBOLS (Continued)

$V_{p_{t1}}$, $V_{p_{t2}}$ = particle velocity component in the direction tangential to the surface before and after impact

$V_{p_{tr}}$ = residual horizontal velocity component following impact

V_x, V_m, V_r, V_θ = gas velocity components in the x, m, r and θ directions

W = relative gas velocity

W_m, W_θ = relative gas velocity in the m and θ directions

W_{st} = turbine stage work

w = blade-to-blade mass flow rate

x = axial coordinate

$\dot{x}_p$, $\dot{r}_p$, $\dot{\theta}_p$ = particle velocity components in the x, r and θ directions

$\ddot{x}_p$, $\ddot{r}_p$, $\ddot{\theta}_p$ = particle acceleration components in the x, r and θ directions

α_3 = flow angle at stator exit

β = gas velocity vector, meridional plane angle

β_{max} = impact angle for maximum erosion

β_0 = erosion reference angle

β_1, β_2 = particle incidence angle before and after impact

β_4 = relative flow angle at rotor exit

α = specific heat ratio

ε = threshold energy for brittle erosion

ε_i = inlet prerotation

VI. LIST OF SYMBOLS (Continued)

θ = circumferential coordinate

θ_1, θ_2 = circumferential coordinate at lower and upper boundaries

λ = turbine axis, streamline direction angle

μ_g = gas viscosity

ρ = gas density

ρ_p = particle density

ρ_i = inlet gas stagnation density

ϕ = threshold energy for ductile erosion

ψ = stream function

ω = blade rotational speed

VII. INTRODUCTION

The idea of using coal as a fuel for gas turbines has been a topic of considerable research since the mid 1940's. Most of the early research programs attempted to use coal in its raw form, crushing it into a fine powder and then burning it. The early programs usually proposed a conventional or exhaust-heated open cycle gas turbine for the production of power from coal (1)*. In the early 1970's, energy shortages led to extensive research programs in the fields of coal gasification and coal liquifaction. Consequently, the use of coal derived liquids or gases as a fuel for gas turbines has become a topic of considerable recent interest (2, 3, 4, 5). Presently, both open cycles burning crushed coal or a coal-derived fuel as well as closed cycles using coal to exchange heat with a helium working fluid are being developed (6, 7, 8).

A direct-fired coal-burning gas turbine, or one that burns coal in its raw form, has a major size advantage over a gas turbine burning a coal-derived fuel. Owing to its smaller size, a direct-fired coal-burning gas turbine is ideally suited for locomotive and marine applications. Since it is uneconomical to transport low calorific 130 - 180 BTU/ft^3 (48,500 - 59,600 kJ/m^3) gasified coal over large distances, gas turbine cycles utilizing gasified coal as their fuel must have the necessary gasifying equipment nearby. In fact, most cycles envisioned will have replaced the gas generator side of the

*Numbers in parentheses refer to references listed at the end of the thesis.

gas turbine with the coal gasifier (6, 7, 8). The high temperature, high pressure product gas from the gasifier will then be expanded through a turbine. Unfortunately, this extra equipment will increase the overall size of the cycle considerably. However, in power plants and other stationary applications, size is not a major factor. Also, liquified coal has many desirable properties, but it has many of the same drawbacks that affect gasified coal.

The main disadvantage of the direct-fired coal-burning gas turbine arises from the nature of its fuel. Due to the particulate nature of the coal dust, combustor designs used in the early research programs had to efficiently burn a substance that took much longer to burn than ordinary fuels (9, 10). Although high combustion efficiencies were eventually attained, the ash in the coal would not burn. Consequently, ash removal equipment was developed to extract a major portion of the ash before the gas passed through the turbine. However, some residual ash passed through the removal equipment, creating serious turbine blade particulate erosion and turbine blade ash deposition problems. Turbine blade erosion and deposition is much less severe in gas turbines burning coal-derived liquids or gases due to the much "cleaner" nature of these fuels. Consequently, the gas passing through the turbine contains less particulate matter, greatly reducing deposition and erosion. In addition, exhaust pollutants are less severe when coal-derived gases or liquids are burned.

The erosion of turbomachinery components has been a topic of considerable interest since the late 1960's. Consequently, several analyti-

cal models have been developed to predict erosion in turbomachinery due to particulates (11, 12, 13). More recent models have suggested theories explaining corosion and deposition as well (14, 15).

VIII. REVIEW OF LITERATURE

Experimental Investigations

During the mid 1940's, several research-oriented organizations around the world began research programs attempting to develop technology forusing coal as a gas turbine fuel. Research in the United States, conducted by the Locomotive Development Comittee (L.D.C.) of Bituminous Coal Research, Inc. was one of the more successful programs. Later continued by the United States Bureau of Mines, this program lasted for nearly thirty years. The research efforts in other countries, notably in Australia, were also somewhat successful.

The Brown Boveri Company of Baden, Switzerland conducted an extensive research and development program during the 1940's attempting to develop a pulverized coal-burning gas turbine. Brown Boveri used an open cycle gas turbine with a combustion air preheater driven by the exhaust gas from the turbine. The cycle developed used a primitive dust extractor that allowed in excess of fifty percent of the ash to pass through the turbine. After 250 hours of operation, deep notches had been cut into the leading edges of many of the blades. Brown Boveri concluded that turbine blade erosion was too severe for the direct-fired coal-burning gas turbine to ever reach commercial operation. Brown Boveri is currently developing gas turbine cycles using coal as a fuel in gaseous and liquified states only (16).

Under mainly government sponsorship, Great Britain conducted a very extensive research and development program beginning in 1949.

The Ministry of Fuel and Power, the major sponsor of the British effort, coordinated work on eight full scale coal-burning gas turbine experiments. The experiments attempted to determine the best method for burning coal in a gas turbine. Four methods were then recognized for doing this: direct firing of coal in an open cycle, gasification of coal and using the producer gas in the gas turbine cycle, the exhaust heated cycle,and the closed cycle (1). In general, the program was a failure. Most of the experiments were never completed. Funding for the program was the major problem.

Another British experiment, sponsored by the Scottish Peat Committee, was more successful. This program attempted to use peat, a geologically young grade of coal, as a fuel for gas turbines. A Ruston and Hornsby 700 KW open cycle gas turbine was used for the peat burning experiments. A cyclone separator removed most of the larger ash particles. The main problem became the adhesion of the finer particles to the turbine blades, causing blockage of blade passages (1).

In 1949, preliminary research began in Melbourne, Australia, at the Aeronautical Research Laboratories (A.R.L.) to develop test apparatus for assessing the problem of burning coal in a gas turbine. In 1958, a Ruston and Hornsby type "TA" open cycle gas turbine was installed at the A.R.L. with testing beginning in 1959. The main modification to the original engine was the redesigning of the combustor. Due to the slow burning rates of coal particles, longer residence times in the combustor were required. The combustor also had some slight aerodynamic modifications incorporated to prevent accumulation of ash

particles (17). Two sets of tests were run, one without ash cleaning equipment and one with the equipment.

The fuel used during all of the tests was dried brown coal from the State of Victoria. Undried, the coal has a relatively high (65 percent) moisture content. After drying, brown coal has the following percentage analysis: moisture content 15.5, ash 1.5, volatile matter 43.5 and fixed carbon 39.5. The coal has a calorific value of 9290 BTU per pound (21,600 kJ/kg) (18). Once dried, the coal was pulverized and injected into an airstream. With relative ease, 60 percent of the coal could be pulverized to less than 10 microns and the remaining 40 percent to less than 50 microns. The coal particles had a 100 millesecond residence time in the combustor. Combustion efficiency eventually reached 97 percent. The brown coal dust released 2.6 MBTU/ft^2 (295 MkJ/m^2) of combustor cross sectional area (19).

The ash separation system used was a multi-cyclone unit designed by the Great Britain Ministry of Power for its peat-burning experiments. The separator used 40 individual cyclones of six in. (.0127 m) diameter. A 30 K temperature loss across the separator was unavoidable so that the actual turbine inlet temperature was 923 K. Of the particles leaving the combustor, an estimated 50 percent were ash particles and 50 percent were unburnt coal. Without the separator, an estimated 9.4×10^{-4} kg solid per kg gas entered the turbine. With the separator, an estimated 3.4×10^{-4} kg solid per kg gas entered the turbine. The separators were completely effective in removing gas-born particles larger than 23 microns, and 50 percent effective in removing particles larger than 10 microns (18).

The major problem faced by the Australian Researchers was not erosion of turbine blades, but ash deposition. An estimated 10,000 hours could be obtained from a set of Nimonic 80 turbine blades before erosion forced their replacement. However, ash deposition leading to blade passage blockage forced shut-down long before then. Without the ash separator, ash deposition was confined to the first and second row of stator blades. After 20 hours of operation, ash deposition rates on the first and second rows of stator blades were 0.161 grams per hour and 0.064 grams per hour, respectively. Two types of deposition were found. On the leading edge of the blades, extending back along the concave face to the trailing edge, a dense sintered material accumulated. This material broke away easily, leaving the blade surface unblemished. The second type of deposition, a light brown powdery surface, confined itself to the convex faces of the blades. Water usually washed away these accumulations (19).

With the ash separation equipment used, the harder concentrations of ash were eliminated. The total weight of the deposition lessened, but the blade area affected by the deposition increased. In addition, the deposition did not confine itself to the first two rows of stator blades, but affected both stator and rotor blades for several stages.

Experiments by Morley (18) established that intermittent water injection into the combustion gases removed most deposits of ash by heat shock. If the water injection proved inadequate, small quantities of a substance called Kaolin removed even the hardest concentrations of ash.

The Australian researchers have continued testing of the Ruston and Hornsby gas turbine. Present blade life is estimated at 51,000 hours for the first stage stator and 31,000 hours for the first stage rotor, proving that erosion rates can be controlled with stronger blade materials and flow field modifications (20).

Research on a coal-fired gas turbine in Canada began in 1949 at McGill University in Montreal. The program, sponsored by the Canadian Department of Mines and several Canadian railroad companies, envisioned the coal-fired gas turbine as a locomotive engine. The Canadian research team concluded that an exhaust-heated cycle was the most practical method for burning coal in a gas turbine. The obvious advantage to this cycle is that only heated air passes through the turbine, eliminating all problems associated with turbine blade erosion and ash deposition. However, high temperature, corrosion resistant, anti-fouling heat exchangers, as required by this cycle, did not exist at the time (21).

By November 1953, the test facilities at McGill University were completed. By March 1955, 1000 hours had been accumulated on the coal-burning aircraft test unit. The first test program proved the engine to be extremely durable. However, severe pressure losses in the cycle reduced the power output. A cyclone furnace, serving as a combustor, burned the aerated crushed coal very efficiently. The heater tubes in the heat exchanger gave no severe slagging problems until the gas temperatures entering the tubes reached 1283 K. Serious corrosion problems were encountered in the heat exchanger tubes owing to the high sulfur content exhaust gases attacking the Nimonic alloyed tubes. Holes

in the tubes developed in several places. The overall heat loss of the cycle was found to be 40 percent (22).

As a result of these problems, modifications were made to the plant in 1955 and 1956. The main modifications attempted to reduce the thermal as well as pressure losses and to improve the coal handling and slag removal equipment. In addition, extensive efforts were made to reduce corrosion of the tubes on the gas side of the heat exchanger.

During 1956, an additional 850 hours of coal-fired operation were accumulated on the modified plant including one 200 hour, non-stop run. Using 446 Ferrite steel tubes in the heat exchanger greatly reduced corrosion. A slight erosion problem developed in these tubes owing to the high velocity and particulate nature of the flow. In addition, the overall thermal as well as pressure losses were reduced to tolerable levels. The furnace-type combustor operated satisfactorily with high combustion efficiencies. The compressor and turbine assembly required only routine maintenance. The ash and slag build-up in the furnace as well as in the heat exchanger tubes continued to be major problems that eventually caused discontinuation of the project in the late 1950's.

One of the most successful research efforts to date toward developing a coal-fired gas turbine was made by the Locomotive Development Committee (L.D.C.) of Bituminous Coal Research, Inc., in their Dunkirk, New York Laboratories during the years 1944-1958. In 1959, the project was transferred to Morgantown, West Virginia where work continued through the late 1960's under the United States Bureau of Mines. The L.D.C. was formed in 1944 by several railroad and coal companies. Its

purpose was to develop technology for the more efficient use of coal as a fuel for locomotives. The newly developed gas turbine offered great promise as a locomotive engine. Consequently, the L.D.C. attempted to burn coal in this engine.

In 1945, very little was known about three major problems facing the L.D.C.: feeding large amounts of coal to a pressurized gas turbine combustor, burning the coal efficiently in the combustor and removal of ash to prevent turbine fouling and wear (23, 24). Tests run during this period proved erosion due to fly ash rapidly diminished for particle sizes less than 20 microns (9).

In 1946, the L.D.C. began development work on the special equipment required for the testing. In 1949, a Houdry-process turbine, on loan from the U. S. Bureau of Mines, began coal burning operation. The maximum turbine inlet temperature for this machine was 839 K. The 1250 hours accumulated on the Houdry unit proved the major problem was turbine blade erosion. Since the Houdry unit had no fly ash removal equipment, erosion was severe (1).

In 1951, the L.D.C. errected a 4,250 HP (3168 KW) Allis Chalmers locomotive gas turbine. By 1955, 3907 hours of coal-burning operation had been accumulated on this machine, of which 569 hours attempted to simulate actual railroad conditions through locomotive cycle operations. One of the major problems found was the inefficient operation of the gas turbine while idling (10).

Still, the major problem facing the L.D.C. continued to be turbine blade erosion. However, the use of 19-9DL alloy for the 1955 tests

(1721 hours) prevented erosion more effectively than the S-590 alloy used before reblading in 1952 (756 hours). The erosion in the 1955 tests was confined to the roots of the third and fourth rows of stator blades. Notches developed in most of the trailing edges of these blades, causing cracks to develop in 27 blades owing to stress concentrations. By 1955, combustion efficiencies were consistently above 95 percent (10).

In late 1955, several modifications were made to the plant. An aerated coal system enabled easier handling of the coal. Redesign of the turbine blades was the topic of considerable research. After consulting the National Advisory Committee for Aeronautics (N.A.C.A.), it was discovered that secondary flow phenomena produced a large fraction of the erosion (25). By thickening the lower trailing edges while using newly developed GMR-235 and HS-31 alloys and skimmers to remove ash concentrations, the L.D.C. hoped to further reduce reosion.

In 1957, further testing accumulated 1100 more hours. Thermal efficiency rose from 16 percent in 1952 to nearly 20 percent in 1957. Use of new separation and pulverizing equipment eliminated the trailing edge erosion. However, leading edge notches on the second, third and fourth rows of stator blades developed. This erosion, predicted by the N.A.C.A. investigation, was caused by tip leakage from the rotor blades. No significant ash concentrations developed (25).

In 1957, funding from Bituminous Coal Research terminated. The U. S. Bureau of Mines took over the project in 1959, its preliminary objective to reduce blade erosion. By fabricating new blades made of Stellite, inserting titanium carbide wear strips at points of maximum

ash concentration and velocity, thickening the trailing edges of the rotor blades and thinning those of the stator blades to reduce secondary flows, the Bureau of Mines hoped to reduce erosion further. In addition, the first stage rotor and second stage stator rows were completely removed to provide an annular space for the ash to centrifuge toward the outer casing, eroding the blade tips instead of the highly-stressed blade roots (26).

During 1962, the Bureau of Mines conducted two tests totaling 1963 hours with the new blade design. After 878 hours, heavy ash deposits caused compressor surge, necessitating shut-down. Erosion was confined to the blade tips in stages two through five (27).

After cleaning and modifications to the ash separation equipment, a second test lasting 1085 hours was conducted. Ash concentrations were much less noticeable, but erosion increased. Large notches developed in the leading edges of the stator blades in rows two through four. Trailing edge erosion of these blades was more pronounced than in the first test. The rotor blades were in good condition, showing few signs of wear. The estimated life of the rotor blades now reached 20,000 - 30,000 hours; while the stator blade estimated life remained 5000 - 7500 hours. Ash deposits had become a more severe problem than erosion (28, 29).

During the early part of the program, the Bureau of Mines contracted the Gas Turbine Division of General Electric Company to develop a new turbine blade design aimed at minimizing ash concentrations and erosion. The new blade design, later used in the 1962 tests, attempted

to divert the ash particles to the outer sidewalls. The General Electric findings indicated many secondary flow phenomena occurring in the blade passages (27). The new blade design attempted to reduce these secondary effects by minimizing flow separation and end whirl from the stator blading. The trailing edges of the stator blading were made as thin as possible, enabling longer blade life for the rotor, but shorter life for the stator blading (30, 31).

The Bureau of Mines made no more additional tests with the Allis Chalmers unit. Further testing with a turbocompressor utilizing ash injection into a 1250° F airstream still produced unacceptable levels of turbine blade wear (32, 33).

One significant result of nearly 30 years of research by the Bureau of Mines and the L.D.C. was the development and testing of the first and only coal-burning gas turbine locomotive. In October 1962, this locomotive began tests with the Union Pacific Railroad. The locomotive was designed and built by the Union Pacific and the American Locomotive Company, using mainly L.D.C. technology. The A unit was a 2000 HP (1491 kW) diesel-electric ALCO locomotive. This unit supplied the power required to start the coal-fired gas turbine and then provided additional power. The 66-ft.-long (20.1 m) A unit had a fuel oil storage tank to supply the fuel oil required for starting the gas turbine. The 101 ft. (30.8 m) B unit contained the coal-fired gas turbine, combustion and ash separation equipment and a small diesel engine used to power the coal handling equipment. The B unit developed an additional 5000 HP (3728 KW) making the total output of the locomotive 7000 HP (5219 KW). A 44 foot (13.4 m) tender, carrying 61 tons (542,000 N) of

coal, followed the B unit. The tender also carried the coal crushing and handling equipment. Crushers reduced the raw coal to fine particles which were then introduced into an airstream, producing fluid-like properties. The fluidized coal was then stored in a 2-1/2 ton (22,400 N) bin. Two coal pumps fed the raw coal to the pulverizers as required. A control system prevented the crushed coal from building up in the bin, crushed coal being supplied only as needed. In its fluidized state, the coal was fed to the gas turbine combustors in the B unit. The gas turbine utilized a 15-stage axial flow compressor with a 6:1 pressure ratio. Maximum turbine inlet temperature was 1061 K (34, 35).

The locomotive was road tested for nearly a year. Severe turbine blade erosion prevented economical commercial operation of the locomotive.

Currently, the only experimental work in the direct coal-fired gas turbine field is being done in Australia. Both the General Electric Company and the Westinghouse Electric Company are currently in the design stages of developing gasified coal power plants. Under funding from the United States Energy Research and Development Administration (E.R.D.A.), these two companies have been preparing an Energy Conversion Alternatives Study (E.C.A.S.) (6, 7). One of the most promising methods studied has been the open cycle gas turbine using a coal gasifier. Both companies will soon begin experimental work in this field. Erosion of turbine blades due to particle impact still appears to be a problem even though scrubbing and cleaning of the combustion products will effectively remove particles larger than 2-3 microns (8).

Analytical Investigations

The earliest analytical investigations of erosion prediction were conducted by the N.A.C.A. and the General Electric Company in support of the L.D.C./Bureau of Mines experimental work discussed above. In the late 1960's, Tabakoff (36) began an investigation on sand ingestion in low-flying military gas turbines. This investigation later led to an erosion study of turbomachinery components in general (11, 12, 37, 38, 39). Using a computer program developed by Katsanis (40), Hussein and Tabakoff developed a computer program in 1972 that predicted particle trajectories in axial-flow turbine cascades (41, 42). Clevenger and Tabakoff (43, 44, 45, 46, 47) later extended this to radial inflow turbines. However, none of these models actually predict erosion rates or include any secondary flow effects.

Menguturk and Sverdrup (13) of the Westinghouse Electric Corporation developed a particle trajectory model similar to the axial flow model developed by Tabakoff. However, the Westinghouse model predicts erosion rates. This erosion model is based on work by Bitter (48, 49) and Finnie (50, 51). Both of these works support the theory of brittle and ductile mode response exhibited by most materials during particle impact. Particles striking a ductile material cause greatest erosion rates at an impact angle of 20° to 30°. For a brittle material, this angle is 90° (52). Bitter maintained that an erosion model must include the elastic and plastic material properties, with plastic deformation beginning once the energy threshold of the material is exceeded. On the other hand, Finnie maintains that erosion is com-

pletely plastic and results from the cutting of the surface by the particle. The erosion model used by Westinghouse is based on Bitter's theory. No related experimental results exist for coal ash particles striking typical turbine blade materials. A comparison of data for erosion due to siliconcarbide particles conducted by Finnie with experiments with callide coal ash by Brasinikas (53) showed that silicon-carbide particles produce erosion rates 25 times greater than coal ash particles. This is the model used in the Menguturk and Sverdrup work. The resulting computer program predicts that particles as small as one micron can still cause considerable damage to turbine blades. Damage is confined to the pressure surfaces of both rotor and stator blades, with 12 micron particles yielding erosion rates 9 times greater than 1 micron particles. Impact angles and particle velocities are also important parameters. The order of magnitude of blade erosion was found to be 10^{-1} cubic mm/hour (54).

Ulke (15), working with Westinghouse, added secondary flow phenomena such as end wall boundary layers, radial flows and blade wakes to the original inviscid solution. This turbine blade erosion model is the most advanced developed to date. With the addition of boundary layers, ash deposition is partially explained. Due to the low velocities in the boundary layers, many particles are "caught" as they strike the blade. The reduced velocities of these "caught" particles are low enough to allow chemical interactions to bind them to the surface. Erosion and deposition predictions made by this model appear to clarify results obtained in previous testing of gas turbines.

IX. THE ANALYSIS

This investigation was directed toward discovering the main parameters affecting erosion rates in axial-flow turbines subjected to particulate flow conditions adding to the work of Menguturk and Sverdrup (13). The investigation was entirely analytical, employing two computer programs. The first program used a finite difference, blade-to-blade solution to determine the fluid flow field, without particles, in an axial-flow turbine cascade. The second program determined particle trajectories and erosion rates, using the flow field established by the first program. A description of these programs and assumptions is included below.

Quasi-Three-Dimensional Inviscid Main Flow

(Following the Methods of Reference 13)

Solution Technique

The main flow field was determined by a FORTRAN program for calculating transonic velocities on a blade-to-blade stream surface of revolution. This program was developed by Katsanis (40). The actual program used, developed by Menguturk and Sverdrup, is a modification of the Katsanis program. The modifications made to the Katsanis program were directed toward linking this program to the particle trajectory programs. None of the modifications, except for a blade trailing edge flow field alteration, changed the predicted flow field; so the assumptions and theoretical developments of the Katsanis program are applicable to the modified Katsanis program. The method of solution

assumes the following (taken from Reference 40):

1. The flow is steady relative to the blade.
2. The fluid is a perfect gas (constant specific heat) or is incompressible.
3. The fluid is nonviscous, and there is no heat transfer, i.e., isentropic.
4. The flow is irrotational.
5. The blade-to-blade surface is a surface of revolution (this does not exclude straight, infinite cascades).
6. The velocity component normal to the blade-to-blade surface is zero.
7. The stagnation temperature is uniform across the inlet.
8. The velocity magnitude and direction are uniform across both the upstream and downstream boundaries.
9. The only forces are those due to momentum and pressure gradients.
10. The flow is essentially subsonic.

The program calculates along a blade-to-blade stream surface of revolution as shown in Figure 1. The general equations are normally written in three spatial variables: r, θ and x. Since the stream surface is defined as input to the program, r and x are not independent. These two variables are replaced by the meridional streamline distance, m, a stream channel thickness, h, and a meridional streamline radius, r, as shown in Figure 2.

The actual solution is calculated in two steps. The weight flow passing through the stream channel is reduced by a reduction factor so

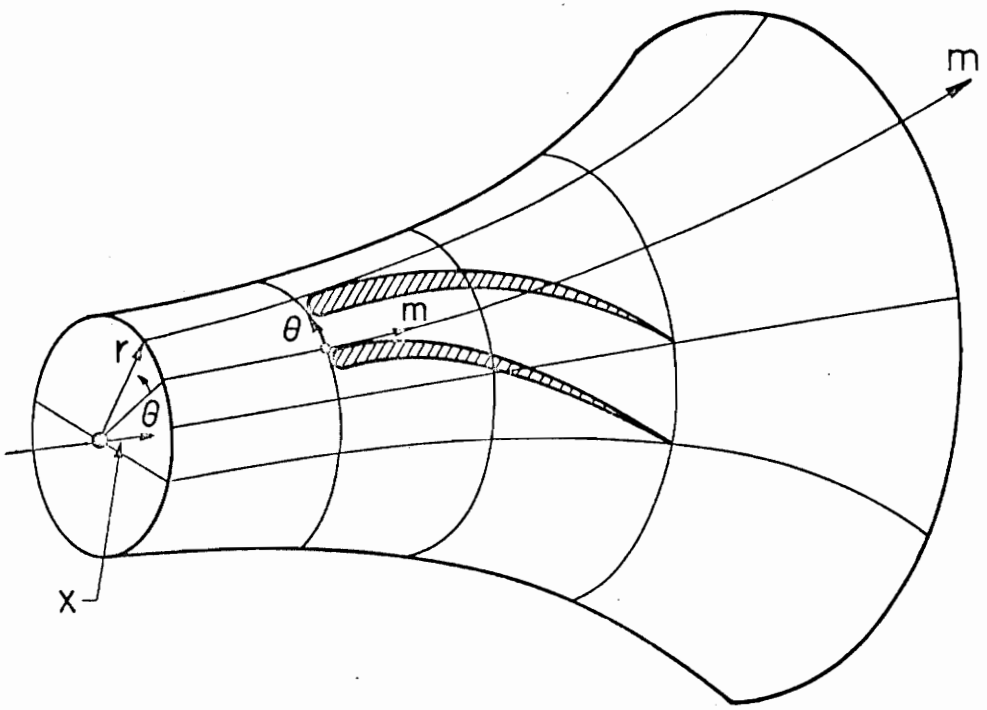

FIG. 1. BLADE-TO-BLADE STREAM SURFACE OF REVOLUTION
(as taken from Reference 13)

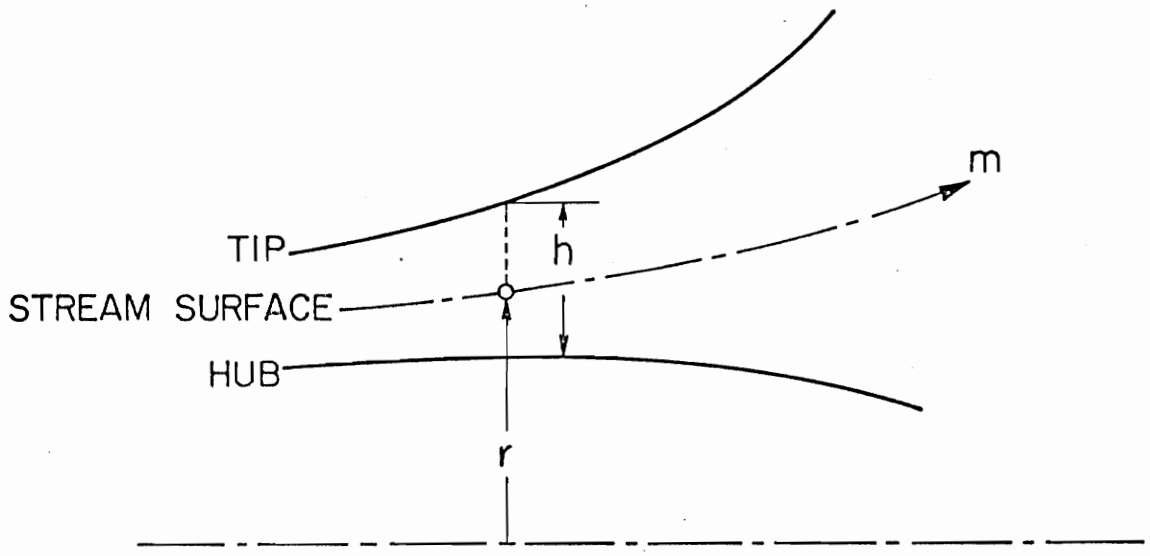

FIG. 2. STREAM CHANNEL (as taken from Reference 13)

that the flow is subsonic throughout the channel. Once the subsonic solution is solved, the velocity distribution corresponding to the full weight flow is solved using velocity gradient techniques. The solution must be determined in two parts, since the stream function equation is elliptic, while the transonic flow field model is parabolic in nature.

The reduced weight flow solution assumes a stream function defined by

$$\frac{\partial \psi}{\partial \theta} = \frac{rh\rho}{w} W_m$$

$$\frac{\partial \psi}{\partial m} = \frac{-h\rho}{w} W_\theta \qquad (1)$$

where W_m and W_θ are the gas velocities in the m and θ directions relative to the blade, ρ is the gas density and w is the stream channel mass flow rate.

The stream function equation for this geometry is

$$\frac{\partial^2 \psi}{\partial m^2} + \frac{1}{r^2} \frac{\partial^2 \psi}{\partial \theta^2} - \frac{1}{r^2 \rho} \frac{\partial \rho}{\partial \theta} \frac{\partial \psi}{\partial \theta} + \left[\frac{\sin\lambda}{r} - \frac{1}{\rho h} \frac{\partial (\rho h)}{\partial m} \right] \frac{\partial \psi}{\partial m} = \frac{2h\rho}{w} \omega \sin\lambda \qquad (2)$$

where λ is the turbine axis, streamline direction angle and ω is the rotational speed of the blade.

With the boundary conditions shown in Figure 3 and the density distribution, the reduced weight flow field is determined.

The temperature field is determined by the energy equation,

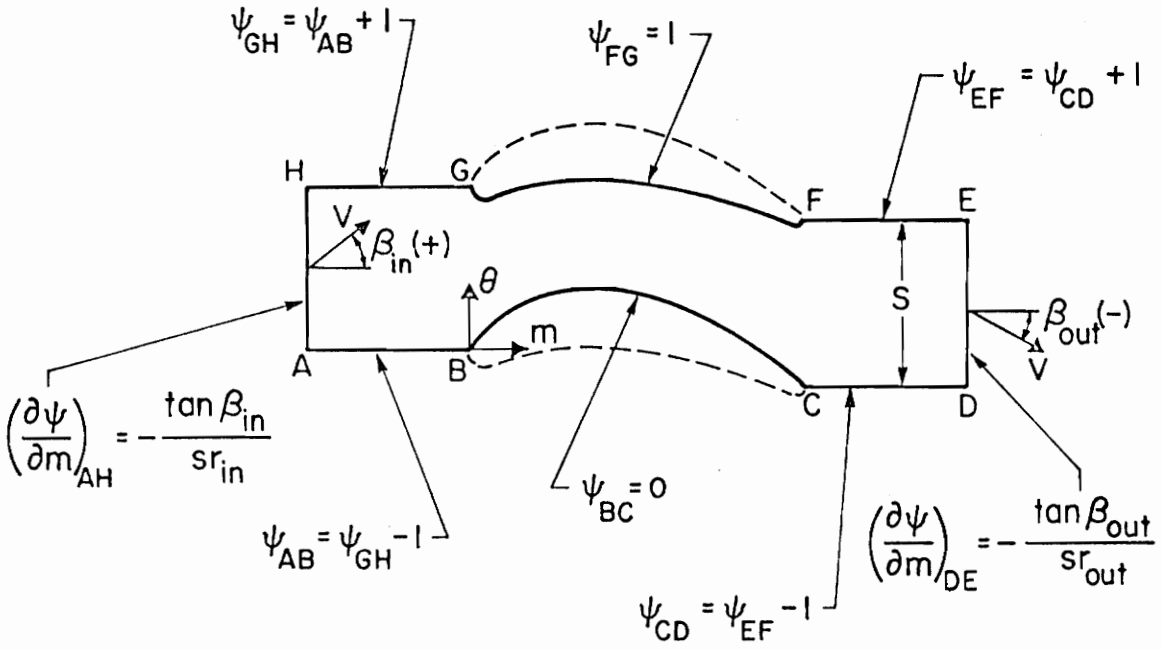

FIG. 3. STREAM CHANNEL BOUNDARY CONDITIONS (as taken from Reference 13)

$$\frac{T}{T_{o_3}} = \frac{1 - (V_m^2 + V_\theta^2) + 2\omega\varepsilon_i - (\omega r)^2}{2CpT_{o_3}} \tag{3}$$

where ε_i = inlet prerotation

T = gas temperature

T_{o_3} = inlet stagnation temperature

Cp = specific heat of gas at constant pressure.

From the isentropic relation,

$$\frac{\rho}{\rho_i} = \left[\frac{T}{T_{o_3}}\right]^{\frac{\alpha-1}{\alpha}} \tag{4}$$

where ρ = gas density

ρ_i = inlet gas density

α = specific heat ratio,

the density field is determined.

For the full weight flow solution, the stream function is not elliptic throughout the region. A velocity gradient solution based on the following equation is used to solve the flow field:

$$\frac{\partial W}{\partial \theta} = AW + A_1 \tag{5}$$

where $A = r^2\cos^2\beta \frac{d^2\theta}{dm^2} + \sin\lambda \tan\beta (1 + \cos^2\beta)$ (6a)

on the blade surface, and

$$A = \sin^2\beta \left[\frac{2\frac{\partial^2\psi}{\partial\theta\partial m} - \frac{\partial\psi}{\partial\theta}\frac{\partial^2\psi}{\partial m^2}}{\frac{\partial\psi}{\partial m}\left(\frac{\partial\psi}{\partial m}\right)^2} - \frac{\frac{\partial^2\psi}{\partial\theta^2}}{\frac{\partial\psi}{\partial\theta}} \right] + \sin\lambda \tan\beta (1 + \cos^2\beta) \tag{6b}$$

is used in the interior of the finite difference mesh.

Finally,

$$A_1 = r\tan\beta \frac{\partial W}{\partial \theta} + \frac{2\omega r \sin\lambda}{\sin\beta} \tag{7}$$

where β is the velocity vector, meridional plane angle.

The velocity distribution based on full weight flow is calculated by Equation (5) and the continuity equation:

$$\int_{\theta_1}^{\theta_2} \rho W\cos\beta \, hrd\theta = w \tag{8}$$

where θ_1 and θ_2 are the values at the upper and lower boundaries. Equation (5) and Equation (8) are solved iteratively until a solution converges, yielding the velocity gradient along a vertical mesh line.

Solution Validity

In most of the stream channel, this method of solution is quite accurate. The boundary layers around the blades are usually quite small owing to the high velocities, making their effect on the main flow insignificant. However, the development of large boundary layers on the casing and hub walls and the development of blade wakes will reduce the effective flow area considerably, increasing the exit velocities from the blade rows. Whether these effects will significantly alter particle trajectory calculations has yet to be determined.

Dynamics of Particles in Fluid Flow Fields

(Following the Methods of Reference 13)

Solution Technique

Particle trajectories are determined by one of two programs developed by Menguturk and Sverdrup (13). The single-row particle trajectory program is capable of calculating trajectories of particles for only one blade row at a time, while the single-stage particle trajectory program can calculate trajectories for a complete stage.

The main assumptions used by these programs are:

1. The particle is relatively small (less than several hundred microns).
2. The particles are spherically shaped.
3. The particles do not significantly alter the flow field established by the Katsanis program.

The main forces acting on particles in a fluid flow field are the pressure force, the viscous drag force and the particle's inertia. Hussein (41) showed that the pressure force can be neglected for small particle sizes. For a spherical particle and a small Reynolds number (based on the relative velocity between the fluid and the particle), the drag force is given by Stokes' Law:

$$\vec{F}_D = 3\Pi\mu_g d_p \, (\vec{V}_G - \vec{V}_P) \, f(Re) \tag{9}$$

where $\vec{F}_D$ = drag force

μ_g = gas viscosity

d_p = particle diameter

$\vec{V}_G$ = absolute gas velocity

$\vec{V}_P$ = absolute particle velocity

$f(Re) = Cd \frac{Re}{24}$

Cd = drag coefficient.

The drag coefficient equations as a function of Reynolds number are:

$$Cd = 24/Re \qquad (0 < Re \leq 0.1)$$

$$Cd = 22.73/Re + 0.093/(Re)^2 + 3.69 \qquad (0.1 < Re \leq 1)$$

$$Cd = 38.80/Re - 12.65/(Re)^2 + 0.36 \qquad (1 < Re \leq 10)$$

$$Cd = 46.50/Re - 116.667/(Re)^2 + 0.61667 \qquad (10 < Re \leq 100)$$

$$Cd = 98.33/Re - 2778/(Re)^2 + .3644 \qquad (100 < Re \leq 1000)$$

$$Cd = 148.62/Re - 47500/(Re)^2 + .35713 \qquad (1000 < Re \leq 5000) \qquad (10)$$

where the Reynolds number is based on the relative velocity between the gas and the particle and on the particle diameter.

By Newton's Second Law, the acceleration and mass of a particle can be related to the net force acting on it. In x, r, θ coordinates as shown in Figure 4, the equations of motion are:

$$\ddot{x}_p = G(V_x - \dot{x}_p)$$

$$\ddot{\theta}_p = \frac{G}{r}(V_\theta - r\dot{\theta}) - \frac{2\dot{r}_p}{r}(\dot{\theta}_p + \omega)$$

$$\ddot{r}_p = G(V_r - \dot{r}_p) + r(\dot{\theta}_p + \omega)^2 \qquad (11)$$

where $(\dot{})$ denotes a time derivative, V_r, V_θ and V_x are the gas velocities in the r, θ and x directions respectively and

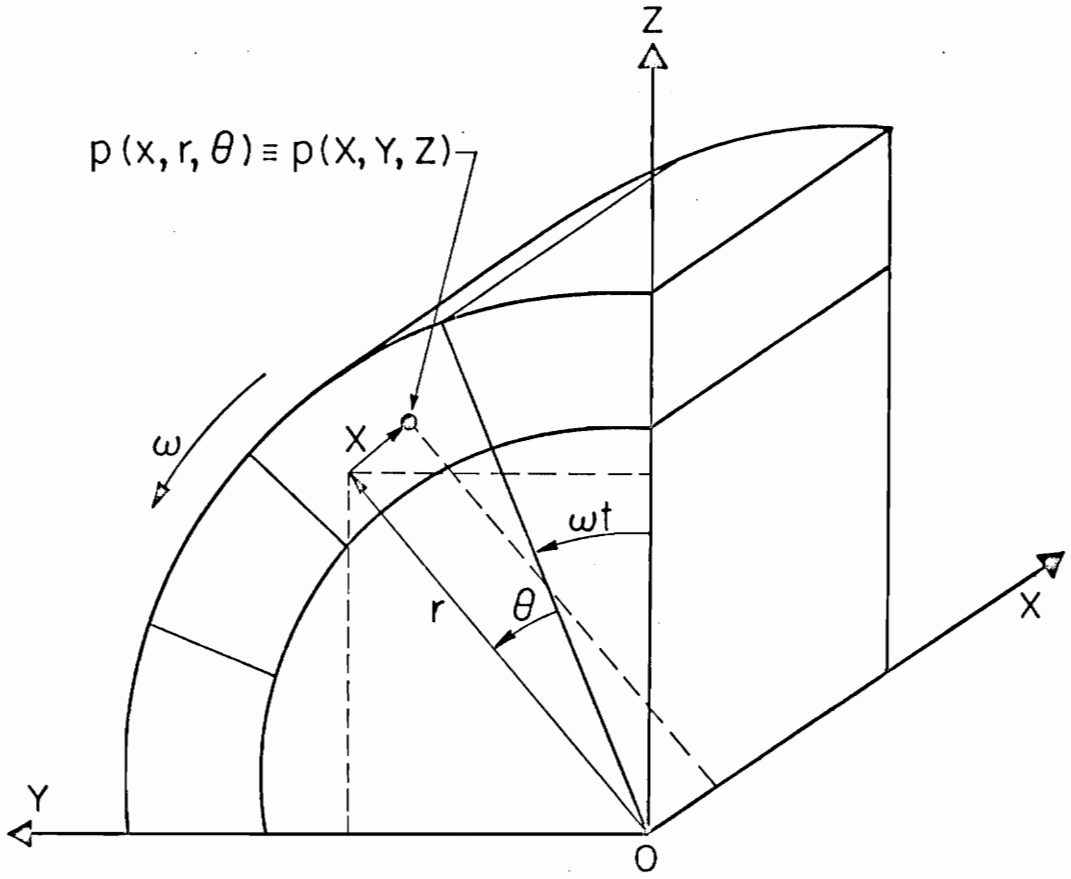

FIG. 4. PARTICLE MOTION COORDINATE SYSTEM (as taken from Reference 13)

$$G = \frac{18\,\mu_g}{d_p^2\,\rho_p}\,f(Re) \tag{12}$$

Equation (11) can be numerically integrated for the particle trajectories, interpolating the gas velocities through the mesh. To account for particle collisions with the blade surface, the results obtained by Hussein (41) are used. The experimental results, which were obtained by using poppy seeds and corn cups with stainless steel blades, shown in Figure 5 can be approximated by the equations

$$\frac{V_{p_2}}{V_{p_1}} = \frac{V_{p_{n2}}}{V_{p_{n1}}} \left[\frac{1 + \cot^2\beta_2}{1 + \cot^2\beta_1} \right]^{\frac{1}{2}}$$

$$\frac{\beta_2}{\beta_1} = \frac{1}{\beta_1} \cot^{-1} \left[\frac{V_{p_{t2}}}{V_{p_{t1}}} \frac{V_{p_{n1}}}{V_{p_{n2}}} \right] \cot\beta_1$$

$$\frac{V_{p_{t2}}}{V_{p_{t1}}} = 0.95 + .00055\beta_1$$

$$\frac{V_{p_{n2}}}{V_{p_{n1}}} = 1.0 - 0.02108\beta_1 + 0.0001417\beta_1^2 \tag{13}$$

where V_p is the velocity of the particle and β_1 is the impact incidence angle. Subscripts 1 and 2 refer to pre-impact and post-impact conditions. Subscripts t and n refer to tangential and normal velocity components.

With this particle rebound model, the particle trajectories following impact can be determined.

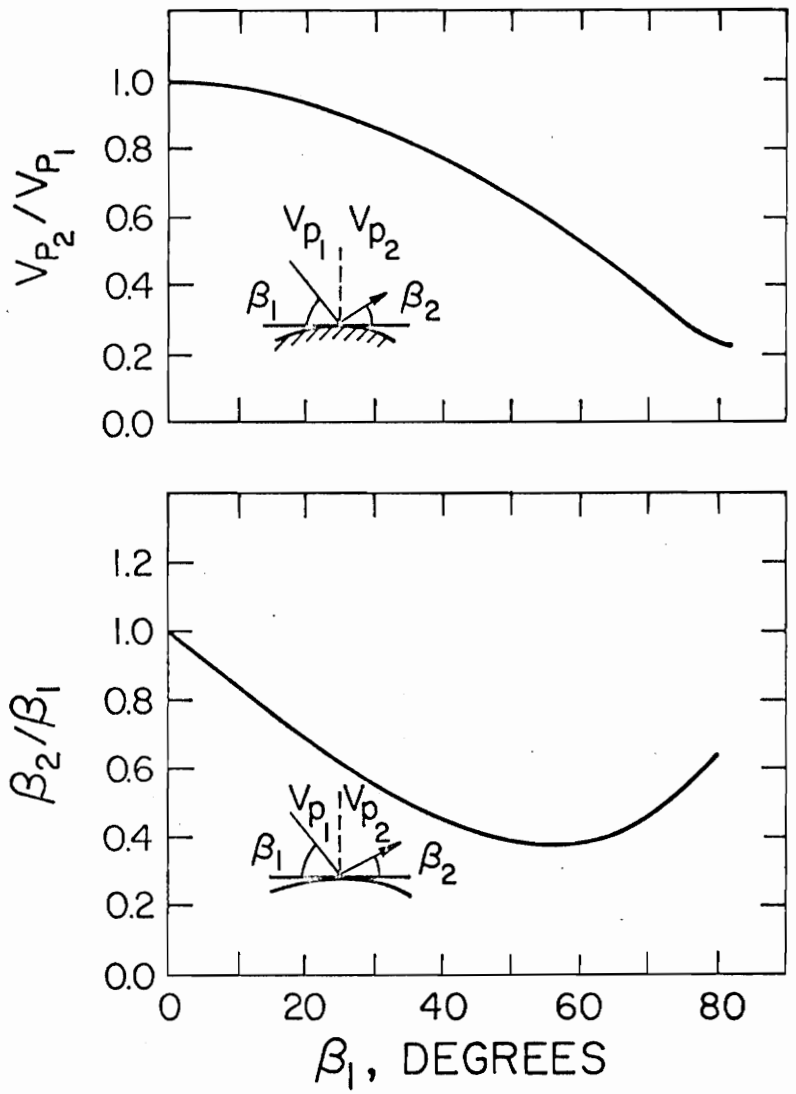

FIG. 5. PARTICLE REBOUND DATA (as taken from Reference 41)

Solution Validity

This procedure has already been used by Ulke (15) to determine particle trajectories in turbine cascades with good results. Since the associated flow model is essentially inviscid, deposition or corrosion of blades cannot be accurately predicted. The inclusion of blade boundary layers, although not affecting the main flow field appreciably, could have a major influence on particle trajectories, especially for those particles having long residence times in the boundary layer, which are likely to deposit on the blade.

Erosion Model

(Following the Methods of Reference 13)

Solution Technique

Blade erosion rates are determined by either of the particle trajectory programs, for a single blade row or for a stage. The erosion model assumes that materials behave in both ductile and brittle modes when struck by particles in the flow field. Ductile erosion occurs at moderate angles of impact, resulting in a gouging-out of the surface. Brittle erosion occurs at high impact angles, resulting in cracking and spalling of material. Since no materials are perfectly brittle or perfectly ductile, particle impacts cause both brittle and ductile erosion.

Bitter (48, 49) determined erosion loss rates and equated them by

$$S = \frac{1}{2} M \frac{(V_p^2 \cos^2\beta_1 - V_{p_{tR}}^2)}{\phi} + \frac{1}{2} \frac{M(V_p \sin\beta_1 - V_{p_{el}})^2}{\varepsilon} \quad (14)$$

where S = volume of material eroded per particle impact

M = mass of particle

$V_{p_{el}}$ = velocity of particle corresponding to elastic deformation

ε = threshold energy for brittle erosion

V_p = particle velocity

ϕ = threshold energy for ductile erosion

β_1 = impact angle

$V_{p_{tR}}$ = residual horizontal velocity component after impact.

With generalized velocity exponents m_1 and m_2, amplitudes of brittle and ductile modes K_2 and K_1, and $E = S/M$, equation (14) becomes:

$$E = K_1 (V_p \cos\beta_1)^{m_1} \left[1 - \frac{V_{p_{tR}}}{(V_p \cos\beta_1)}^{m_1} \right] + K_2 (V_p \sin\beta_1 - V_{p_{el}})^{m_2} \quad (15)$$

This equation is further simplified, assuming that the residual horizontal velocity component is a function of impact velocity, impact angle, and various material properties, to

$$E = K_1 (V_p \cos\beta_1)^{m_1} f(\beta_1) + K_2 (V_p \sin\beta_1 - V_{p_{el}})^{m_2} \quad (16)$$

where $f(\beta) = \sin(n\beta_1)$ for $\beta_1 \leq \beta_0$

$= 1$ for $\beta_1 > \beta_0$

where β_0 is a reference angle determined by experiment. $V_{p_{el}}$ is

usually small in a gas turbine so it can be neglected.

The erosion equations now become:

$$E = K_1 (V_p \cos\beta_1)^m \sin(n\beta_1) + K_2 (V_p \sin\beta_1)^m \quad \text{for } \beta_1 \leq \beta_0$$

$$E = K_1 (V_p \cos\beta_1)^m + K_2 (V_p \sin\beta_1)^m \quad \text{for } \beta_1 > \beta_0 \qquad (17)$$

A typical plot of the results from these equations is shown in Figure 6. The coefficients K_1 and K_2, the velocity exponent and β_0 are all determined experimentally. For silicon carbide particles striking nickel cobalt alloy, the following experimental results by Smeltzer (55) can be used:

β_{max} (deg.)	β_0 (deg.)	K_1 ($\frac{mm^3/gm}{(ft/sec)^2}$)	K_2 ($\frac{mm^3/gm}{(ft/sec)^2}$)
10	10.3	7.44×10^{-8}	2.4×10^{-8}
20	22.7	8.35×10^{-8}	2.4×10^{-8}
30	45.3	1.12×10^{-7}	2.4×10^{-8}
90	90	0	7.18×10^{-8}

where β_{max} is the angle of maximum erosion and the velocity exponent is assumed to be 2.5.

Experimental data for coal ash particles by Brasinikas (53) was used to estimate the relative erosion rates between silicon carbide particles and coal ash particles. It was found that coal ash particles are only 1/25 as erosive as silicon carbide particles impacting a nickel alloy at room temperature. By using this ratio, the silicon carbide erosion model presented above was used in the computer program to predict coal ash erosion.

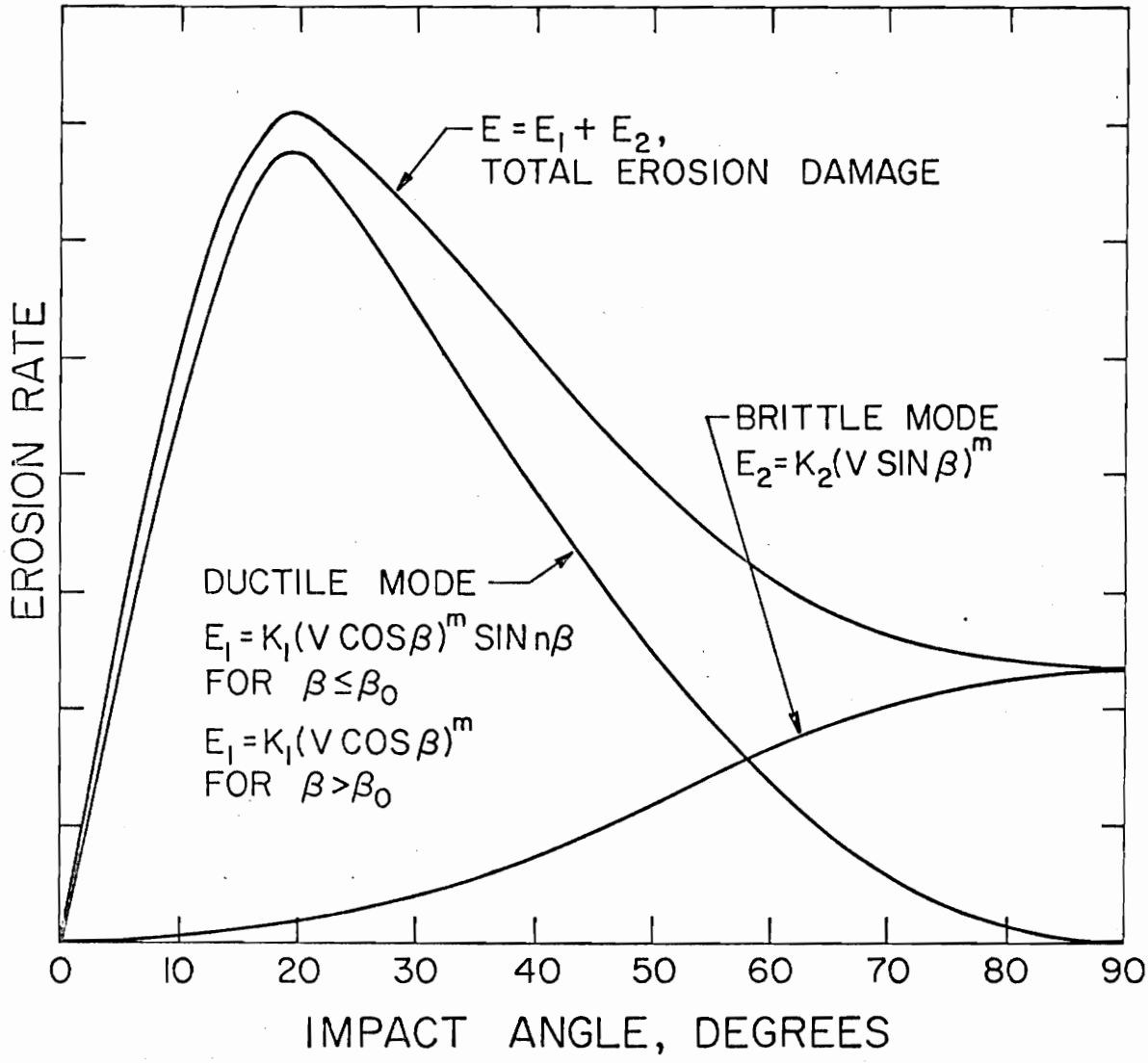

FIG. 6. BRITTLE AND DUCTILE MODES OF EROSION (as taken from Reference 13)

Solution Validity

The values of the constants K_1, K_2, m, β_0 and β_{max} have yet to be determined for coal ash particles striking typical turbine blade materials. Experimental results for these values would make the erosion model presented above more accurate. The effect of the blade boundary layer has yet to be determined. A particle entering the boundary layer may have its velocity and impact angle significantly changed so that the erosion model presented above could be in error.

X. THE INVESTIGATION

The investigation can be divided into three main sections corresponding to the three main parameters to be studied: blade profile variation, gas temperature variation and particle size and density variations. The investigation centered on the total erosion damage to blading caused by the variations of the parameters. No effort was made to determine the erosion distribution over the blade surfaces although this capability existed in the computer programs used.

Blade Profile Variation

The design of the basic stator and rotor blade shapes and the modifications made to these shapes in order to vary flow turning angles and blade leading edge thicknesses are discussed in detail in Appendix B. The main criterion used in determining the acceptability of these shapes for the erosion programs was the surface velocity distribution plotted by the modified Katsanis program. Once deemed acceptable, the data sets generated by the modified Katsanis program were placed in the single-row particle trajectory program. The erosion rates and particle trajectories were then determined for the twelve blade shapes used.

The initial conditions required by the single-row particle trajectory program were the number of particle trajectories, the initial m and θ coordinates of each particle relative to the blade, the initial flow angles in the m-θ plane and m-r plane and the initial size and density of each particle.

For the blade profile variation portion of the investigation, it was decided that the particle size should be 10 microns. This size might appear to be somewhat large since hot gas clean-up facilities can effectively remove most (but not all) particles larger than 2-3 microns. However, particles of this latter size produce small erosion rates (29). The larger particles, although less numerous, will apparently be responsible for most of the erosion damage; thus, 10 micron particles were assumed for the majority of this study.

The particle density for the blade profile variation was chosen as 1.5 gm/cc, corresponding to that of a typical coal ash particle.

The initial particle position and velocity specification varied for the rotor and the stator blades because these parameters had to be specified relative to the blade. The number of particle trajectories for the stator and the rotor passages differed because there are twice as many rotor blades as there are stator blades in the first stage of the gas turbine investigated. This resulted in two particles entering a stator passage for every particle entering a rotor passage. The maximum number of particle trajectories allowable in the single-row particle trajectory program was nineteen, imposing limitations on the detail or "fineness" of the results.

For all of the stator blades analyzed in the blade profile variation study, the number of particle trajectories was nineteen. The initial particle m-coordinate was chosen as -0.15 ft (-.046 m). Since the flow ahead of the blade passage is affected by the blades, it was desired to let the particle adjust to this flow before entering the

passage. For this reason, the initial m-coordinates of the particles were chosen as far from the blade as permitted by the computer program.

The initial particle velocity was chosen as 552 ft./sec. (140 m/sec.) for all of the stator blades analyzed since this velocity corresponded (to within 25 ft./sec. (6.35 m/sec.)) to the flow velocities for all of the stator blades at the initial m-coordinate. The initial particle trajectory angles, α_p and β_p, were chosen at 0° for all of the stator blades. It should be noted that the initial particle trajectory angles and particle velocities were required to be only approximate since particles as small as 10 microns quickly adjust to the surrounding flow field. Table 1 shows the initial particle conditions for all nineteen trajectories. Every other trajectory was plotted to avoid clutter. Those plotted are denoted by the * symbol. These plots appear in Appendix C.

The initial particle conditions for the rotor blades were more difficult to determine since these blades required relative trajectory angles and velocities. Rather than "aiming" the particles through the desired blade channel from a position in front of the blade, it was decided to "force" the particles through the channel by specifying the initial m-coordinate as 0.0000 ft. This specification required each particle to have the correct flow angle and velocity since the particle would have little time to adjust to the flow before traveling well into the blade channel. The flow angles and velocities were found from the output of the modified Katsanis program for each blade at the rotor inlet plane for varying θ-coordinates. The single-row particle trajectory program will actually allow for particles to "spill" over into

TABLE 1.

INITIAL PARTICLE CONDITIONS FOR THE STATOR BLADES
(BLADES 1-3, 7-9)

ρ_p = 1.5 mg/cc $\quad\quad$ $\alpha_p = 0°$

T_{o_3} = 2465°R $\quad\quad$ $\beta_p = 0°$

$d_p = 10\mu$ $\quad\quad$ V_p = 552 ft./sec.

Trajectory number	X (ft.)	θ (radians)
1*	-0.15	0.0000
2	-0.15	0.0069
3*	-0.15	0.0137
4	-0.15	0.0207
5*	-0.15	0.0276
6	-0.15	0.0344
7*	-0.15	0.0413
8	-0.15	0.0482
9*	-0.15	0.0551
10	-0.15	0.0620
11*	-0.15	0.0689
12	-0.15	0.0758
13*	-0.15	0.0827
14	-0.15	0.0896
15*	-0.15	0.0964
16	-0.15	0.1033
17*	-0.15	0.1102

TABLE 1.

(Continued)

Trajectory number	X (ft.)	θ (radians)
18	-0.15	0.1171
19*	-0.15	0.1240

the next channel by adding or subtracting the blade pitch, permitting the particle to travel through the desired channel. However, this procedure produced cluttered trajectory plots, so the particles were forced through the desired channel by the method above. The method used was later compared to results obtained from the single-stage particle trajectory program with identical initial rotor flow conditions yielding nearly identical erosion results. Use of the single-stage program would have avoided the "forcing" requirement for the rotor blades. However, only the single-row program was available for the initial portion of the investigation.

For programming convenience, the number of particle trajectories for the rotor was chosen at sixteen instead of the nineteen used for the stator blades. One might question this choice since one would expect to find half as many particles entering a rotor passage than those entering the stator passages. However, no effort was made to compare the total erosion damage for complete stages because the matching flow between blade rows was not determined.

Rotor blade pairs 4 and 10, 5 and 11 and 6 and 12 have the same initial particle conditions because they have the same leading edge configurations. Tables 2 through 4 show the initial particle conditions for these three sets of rotor blades. Again, those trajectories actually plotted are denoted by the * symbol.

Temperature Variation

The single-row particle trajectory program was used to analyze the effect of turbine inlet temperature variations by two different

TABLE 2.

INITIAL PARTICLE CONDITIONS FOR THICK LEADING EDGE ROTOR BLADES
(BLADES 4, 10)

ρ_p = 1.5 mg/cc $\alpha_p = 0°$

T_{o_3} = 2465°R

d_p = 10μ

Trajectory number	X (ft.)	θ (radians)	BETAP (deg.)	VPART (ft./sec.)
1*	0.0	0.0000	22.1	850.
2	0.0	0.0041	45.6	822.
3*	0.0	0.0083	46.7	840.
4	0.0	0.0124	45.4	844.
5*	0.0	0.0165	44.8	850.
6	0.0	0.0207	44.2	844.
7*	0.0	0.0248	43.8	838.
8	0.0	0.0289	43.9	834.
9*	0.0	0.0331	44.0	835.
10	0.0	0.0372	44.1	835.
11*	0.0	0.0413	44.3	836.
12	0.0	0.0455	43.9	832.
13*	0.0	0.0496	43.6	824.
14	0.0	0.0537	43.1	818.
15*	0.0	0.0579	42.8	814.

TABLE 2.

(Continued)

Trajectory number	X (ft.)	θ (radians)	BETAP (deg.)	VPART (ft./sec.)
16	0.0	0.0620	39.4	831.

TABLE 3.

INITIAL PARTICLE CONDITIONS FOR MEDIUM THICKNESS LEADING EDGE ROTOR BLADES
(BLADES 5, 11)

ρ_p = 1.5 gm/cc $\alpha = 0°$

$T_{o_3} = 2465°R$

$d_p = 10\mu$

Trajectory number	X (ft.)	θ (radians)	BETAP (deg.)	VPART (ft./sec.)
1*	0.0	0.000	28.4	810.
2	0.0	0.0041	48.5	818.
3*	0.0	0.0083	48.8	850.
4	0.0	0.0124	48.7	865.
5*	0.0	0.0165	48.4	876.
6	0.0	0.0207	48.1	864.
7*	0.0	0.0248	47.5	854.
8	0.0	0.0289	47.4	851.
9*	0.0	0.0331	47.2	844.
10	0.0	0.0372	47.0	831.
11*	0.0	0.0413	46.9	822.
12	0.0	0.0455	47.0	820.
13*	0.0	0.0496	47.1	819.
14	0.0	0.0537	47.2	812.
15*	0.0	0.0579	47.3	802.
16	0.0	0.0620	39.4	822.

TABLE 4.

INITIAL PARTICLE CONDITIONS FOR THIN LEADING EDGE ROTOR BLADES (BLADES 5, 11)

Trajectory number	X (ft.)	θ (radians)	BETAP (deg.)	VPART (ft./sec.)
1*	0.0	0.0000	26.1	851.
2	0.0	0.0041	51.9	830.
3*	0.0	0.0083	51.7	865.
4	0.0	0.0124	50.7	859.
5*	0.0	0.0165	50.6	861.
6	0.0	0.0207	50.5	849.
7*	0.0	0.0248	50.3	845.
8	0.0	0.0289	50.3	841.
9*	0.0	0.0331	50.2	835.
10	0.0	0.0372	50.2	831.
11*	0.0	0.0413	50.3	826.
12	0.0	0.0455	50.4	817.
13*	0.0	0.0496	50.5	824.
14	0.0	0.0537	50.6	819.
15*	0.0	0.0579	50.9	818.
16	0.0	0.0620	42.1	838.

methods. One method varied only turbine inlet temperature. The other method varied both turbine inlet temperature as well as mass flow (w) so that the parameter $w\sqrt{T_{o_3}}$ was held constant. This parameter, when divided by the turbine inlet stagnation pressure is the "non-dimensional mass flow" used in a gas turbine performance analysis.

For all of the temperature variation calculations, the particle density was 1.5 gm/cc. Only Blades 2 and 5 (the reference blade shapes used in this investigation) were analyzed. The initial particle conditions can be found in Table 1 for Blade 2 and Table 2 for Blade 5.

Particle size was also varied along with temperature and mass flow. Both 1 and 10 micron particles were used in the temperature investigation. The three turbine inlet temperatures studied were 2365, 2465 and 2565 °R (1314, 1369, 1425 °K). These temperatures and particle sizes were varied at constant design mass flows of 0.435 slugs/sec. (6.34 kg./sec.) for Blade 2 and 0.217 (3.16 kg./sec.) for Blade 5. The design mass flows were then used to determine the constant $w\sqrt{T_{o_3}}$ for Blades 2 and 5. Then, turbine inlet temperature was varied and the new mass flows corresponding to holding $w\sqrt{T_{o_3}}$ constant were calculated. The investigation was repeated using these new mass flows.

Particle Size and Density Variation

This portion of the study was designed to investigate the effect of particle size and density changes on predicted erosion. The two particle sizes investigated were 1 and 10 microns. The two particle densities studied were 1.5 gm/cc and 2.5 gm/cc. The second density corresponds to a typical dolomite particle found in the producer gas from coal gasifiers. The blades used were Blade 2 and Blade 5. The

single-stage particle trajectory program was used to determine the rotor erosion rates in this study as well as to check the methods used for the rotor blades in the single-row particle trajectory program. As previously noted, the single-stage particle trajectory program was not used for all of the rotor blade calculations because of late availability. Since the results from the single-row particle trajectory program proved to be very similar to those predicted by the single-stage particle trajectory program for the several cases tested, single-row particle trajectory program results are reported in this thesis, except for the particle size and density variation studies.

The initial conditions used in the single-stage particle trajectory program were as follows: one particle in the stator passage with initial m and θ coordinates of -0.15 ft. (-.046 m) and 0.0000 ft. respectively and sixteen particles in the rotor passage at the θ-coordinates found in Table 3. The single-stage particle trajectory programs had to be run twice since the maximum number of trajectories for this program was ten. The erosion rates for variations of particle size and density in the stator passages were more easily determined by the single-row particle trajectory program because of its simpler method of inputting large numbers of particles for these blades. This program was used to determine the stator blade erosion rates for variations of particle size and density.

XI. RESULTS

Stator

Blade Profile Variation

The single-row particle trajectory program was used to determine the total erosion damage for the six stator blade shapes. The initial particle conditions are found in Table 1. The results of these geometry variations are presented in Figure 7. The calculated erosion damages are non-dimensionalized with the Blade 2 (reference blade at 66.7° turning angle) erosion damage. As can be seen from Figure 7, a decrease in flow turning angle results in corresponding decreases of erosion damage in stator blades with thickened leading edges only. Interestingly, for thin leading edge stator blades, a decrease in turning angle yields higher predicted total erosion damage. The standard first stage stator blade (medium leading edge) shows only a slight reduction in erosion damage for the 6.7° turning angle reduction used in this investigation.

Temperature Variation

The single-row particle trajectory program was used to determine the effect of temperature and mass flow variations for the standard first stage stator blade. The results of this investigation are shown in Figure 8 for the two particle sizes examined. The erosion damages are non-dimensionalized with the Blade 2 erosion damage at design conditions. As can be seen from Figure 8, variations of 100° R yield very little variation in total erosion damage for both the 1 and 10

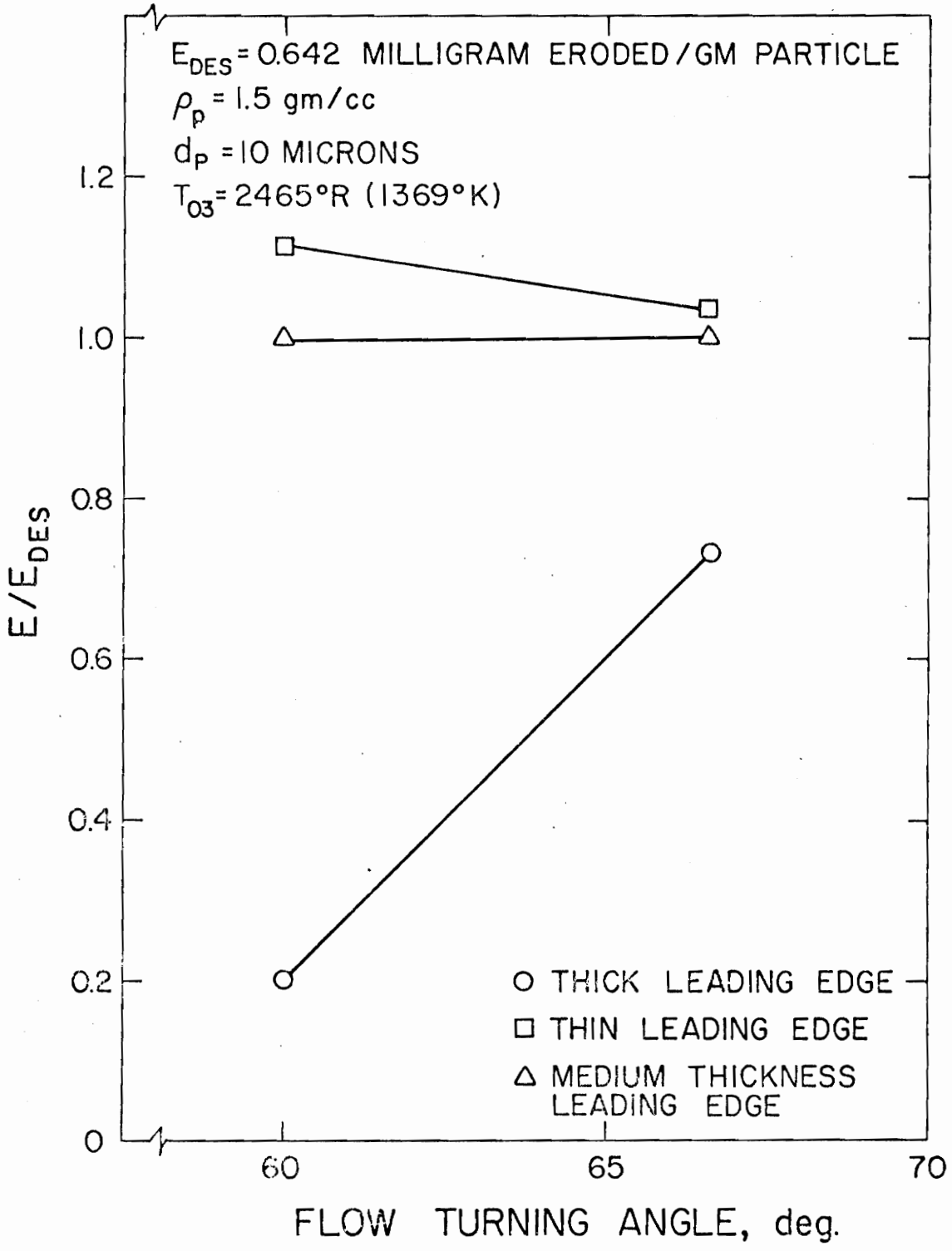

FIG. 7. EROSION RATE OF STATOR BLADES AS A FUNCTION OF TURNING ANGLE

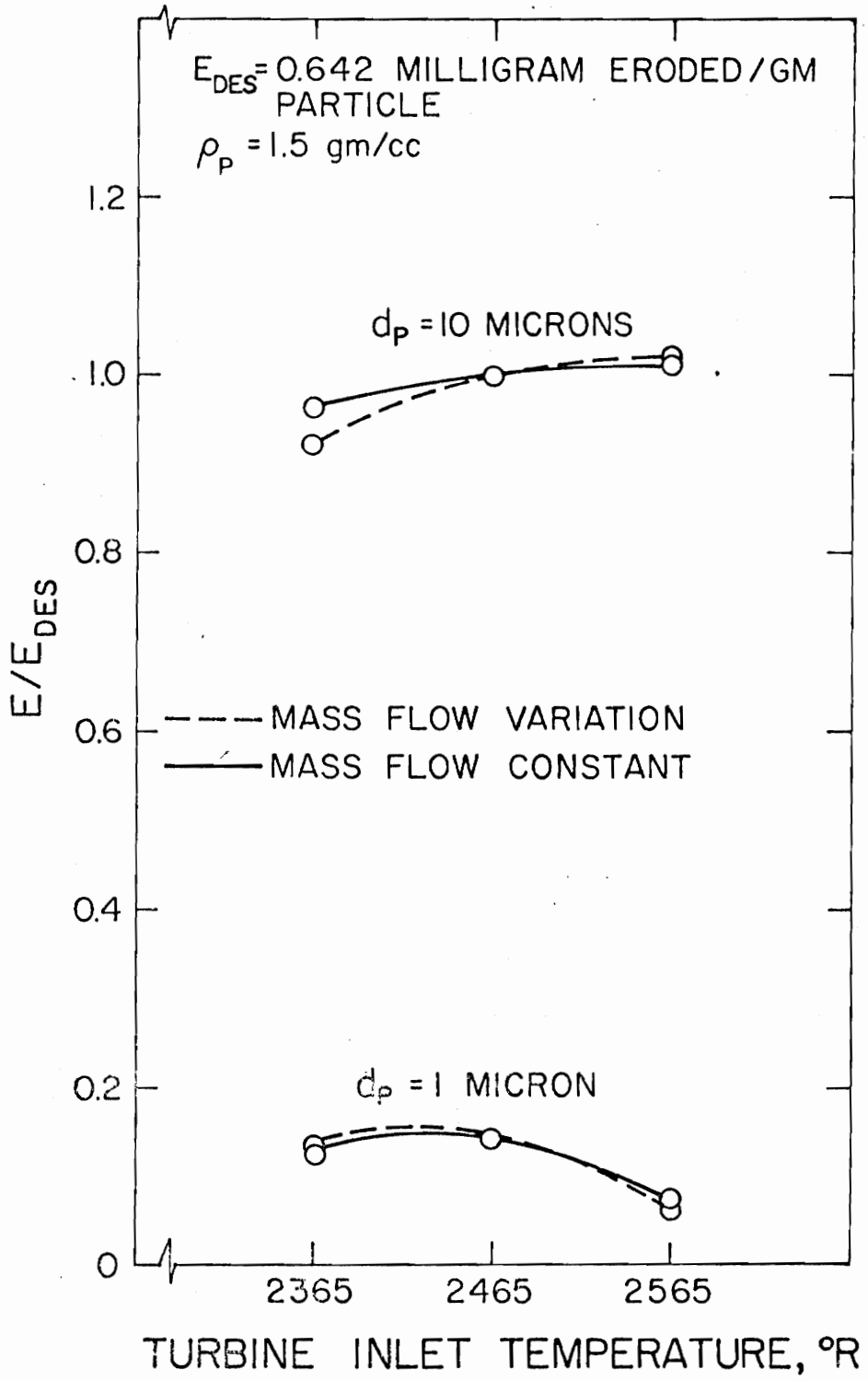

FIG. 8. EROSION RATE OF STATOR AS A FUNCTION OF INLET STAGNATION TEMPERATURE (BLADE 2)

micron particles. Variations in mass flow corresponding to holding $w\sqrt{T_{o_3}}$ constant also yielded insignificant changes in total erosion rates. For the 1 micron particles, a slight decrease in total erosion damage is noticed for higher turbine inlet temperatures. However, this trend is not evident for 10 micron particles.

Particle Size and Density Variations

Figure 9 shows the non-dimensional erosion damage in the stator as a function of particle size and density for the standard first stage stator blade. As can be seen in Figure 9, reductions in particle size and particle density resulted in the lowest predicted erosion rates. This result was also found in the Menguturk and Sverdrup study (13). In Figure 9, the plot is arranged on 3 axes.

Rotor

Blade Profile Variation

The single-row particle trajectory program was used to determine the total erosion damage for the six rotor blade shapes. The initial particle conditions are found in Tables 2 through 4. The results of the blade profile variation are shown in Figure 10. The erosion damages are non-dimensionalized to the Blade 5 (reference blade) erosion damage at design conditions. As can be seen from Figure 10, decreases in flow turning angle result in decreases in total erosion damage for all of the leading edge thicknesses investigated. The combination of a thick leading edge and a lower turning angle yielded the most significant

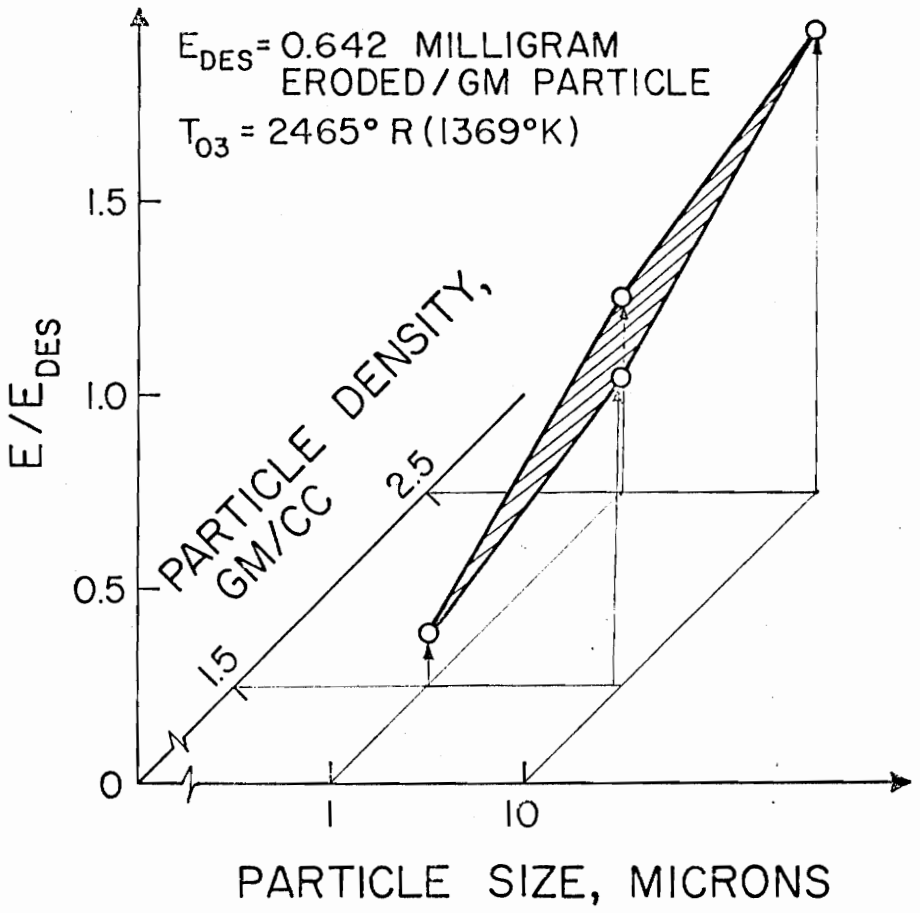

FIG. 9. EROSION RATE OF STATOR AS A FUNCTION OF PARTICLE SIZE AND DENSITY (BLADE 2)

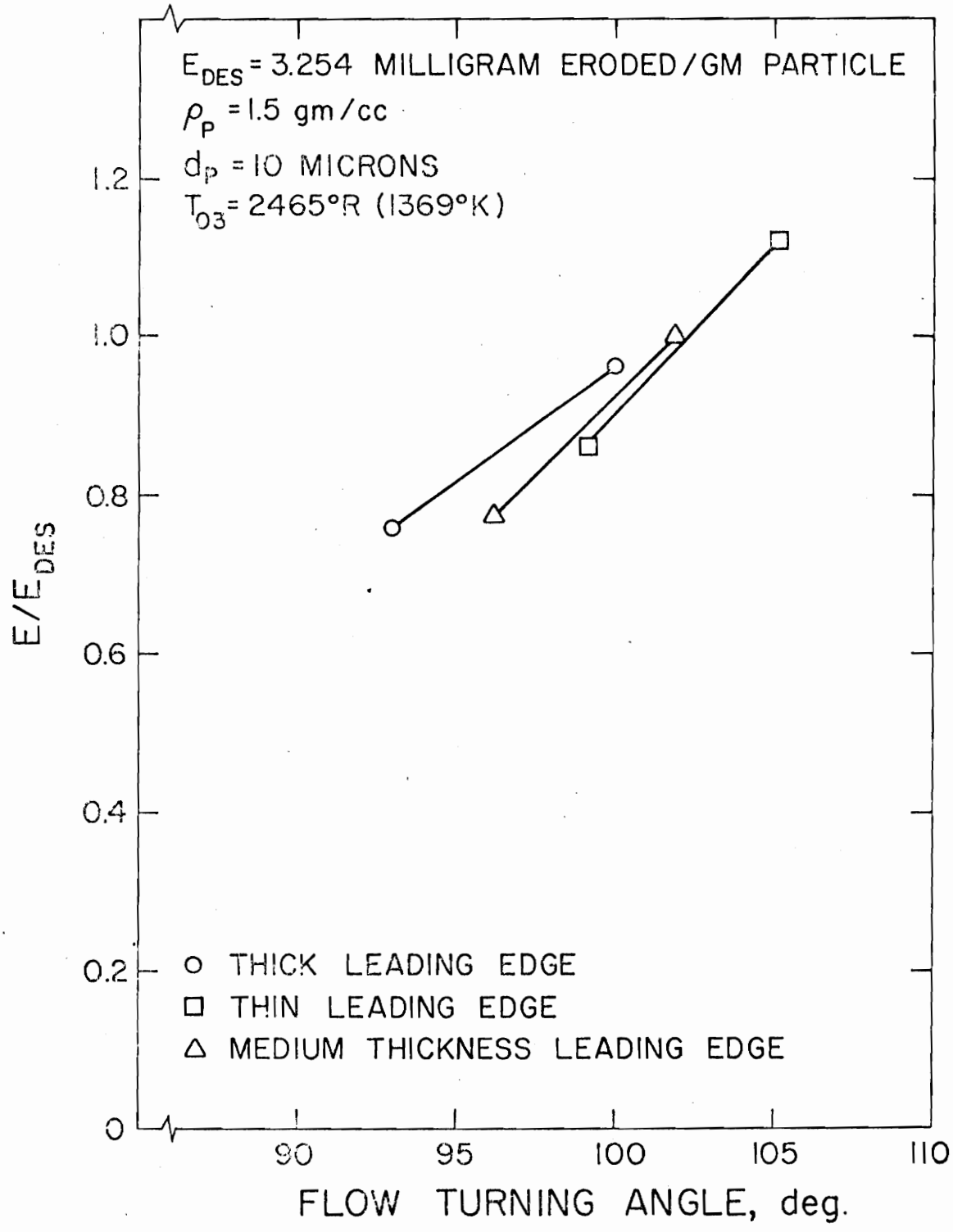

FIG. 10. EROSION RATE OF ROTOR AS A FUNCTION OF TURNING ANGLE

reduction in total erosion damage, as was found for the stator blades.

Temperature Variation

The single-row particle trajectory program was used to determine the total erosion damage for the standard first stage rotor blades for variations in temperature and mass flow. These results appear in Figure 11. The total erosion damages are non-dimensionalized to the Blade 5 erosion damage at design conditions. The results for the rotor blades are very similar to those found for the stator blades: temperature and mass flow variations have little effect on total erosion damage.

Particle Size and Density Variation

The results of the particle size and density variation for the standard first stage rotor blades are presented in Figure 12. Again, the total erosion damages are non-dimensionalized to the Blade 5 erosion damage at design conditions. As can be seen from Figure 12, the total erosion damage is minimized for small particle sizes and densities, as was found for the stator blades. This is also in agreement with the findings of Menguturk and Sverdrup (13).

Collective Results

The plots of total erosion damage as a function of turbine inlet temperature, flow turning angle and blade leading edge thickness for 10 micron particles with densities of 1.5 gm/cc are collectively presented in Figure 13 for the stator blades and Figure 14 for the

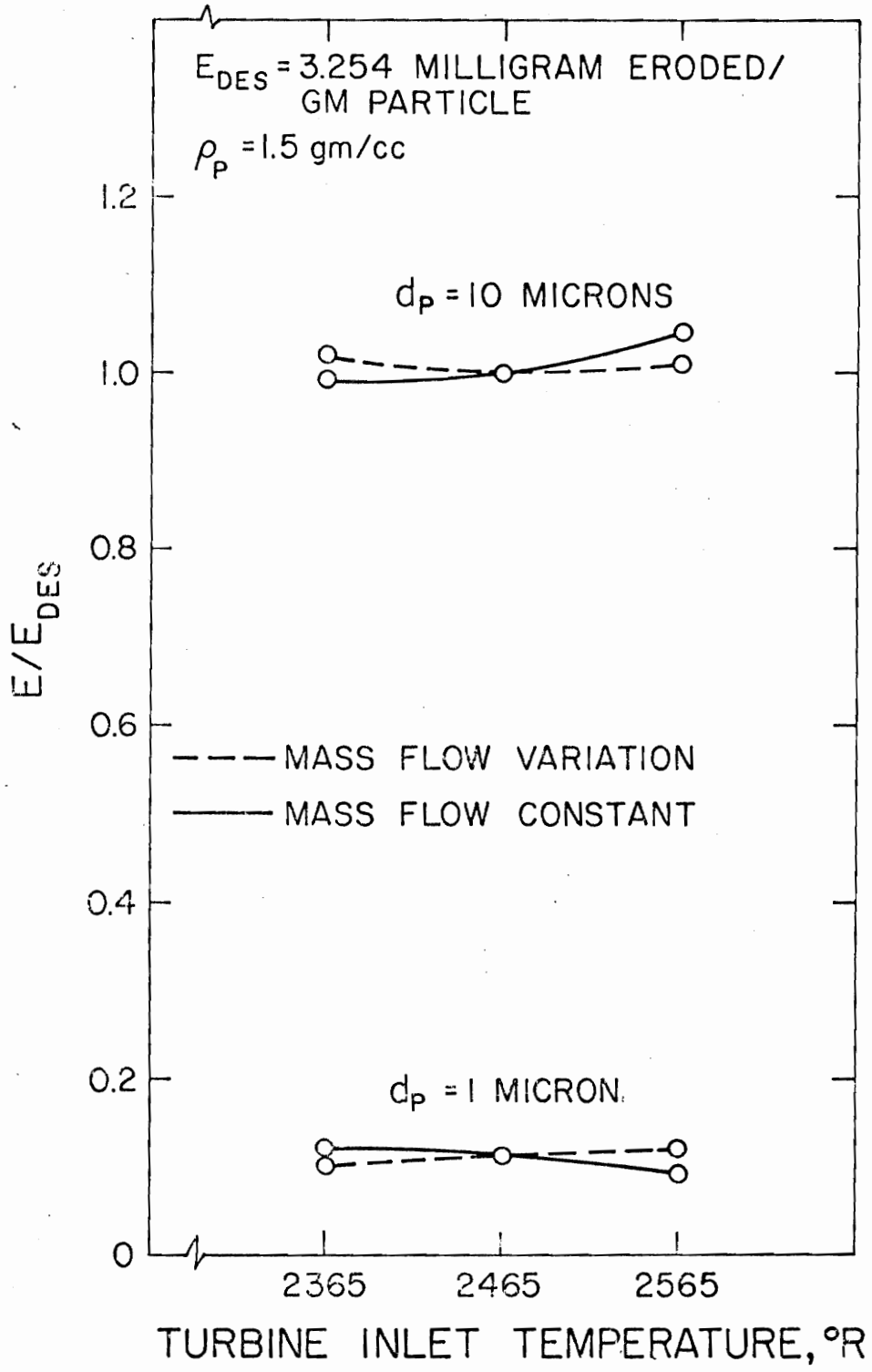

FIG. 11. EROSION RATE OF ROTOR AS A FUNCTION OF INLET STAGNATION TEMPERATURE (BLADE 5)

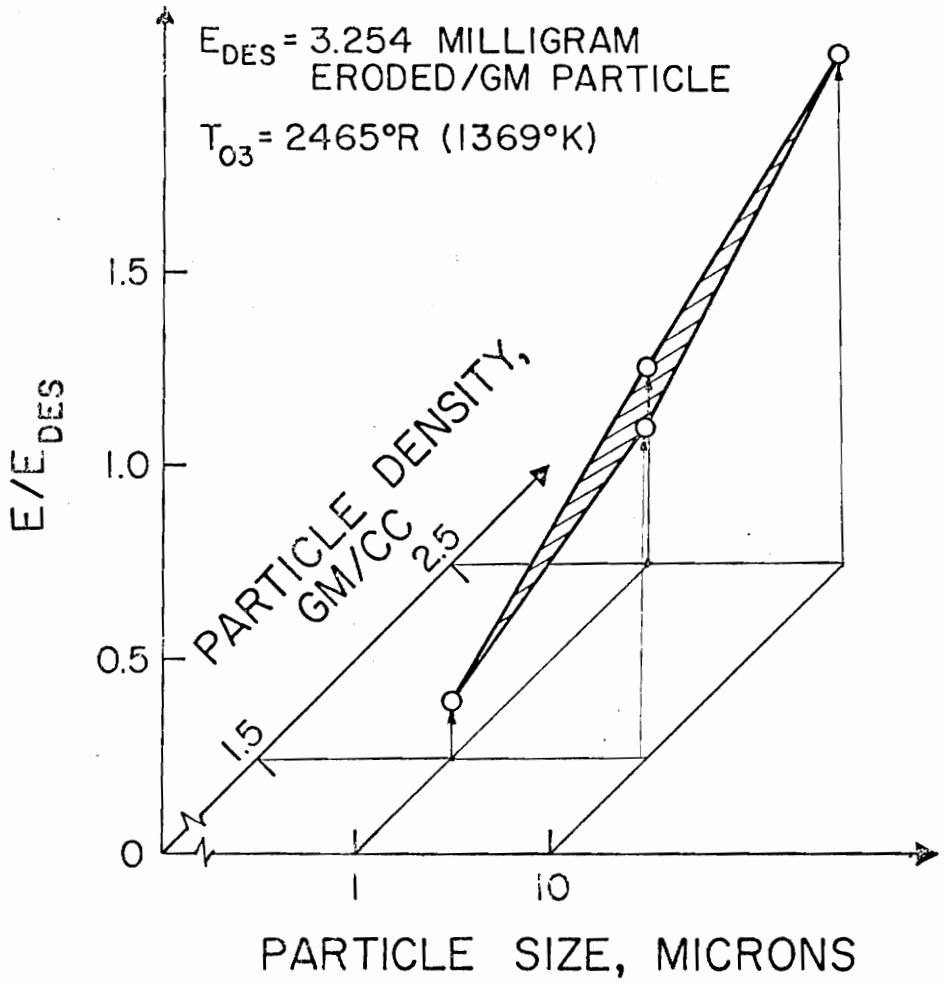

FIG. 12. EROSION RATE OF ROTOR AS A FUNCTION OF PARTICLE SIZE AND DENSITY (BLADE 5)

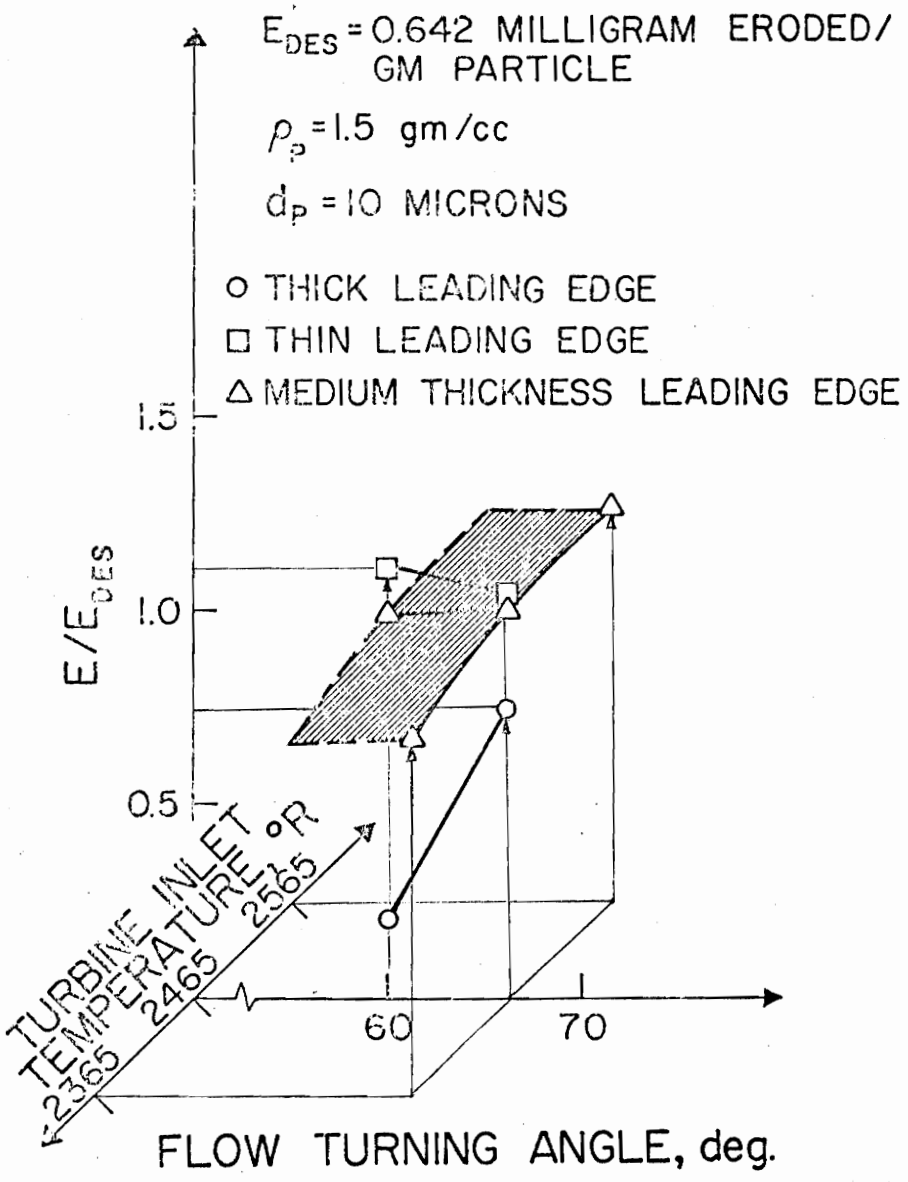

FIG. 13. EROSION RATE OF STATOR AS A FUNCTION OF TURNING ANGLE AND TEMPERATURE

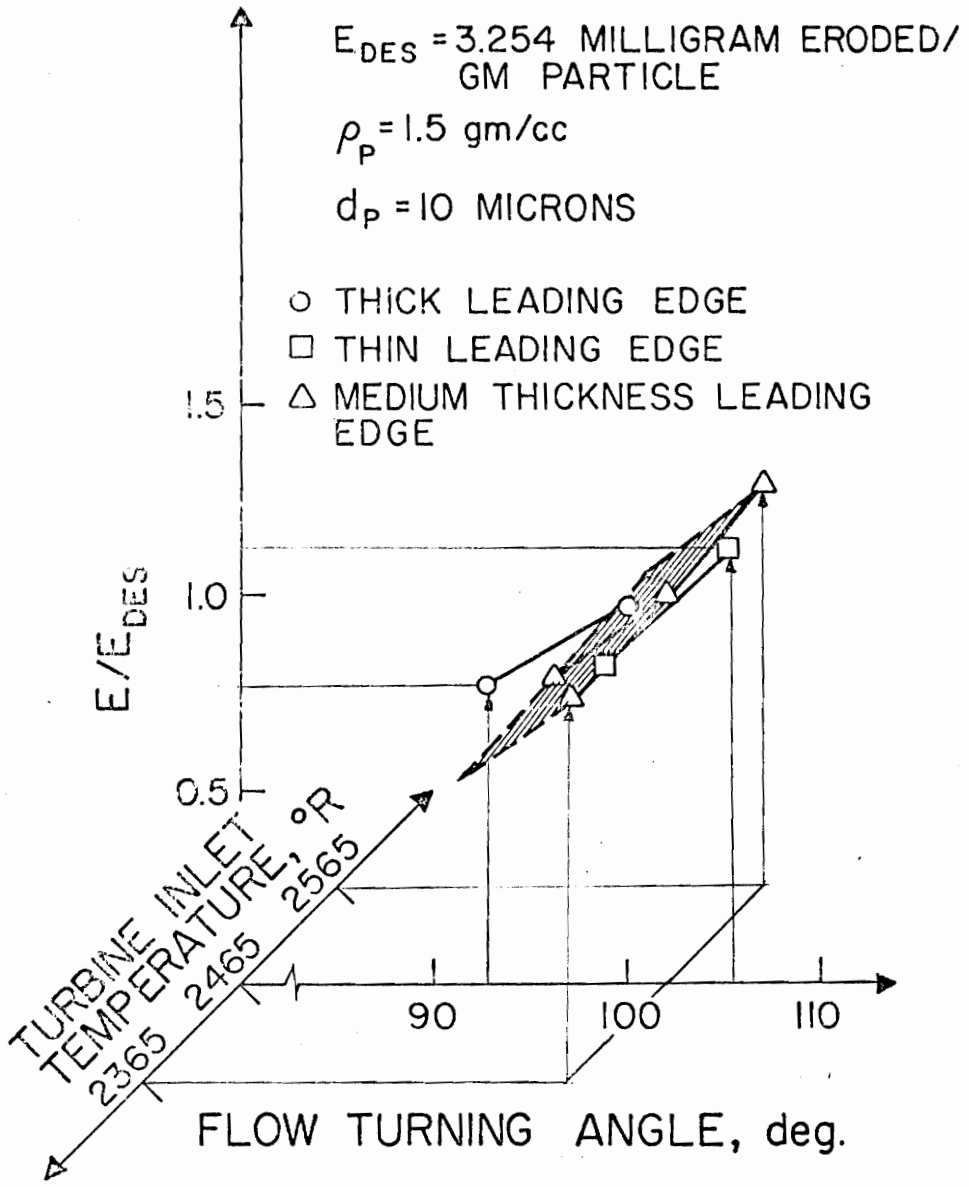

FIG. 14. EROSION RATE OF ROTOR AS A FUNCTION OF TURNING ANGLE AND TEMPERATURE

rotor blades. Dashed lines indicate extrapolated results that have yet to be established. Solid lines indicate results established by this investigation. As can be seen from Figures 13 and 14, large areas have yet to be investigated.

During all of the investigation, several trends were noticed. Maximum erosion rates for the stator blades appeared to be confined to the immediate area around the leading edge and also near the trailing edge on the pressure side of the blades. The leading edges of the stator blades received high impact angles. These angles decreased as the impact positions approached the trailing edges. The rotor blades received a more even distribution of impact angles along the pressure surfaces, yielding a more even distribution of erosion damage. However, predicted erosion damage for both the stator and rotor blades appeared to be confined to the pressure surfaces and the leading edges. Since a rather small number of particles were passed through the blade passages for these initial investigations, the above results are not quantitatively reported. A larger number of particles would determine an erosion distribution that would presumably confirm these results and provide increased detail, but this study was considered beyond the scope of the present investigation.

XII. DISCUSSION OF RESULTS

Stator

The results for the stator blade geometry variation were shown in Figure 7. The particle trajectory plots for these blades appear in Figures C-1 through C-3 and Figures C-7 through C-9. These figures are not consecutive since the figure number corresponds to the blade number. The predicted reduction of total erosion damage for the thick leading edge blades with reduced turning angle is not a surprising result. This trend was expected since fewer particles will impact the surfaces if the turning angle is reduced. However, the increase in erosion damage noticed for the thin leading-edged blades for smaller turning angles was not expected. From the computer results, it was noted that fewer impacts actually took place for the reduced turning angle blades. However, more of the impacts occurred at angles between 20° and 30°, so the total erosion damage was more than the damage received by the high turning angle blade. This trend was noticed for the stator blades with both medium thickness and thin leading edges. The stator blade with the thick leading edges had a noticeable decrease in erosion damage as the turning angle was decreased. This resulted from the thickened leading edge absorbing some of the impacts at high incidence angles. These same particles would have impacted the blade surfaces further back at a lower incidence angle, yielding high erosion damage, had the leading edge not been thickened. Thickening the leading edge also gives the flow larger tangential velocity components

as the flow accelerates around the blade. These larger velocity components in the tangential direction have a tendency to direct the particles away from the blade surface.

The fact that erosion damage was confined to the pressure surfaces and leading edges of the blades is not surprising. Erosion of the suction surfaces has been found to be less than that observed for the pressure surfaces in experiments (27, 28).

The results for the stator blade inlet temperature variations appear in Figure 8 with the corresponding trajectory plots appearing in Figures C-13 through C-17. The fact that turbine inlet temperature variations failed to produce variations in total erosion damage is somewhat surprising. It was expected that reductions in turbine inlet temperature would decrease the relative velocities in the blade passages, thus decreasing erosion rates. Although velocities were reduced, erosion was not. The "variations of mass flow" calculations attempted to discover the effect of varying turbine inlet temperature in similar velocity fields by holding the parameter $w\sqrt{T_{o_3}}$ constant. Velocity fields are similar because decreases in turbine inlet temperatures were associated with increases in mass flow rates. It is possible that the variations were too small to disclose erosion damage variations.

The reduction in predicted erosion damage for small particles and lower densities was expected since these particles have the smallest mass and are more likely to follow the streamlines than larger particles. In this investigation, particles with diameters of 10 microns yielded erosion damage predictions seven times higher than 1 micron particles for both densities tested. The variation

with particle density was also clear. Particles with 2.5 gm/cc densities produced erosion rates nearly twice that produced by 1.5 gm/cc particles.

Rotor

The results for the rotor blade geometry variation are shown in Figure 10 with the trajectory plots appearing in Figures C-4 through C-6 and Figures C-10 through C-12. The major differences noticed between the results found for the stator blades and those found for the rotor blades was that decreases in rotor blade turning angle resulted in predicted reductions of total erosion damage for all leading edge thicknesses. This trend appears reasonable, since particles enter the rotor passages at such high angles that the rotor blade leading edges do not alter their trajectories enough to significantly change the number or angle of impacts. This allows a decrease in turning angle to reduce predicted erosion damage for all leading edge thicknesses. From the computer output, it was noted that several particles did not impact in the low turning angle rotor blades but these same particles impacted the high turning angle blades. This result was noted for all leading edge thicknesses.

The results for the rotor blade turbine inlet temperature variation study are shown in Figure 11 with trajectory plots appearing in Figures C-18 through C-22. The turbine inlet temperature variation results for the rotor blades were similar to those found for the stator blades. Again, larger variations in turbine inlet temperature and mass flow might have yielded larger changes in total erosion damage.

The variations of particle size and density for the rotor blades produced results similar to those for the stator blades. Smaller particles with smaller densities follow streamlines more closely than larger particles do, resulting in fewer impacts and less erosion damage.

XIII. CONCLUSIONS

The following conclusions can be drawn from the parameter study:

1. A decrease in flow turning angle significantly reduced predicted erosion damage for rotor blades subjected to particulates in the flow for all three leading edge thicknesses studied. Decreases in flow turning angles resulted in corresponding decreases in erosion damage for stator blades only with thickened leading edges.

2. Variations of mass flow and turbine inlet temperatures within the range of the study did not substantially alter total erosion damage. This was true for both rotor and stator blades.

3. Decreases in particle size and density resulted in reductions of predicted total erosion damage for both rotor and stator blades.

4. Predicted erosion damage appears to be confined to the pressure surfaces and leading edges of both rotor and stator blades. This conclusion was not quantitatively substantiated since the major emphasis of this investigation was to discover total erosion damage associated with variations of different parameters. A more detailed study is required to determine specific areas of erosion damage.

XIV. RECOMMENDATIONS FOR FUTURE WORK

1. An experimental investigation should be made to determine if the erosion model used is accurate for typical blade materials and flow conditions. This investigation should determine erosion rates due to impact, deposition rates and rebound data for coal ash particles.

2. A parameter study using computer programs that include additional flow effects should be undertaken. The primary additional effects should be radial flows, blade wakes and blade boundary layers.

3. An accurate analytical model should be developed to explain the deposition and corrosion aspects of particulate flow.

4. The existing programs should be modified to calculate blade recession rates. Particle concentration is not a direct input to either erosion program. This parameter should be included.

5. A more realistic erosion model could be developed by using a random number generator to inject different sized particles at different tangential positions. Using this program for several hundred particles would more nearly simulate actual flow.

XV. REFERENCES

1. Mordell, D. L., Conference on Coal Burning Gas Turbines, Proceedings, McGill University, Montreal, Quebec, 1956.

2. Furlong, D. A. and Wade, G. L., "Use of Low Grade Solid Fuels in Gas Turbines", ASME Paper No. 74-WA/Ener-5, 1974.

3. Perry, H., and Jones, J. F., "Electricity from Coal: The Cycles", Mechanical Engineering, November 1953, pp. 32-46.

4. Schiefer, R. B. and Sullivan, D. A., "Low BTU Fuels for Gas Turbines", ASME Paper No. 74-GT-21, 1974.

5. Tilly, G. P., Sage, W., "Military Gas Turbine Sand Ingestion Specifications", ASME Paper No. 69-WA/MET-6, 1969.

6. Amos, D. J., "Energy Conversion Alternatives Study, Westinghouse Phase 1, Volume 4: Open Recuperated and Bottomed Gas Turbine Cycles", Westinghouse Research Laboratories, Pittsburgh, PA, 1976.

7. Brown, D. H., and Shleton, N. E., "Energy Conversion Alternatives Study, General Electric Phase 1, Volume 2: Advanced Energy Conversion Systems, Part 1, Open Cycle Gas Turbines", General Electric Co., 1976.

8. Thomas, D. E., "Energy Conversion Alternatives Study, Westinghouse Phase 1, Volume 2: Materials Considerations", Westinghouse Research Laboratories, Pittsburgh, PA, 1976.

9. Yellot, Y. I., "Progress Report, 1953", The Coal Burning Gas Turbine Locomotive, Locomotive Development Committee of Bituminous Coal Research, Inc., Dunkirk, NY, 1953.

10. Yellot, Y. I., "Annual Report, 1955", The Locomotive Development Committee of Bituminous Coal Research, Inc., Dunkirk, NY, 1955.

11. Tabakoff, W., Hussein, M., "Properties and Particle Trajectories of Gas-Particle Flows in Cascades", Department of Aerospace Engineering, University of Cincinnati, Cincinnati, Ohio, 1972.

12. Tabakoff, W., and Hussein, M., "Effect of Solid Particles on Turbine Performance", ASME Paper No. 75-GT-41, 1975.

13. Menguturk, M., and Sverdrup, E. F., "Tolerance of a Large Electric Utility Turbine to Erosion Damage by Coal Ash Particles", Westinghouse Research and Development Center, Pittsburgh, PA, to be presented to ASTM Symposiym on Erosion, Vail, Colo., October, 1977.

14. Ulke, A. and Rouleau, W. T., "The Effects of Secondary Flows on Turbine Blade Erosion", ASME Paper No. 74-GT-74, 1974.

15. Ulke, A., An Approximate Analysis of the Effect of Secondary Flows on the Motion of Particulates in an Axial Flow Gas Turbine, Ph.D. dissertation, Carnegie Mellon University, 1975.

16. Pfenninger, H., "Coal as a Fuel for Steam and Gas Turbines", Brown Boveri Review, October, November, 1975, pp. 21-33.

17. Warren, T. E. and Roberts, T. L., "Coal-fired Gas Turbines", Mining Society of Nova Scotia, Bulletin, Sept., 1952, pp. 524-531.

18. Morley, W. J., "Brown Coal Ash Deposition in the Open-cycle Gas Turbine", Journal of the Institute of Fuel, May, 1964, pp. 187-200.

19. Wisdom, J. C., "Brown Coal Burning Gas Turbines", The Engineer, Aug. 29, 1958, pp. 328-331.

20. Aeronautical Research Laboratories, "Report of the Interdepartmental Steering Committee, The Coal Burning Gas Turbine Project", Australian Government Publishing Service, Canberra, 1973.

21. Mordell, D. L., "Indirect-fired Gas Turbines", The Engineer, February 1957, pp. 210-213.

22. Mordell, D. L. and Tyndall, K. T., "Test of an Experimental Coal-burning Turbine", Transactions of the ASME, November 1956, pp. 1807-1821.

23. Marks, C. H., Broadly, P. R. and Yellot, Y. I., "Flow Characteristics of Aerated Crushed Coal", ASME Paper No. 55-A-118, 1955.

24. Nabors, W. M., "Feeding Coal to a Gas Turbine-Operation of Star Wheel Coal Feeding System", Combustion, January, 1964, pp. 41-44.

25. Yellot, Y. I., "Annual Report, 1957", The Locomotive Development Committee of Bituminous Coal Research, Inc., Dunkirk, NY, 1957.

26. McGee, J. P. and Corey, R. C., "Bureau of Mines Coal Fired Gas Turbine Research Project", Combustion, April, 1960, pp. 67-72.

27. McGee, J. P. and Corey, R. C., "Redesign and Assembly of Turbine", United States Department of the Interior, Bureau of Mines, Report of Investigations No. 5958, 1962.

28. Cargill, R. W. and Tennyson, W. L., "Coal Fired Gas Turbine Completes Run With New Blades", Power Engineering, May, 1964, pp. 47-48.

29. Smith, J. and Simpson, W. L., "Test of New Turbine Blade Design", United States Department of the Interior, Bureau of Mines, Report of Investigations No. 6920, 1967.

30. Nabors, W. M., "Bureau of Mines Progress in Developing the Coal-burning Gas Turbine Power Plant", Journal of Engineering for Power, April, 1965, pp. 215-221.

31. Smith, J. and McGee, J. P., "Bureau of Mines Progress in Developing Open and Closed-cycle Coal-burning Gas Turbine Power Plants", Journal of Engineering for Power, October, 1966, pp. 313-322.

32. McGee, J. P. and Smith, J., "Turbine Blade Wear by Coal Ash in Working Fluid at 1200°F", United States Department of the Interior, Bureau of Mines, Report of Investigations No. 7255, 1969.

33. Strimbeck, D. C., "Test of Combustor and Ash Separators for Open Cycle Plant", United States Department of the Interior, Bureau of Mines, Report of Investigations No. 7295, 1969.

34. Joseph, J., "Union Pacific's Coal-burning Gas Turbine-Electric Locomotive", Diesel and Gas Engine Progress, Apr., 1963, pp. 56-57.

35. Morris, R. I., "New Developments in Coal are Leading to New Developments in Coal Fired Gas Turbine", Railway Age, Aug. 5, 1957, pp. 20-23.

36. Grant, G. and Tabakoff, W., "Erosion Prediction in Turbomachinery Due to Environmental Solid Particles", AIAA Paper No. 74-16, 1974.

37. Grant, G. and Tabakoff, W., "An Experimental Study of Certain Aerodynamic Effects on Erosion", Department of Aerospace Engineering, University of Cincinnati, Cincinnati, Ohio, 1972.

38. Hussein, M. F. and Tabakoff, W., "Dynamics and Erosion Study of Solid Particles in a Cascade", Department of Aerospace Engineering, University of Cincinnati, Cincinnati, Ohio, 1971.

39. Tabkoff, W. and Hussein, M., "An Experimental Study of the Effect of Solid Particles on the Pressure at Blade Surfaces in Cascades", Project Themis Report No. 70-9, Department of Aerospace Engineering, University of Cincinnati, Cincinnati, Ohio, 1970.

40. Katsanis, T., "Computer Program for Calculating Velocities and Streamlines on a Blade-to-Blade Surface of a Turbomachine", NASA TN D-4525, Lewis Research Center, 1969.

41. Hussein, M., The Dynamic Characteristics of Solid Particulates in Rotating Turbomachinery", Ph.D. Dissertation, University of Cincinnati, 1972.

42. Hussein, M. F., and Tabakoff, W., "Three Dimensional Dynamic Characteristics of Solid Particles Suspended by Polluted Air Flow in a Turbine Stage", AIAA Paper No. 73-140, 1973.

43. Clevenger, W. B., and Tabakoff, W., "Erosion in Radial Inflow Turbines - Volume I: Erosive Particle Trajectory Similarity" NASA CR-134589, Lewis Research Center, 1974.

44. Clevenger, W. B., and Tabakoff, W., "Erosion in Radial Inflow Turbines - Volume II: Balance of Centrifugal and Radial Drag Forces on Erosive Particles", NASA CR-134616, Lewis Research Center, 1974.

45. Clevenger, W. B., and Tabakoff, W., "Erosion in Radial Inflow Turbines - Volume III: Trajectories of Erosive Particles in Radial Inflow Turbines", NASA CR-134700, Lewis Research Center, 1974.

46. Clevenger, W. B., and Tabakoff, W., "Erosion in Radial Inflow Turbines - Volume IV: Erosion Rates on Internal Surfaces", NASA CR-134677, Lewis Research Center, 1974.

47. Clevenger, W. B., and Tabakoff, W., "Erosion in Radial Inflow Turbines - Volume V: Computer Programs for Tracing Particle Trajectories", NASA CR-134787, Lewis Research Center, 1975.

48. Bitter, J. G. A., "A Study of Erosion Phenomena", Part I, Wear, June, 1965, pp. 5-21.

49. Bitter, J. G. A., "A Study of Erosion Phenomena", Part II, Wear, June, 1965, pp. 169-190.

50. Finnie, I., "An Experimental Study of Erosion", S.E.S.A. Proceedings, Vol. XVII, No. 2, February, 1960, pp. 65-70.

51. Finnie, I., "Erosion of Surfaces by Solid Particles", Wear, Vol. 3, 1960, pp. 87-103.

52. Sheldon, G. L. and Finnie, I., "The Mechanism of Material Removal in the Erosive Cutting of Brittle Materials", ASME Paper No. 65-WA/PROD-8, 1965.

53. Brasinikas, G., "Erosion by Particle Impact - Experiments with Callide Coal Ash", Australian Defense Scientific Service, Aeronautical Research Laboratories, Canberra, Australia, 1970.

54. United States Energy Research and Development Administration, "Coal Gasification", Energy Research and Development Administration Quarterly Report, Fall, 1975, pp. 60-61.

55. Smeltzer, C. E. and Sage, P. L., "Mechanisms of Metal Removal by Impacting Dust Particles", Transactions of the ASME, Journal of Basic Engineering, Sept. 1970, pp. 639-54.

56. Cohen, H., Rogers, G. F. C., Saravanamutto, H. I. H., Gas Turbine Theory, Second Edition, Halsted Press, John Wiley, New York, 1974.

XVI. APPENDICES

APPENDIX A. COMPUTER PROGRAMS

The input listings, symbol definitions and changes made to the original programs are described below. The programs were originally written for use on a UNIVAC computing system. Changes were necessary for compatibility with the available IBM 370 system. The actual programs are proprietary to Westinghouse Electric Corporation and are not listed here. Initial results have been presented in Reference 13.

Input Parameters

The following sections list the input parameters for the three programs used in the investigation. Since some modifications have been made to the particle trajectory program input listings, the complete formats and card numbers will be included with the input listings for these programs. The changes made to the modified Katsanis program yielded an input listing nearly identical to the published version (40).

The units for all of the programs must be consistent. Throughout the investigation, the English system of units was used for input data because of the program requirements.

Modified Katsanis Input Information

(Taken from Reference 40)

GAM	specific-heat ratio
AR	gas constant
TIP	inlet stagnation temperature

RHOIP	inlet stagnation density
WTFL	mass flow per blade for stream channel
OMEGA	rotational speed
ORF	value of overrelaxation factor to be used in the solution of the inner iteration simultaneous equations
BETAI	inlet flow angle with respect to m-direction, deg.
BETAO	outlet flow angle with respect to m-direction, deg.
CHORDF	overall length of blade in m-direction
STGRF	angular θ-coordinate for center of trailing-edge circle of blade with respect to the center of leading-edge circle, radians
REDFAC	factor by which weight flow (WTFL) must be reduced in order to assume subsonic flow throughout passage
DENTOL	tolerance on density change per iteration for reduced weight flow
CUTOFF	per-cent chord for normal successive overrelaxation solution
MBI	number of vertical mesh lines from blade passage entrance to leading edge of blade
MBO	number of vertical mesh lines from blade passage entrance to trailing edge of blade
MM	total number of vertical mesh lines in m-direction, maximum of 100
NBBI	total number of mesh spaces in θ-direction, maximum of 50
NBL	number of blades
NRSP	number of spline points for stream-channel radius (RMSP) and thickness (BESP) coordinates, maximum of 50
RI1, RI2	leading-edge radii of the two blade surfaces
RO1, RO2	trailing-edge radii of the two blade surfaces
BETI1, BETI2	angles (with respect to m-direction) at tangent points of trailing-edge radii with two blade surfaces, deg.

SPLN01, SPLN02	number of blade spline points given for each surface as input, maximum of 50
MSP1, MSP2	arrays of m-coordinates of spline on the two blade surfaces, measured from blade leading edge
THSP1, THSP2	arrays of θ-coordinates of spline points corresponding to MSP1 and MSP2, radians
MR	array of m-coordinates of spline points for the stream-channel radii and stream-channel thickness
RMSP	array of r-coordinates of spline points for the stream-channel radii, corresponding to the MR array
BESP	array of stream channel normal thickness corresponding to the MR and RMSP arrays

A geometric description of these parameters is shown in Figure A-1.

Modified Katsanis Output Variables

BLDAT	all geometric information which does not change from iteration to iteration
AANDK	coefficient array, constant vector, and indexes of all adjacent points for each point in finite difference mesh
ERSOR	maximum change in stream function at any point for each iteration of successive overrelaxation equation
STRFN	value of stream function of each unknown mesh point in region
SLCRD	stream line θ-coordinates of each unknown mesh point in region
INTVL	velocity and flow angle at each interior mesh point for both reduced and actual weight flow
SURVL	m-coordinate, surface velocity, flow angle, distance along surface and W/Wcr based on meridional velocity components

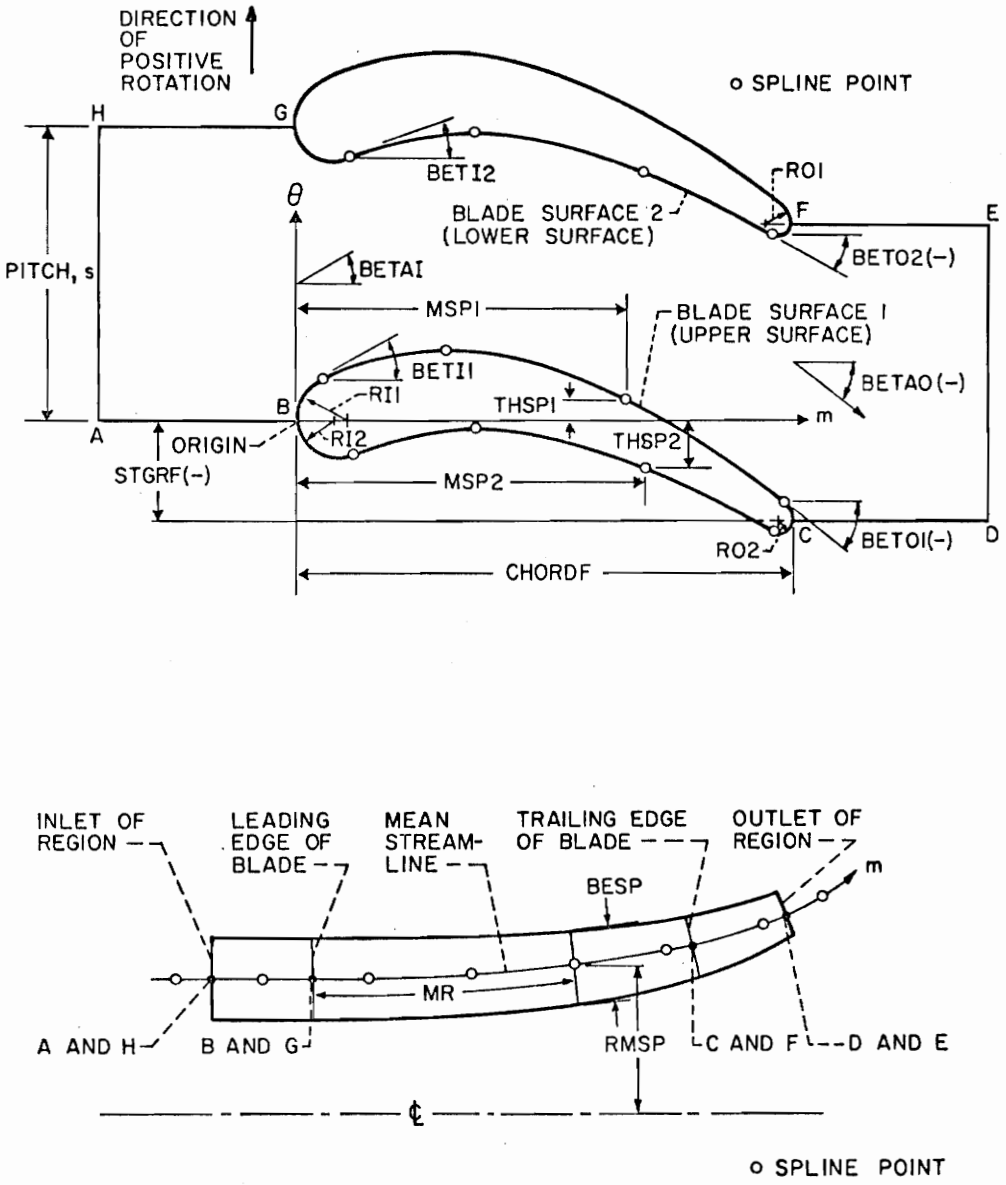

FIG. A-1. DESCRIPTION OF BLADE CHANNEL GEOMETRY (as taken from Reference 40)

The output parameters have values of 1, 2 or 3 depending on the following:

OUTPUT = 1 final iteration printout

OUTPUT = 2 first and final interation printout

OUTPUT = 3 all iteration printout

ICONT	trailing edge m-direction mesh line
JFLOW	dummy variable due to changes in program
NLAST	cutoff m-direction mesh line
JOUT	output parameter, JOUT≠1 generates punched output for particle trajectory programs
JGRAPH	JGRAPH≠2 generates surface velocity profiles

Single-Row Particle Trajectory Program Input Variables

NDATA	number of particle trajectories + 1
INTEG	integration method, set INTEG=2
NINT	initial step size, set NINT=20
NDEP	deposition factor, set NDEP=1
FACT	plotting scale factor
SCAL	scale factor of turbine
DPART	particle diameter, microns
RHOP	particle density, gm/cm^3
TINCR	time increment, usually 0.5×10^{-5} for 10μ particles and 0.5×10^{-4} for 1μ particles
X	initial X-position
THETA	initial θ-position
Z	initial Z-position

VPART	initial particle velocity
BETPAR	initial particle trajectory angle in X-θ plane
ALPHAP	initial particle trajectory angle in Z-X plane

Single-Row Particle Trajectory Program Output Variables

INP	INP=0 no printing of input data
	INP=1 print input data
IPLOT	IPLOT=0 no plotting of particle trajectories
	IPLOT=1 plot particle trajectories
IMACH	IMACH=0 no printing of particle history
	IMACH=1 print particle history
	IMACH=7 print RE, G, X, time
ISW	ISW=1 use program plot routine
	ISW=2 use calcomp plot routines

Single-Row Particle Trajectory Program Data Set Listing

Card 1 FORMAT 16I5
INP, IPLOT, IMACH, NDATA, INTEG, NINT

Card 2 FORMAT 16I5
NDEP, ISW

Card 3 FORMAT 8F10.4
FACT, SCAL

DATA SET FROM MODIFIED KATSANIS PROGRAM

Card 4 FORMAT 8F10.4
DPART, RHOP, TINCR

Card 5 FORMAT 8F10.4
X, THETA, Z, VPART, BETAP, ALPHAP

Go back to Card 4 for NRUNS + 1 trajectories, last trajectory is a dummy.

Single-Stage Particle Trajectory Program Input Variables

DSR	gap size between stator and rotor
SSK	scale factor of turbine
FACT	plot scale factor
ISUR	erosion index ISUR=1 erosion per unit axial length ISUR=2 erosion per unit surface length
NRUNS	number of particled trajectories in stator, last trajectory is a dummy set
NDEP	deposition factor, set NDEP=1
NINT	initial integration step, set NINT=20
NDATA	number of particle trajectories in rotor + 2, last trajectory is a dummy set
DPART	particle diameter
RHOP	particle density
TINCR	initial time increment, set TINCR between $.5 \times 10^{-4}$ and $.5 \times 10^{-5}$ depending on particle size
X	initial X-position of particle
THETA	initial θ-position of particle
Z	initial Z-position of particle
VPART	initial particle velocity
BETAP	initial particle flow angle in X-θ plane
ALPHAP	initial particle flow angle in X-Z plane

Single-Stage Particle Trajectory Program Output Variables

INP	INP=0 no printing of gas properties INP=1 print gas properties
IEROS	IEROS=0 no printing of erosion rates IEROS=1 print erosion rates
IPLOT	IPLOT=0 no plotting of trajectories IPLOT=1 plot particle trajectories
IPRINT	IPRINT =0 no printing of particle histories IPRINT=1 print particle histories

Single-Stage Particle Trajectory Program Data Set Listing

Card 1 FORMAT 3F10.4, I5
DSR, SSK, FACT, NRUNS

Card 2 FORMAT 16I5
IPRINT, IEROS, ISUR, INP, IPLOT, NDATA, NDEP, NINT

STATOR BLADE DATA SET FROM MODIFIED KATSANIS PROGRAM

Card 3 FORMAT 8F10.4
DPART, RHOP, TINCR

Card 4 FORMAT 8F10.4
X, THETA, Z, VPART, BETPAR, ALPHAP

ROTOR BLADE DATA SET FROM MODIFIED KATSANIS PROGRAM

Card 5 FORMAT 8F10.4
TINCR, THETA

Repeat Card 5 for rotor trajectories until NDATA + 1.

Repeat Cards 2-5 (including stator and rotor blade data sets) until NRUNS + 1.

Modifications Made to Original Programs

The original programs developed by Menguturk and Sverdrup were structured for a UNIVAC computer. Several modifications were made to them for compatibility with the available IBM 370 computing system used in this investigation. Most of these changes were minor and are described below.

The modified Katsanis program had extensive modifications made to the main program. The original program could compute external as well as internal (blade passage) flows. In order for the program to calculate more than one data set per run, the external flow field calculating cabability was removed. In addition to this, subroutine E7ES was removed because it was never used. The original plotting routines were changed so that they could be run on the IBM 370 system. Several format statements were changed because of truncation errors. Finally, SK (turbine scale factor) was set equal to 1.0 internally. ITEST (indice for call to subroutine E7ES) was internally set equal to 0.

The single-row particle trajectory program had several modifications made. The main changes incorporated in this program were in its conversion to double precision. All of the functions (sin, cos, etc. . .) had to be changed as well as several subroutine names. This conversion to double precision was necessary to obtain the required program accuracy. Changes were made in the graphing subroutines because some of the Calcomp plotting routines did not coincide. Other minor changes include format statement changes to accept the modified Katsanis program data sets and input headings were omitted.

The single-stage particle trajectory program modifications were identical to those of the single-row particle trajectory program because of their similarity. The graphing subroutine in the single-stage program was modified because of difficulties encountered in conversion to the IBM 370 system. The program in its current form plots particle trajectories in the top view only.

APPENDIX B. BLADE PROFILE VARIATION ANALYSIS

Objectives

One of the main parameters investigated in the particle erosion programs were blade profile variations. These variations were made by altering the basic blade shapes found in the first turbine stage of a large industrial gas turbine engine. The two major variations studied for both rotor and stator blades were blade leading edge thickness and blade turning angle.

The new blade leading edge thicknesses were chosen somewhat arbitrarily. Extreme changes of the existing blade shapes were avoided. The stator blades tested in the erosion programs had much larger variations in leading edge thicknesses than the rotor blades because of difficulties in obtaining valid flow fields from the modified Katsanis program for the rotor blades. In reality, only moderate changes in leading edge thickness could be tolerated so the changes to the rotor blades are perhaps more realistic. Significant changes in leading edge thickness could cause flow separations and viscous losses that the Katsanis program would not predict.

The effects of blade turning angle are clarified by calculating the stage work associated with various combinations of turning angles. The Euler turbine equation (from Reference 56) can be used to estimate the stage work. This equation is:

$$W_{ST} = U_T^2 \left[\frac{Ca_3}{U_T} \left(\text{Tan } \alpha_3 + \text{Tan } \beta_4 \right) - 1 \right] \qquad (18)$$

where W_{ST} = turbine stage work

U_T = tangential rotational velocity

Ca_3 = axial absolute velocity

α_3 = flow angle at stator exit

β_4 = relative flow angle at rotor exit.

The original first stage blades had $\alpha_3 = 66.7°$ and $\beta_4 = 54.1°$. These blades were designated as having large turning angles. The modified blades had these angles reduced to 60° and 48°, respectively. These blades were designated as having small turning angles.

The actual stage work variations for the six rotor blades investigated can be determined from Equation 18 using the rotor blade geometric inlet and outlet flow angles. The results below show the stage work variations with respect to the Blade 5 (reference blade) stage work.

Blade	$W_{ST}/W_{ST_{Blade\ 5}}$
4	0.94
5	1.0
6	1.04
10	0.77
11	0.84
12	0.89

Throughout the investigation, the total number of stator blades (48) and rotor blades (95) remained the same. In addition, the turbine rotational speed remained constant at 3600 rev./min. The chords of all stator blades and all rotor blades remained the same as the reference blades.

Blade Coordinates

The following tables list the X and Y coordinates for the twelve blade shapes used in the investigation. Also included are figures describing the blade profiles. The Katsanis program uses a cubic spline curve fitting routine to interpolate between the blade coordinates.

TABLE B-1.

COORDINATES OF FIRST STAGE STATOR BLADE SURFACES
THICK LEADING EDGE, HIGH TURNING ANGLE (BLADE 1)

(Radius = 2.718 ft.)

X, ft.	Convex Y, ft.	Concave Y, ft.
.04078	-.02443	.04999
.08157	-.02655	.06416
.12236	-.01960	.08334
.16314	-.00272	.10827
.20393	.02672	.14167
.24335	.07085	.18332
.28278	.13131	.22907
.32222	.20551	.28575
.36163	.29076	.34642

Center of Convex Leading Edge Circle; X = .018908 ft., Y = 0.0000

Radius of Convex Leading Edge Circle = .018908 ft.

Center of Concave Leading Edge Circle; X = .05105 ft., Y = 0.0000

Radius of Concave Leading Edge Circle = .05105 ft.

Center of Trailing Edge Circle; X = .39446 ft., Y = .39456 ft.

Radius of Trailing Edge Circle = .006583 ft.

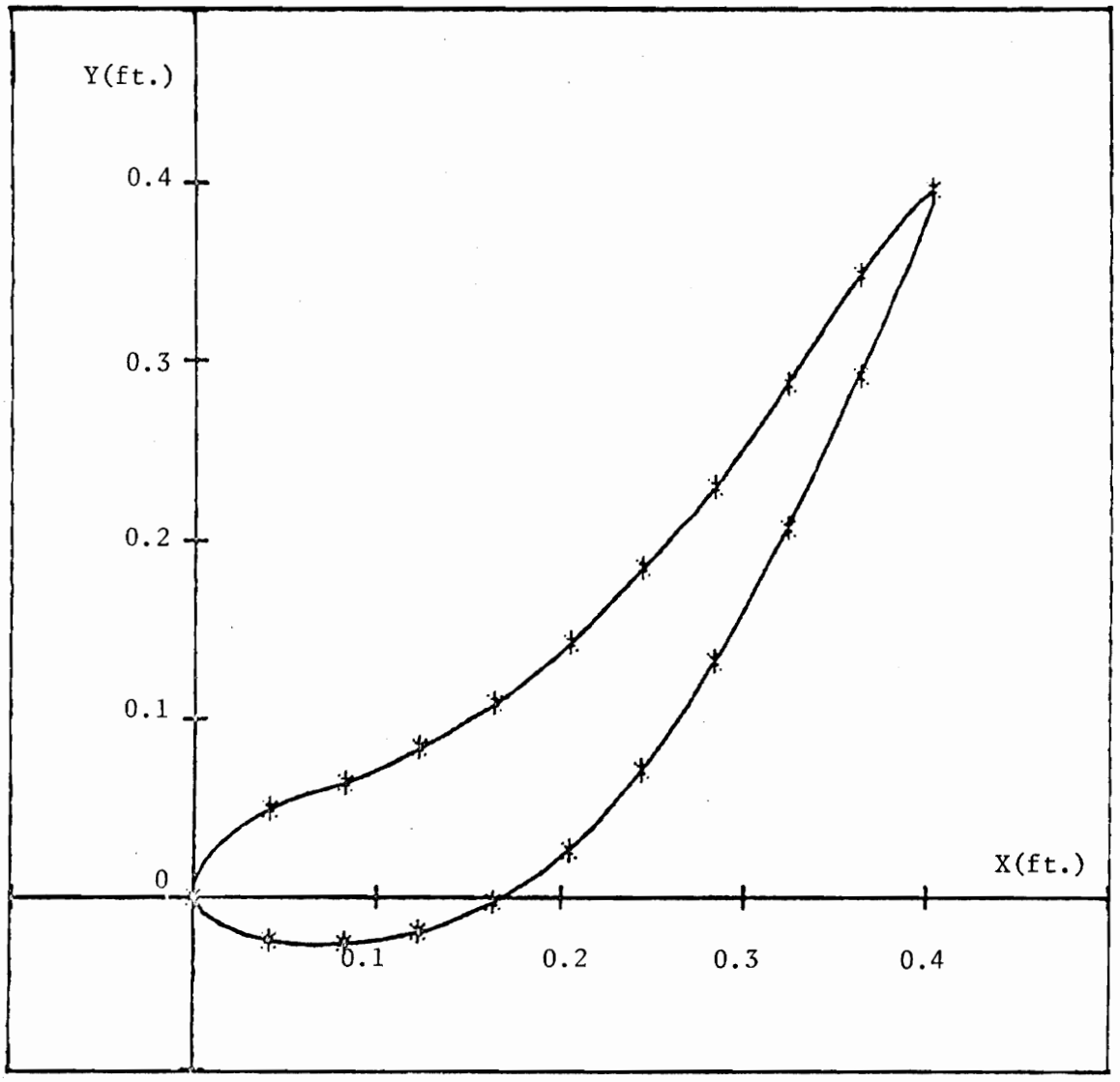

FIG. B-1. CROSS-SECTION OF BLADE 1

TABLE B-2.

COORDINATES OF FIRST STAGE STATOR BLADE SURFACES
MEDIUM THICKNESS LEADING EDGE, HIGH TURNING ANGLE (BLADE 2)

(Radius = 2.718 ft.)

X, ft.	Y, ft. Convex	Y, ft. Concave
.04078	-.02443	.02500
.08157	-.02665	.04536
.12236	-.01960	.06803
.16314	-.00272	.09693
.20393	.02672	.13492
.24335	.07085	.17896
.28278	.13131	.22907
.32222	.20551	.28576
.36163	.29076	.34642

Center of Leading Edge Circle; X = .0018908 ft.,
Y = 0.0000

Radius of Leading Edge Circle = .0018908 ft.

Center of Trailing Edge Circle; X = .39446 ft.,
Y = .39456 ft.

Radius of Trailing Edge Circle = .006583 ft.

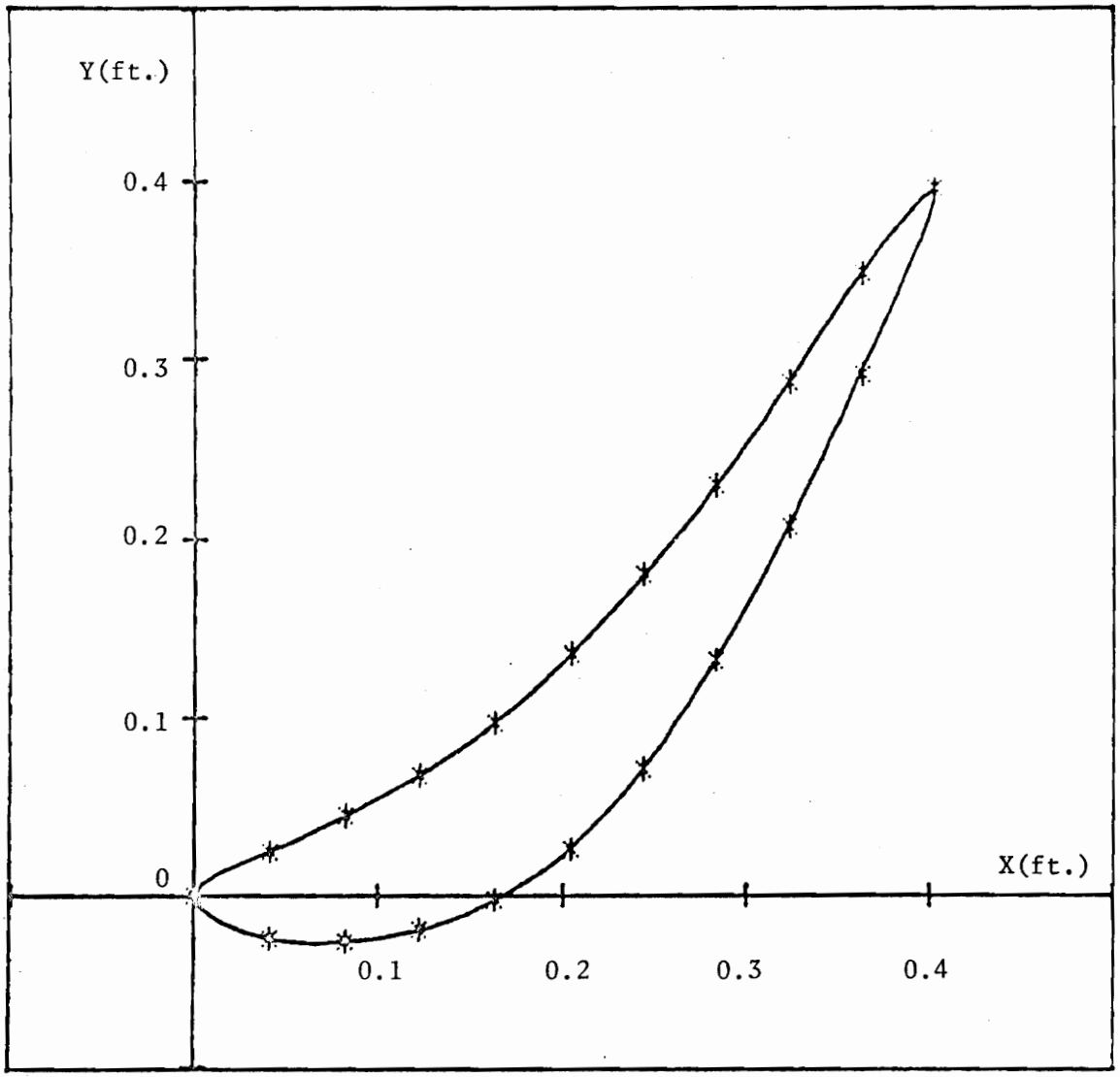

FIG. B-2. CROSS-SECTION OF BLADE 2

TABLE B-3.

COORDINATES OF FIRST STAGE STATOR BLADE SURFACES
THIN LEADING EDGE, HIGH TURNING ANGLE (BLADE 3)

(Radius = 2.718 ft.)

X, ft.	Convex Y, ft.	Concave Y, ft.
.04078	-.02443	.01416
.08157	-.02665	.02499
.12236	-.01960	.04999
.16314	-.00272	.08165
.20393	.02672	.11666
.24335	.07085	.16667
.28278	.13131	.21666
.32222	.20551	.28539
.36163	.29076	.34498

Center of Convex Leading Edge Circle; X = .018908 ft., Y = 0.0000

Radius of Convex Leading Edge Circle = .018908 ft.

Center of Concave Leading Edge Circle; X = .008334 ft., Y = 0.0000

Radius of Concave Leading Edge Circles = .008334 ft.

Center of Trailing Edge Circle; X = .39446 ft., Y = .39456 ft.

Radius of Trailing Edge Circle = .006583 ft.

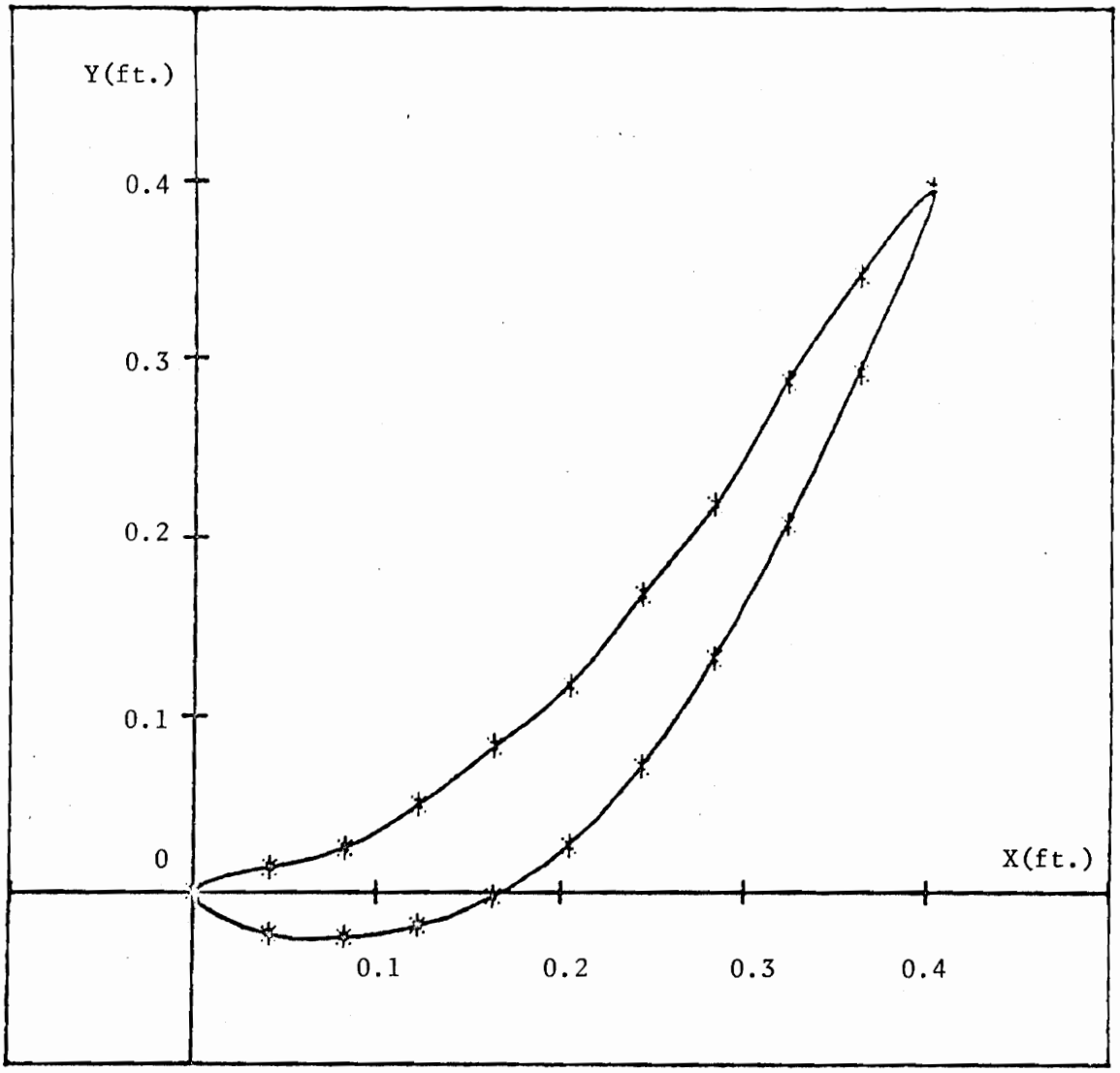

FIG B-3. CROSS-SECTION OF BLADE 3

TABLE B-4.

COORDINATES OF FIRST STAGE ROTOR BLADE SURFACES
THICK LEADING EDGE, HIGH TURNING ANGLE (BLADE 4)

(Radius = 2.702 ft.)

X, ft.	Convex Y, ft.	Concave Y, ft.
.02819	.03646	-.00292
.05638	.05303	.00254
.08458	.05997	.00217
.11277	.05916	-.00208
.14097	.05178	-.00998
.17220	.03589	-.02303
.20334	.01097	-.04194
.23466	-.02405	-.06411
.26589	-.06614	-.09327

Center of Leading Edge Circle; X = .007916 ft.,
Y = 0.0000

Radius of Leading Edge Circle = .007916 ft.

Center of Trailing Edge Circle; X = .29294 ft.,
Y = -.11682 ft.

Radius of Trailing Edge Circle = .004058 ft.

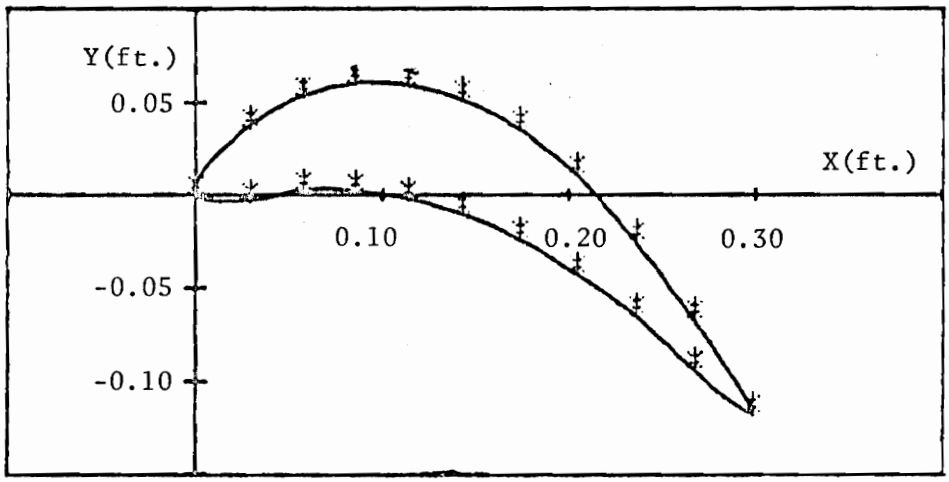

FIG. B-4. CROSS-SECTION OF BLADE 4

TABLE B-5.

COORDINATES OF FIRST STAGE ROTOR BLADE SURFACES
MEDIUM THICKNESS LEADING EDGE, HIGH TURNING ANGLE (BLADE 5)

(Radius = 2.702 ft.)

X, ft.	Convex Y, ft.	Concave Y, ft.
.02819	.03646	-.00219
.05638	.05303	.00265
.08458	.05997	.00241
.11277	.05916	-.00192
.14097	.05178	-.00994
.17220	.03589	-.02302
.20334	.01097	-.04113
.23466	-.02405	-.06411
.26589	-.06614	-.09327

Center of Leading Edge Circle; X = .007916 ft.,
Y = 0.0000

Radius of Leading Edge Circle = .007916 ft.

Center of Trailing Edge Circle; X = .29294 ft.,
Y = -.11682 ft.

Radius of Trailing Edge Circle = .004058 ft.

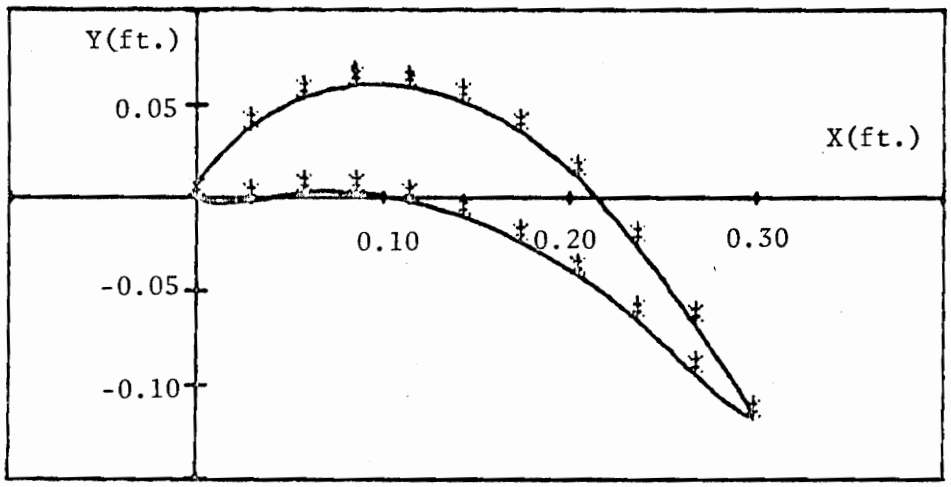

FIG. B-5. CROSS-SECTION OF BLADE 5

TABLE B-6.

COORDINATES OF FIRST STAGE ROTOR BLADE SURFACES
THIN LEADING EDGE, HIGH TURNING ANGLE (BLADE 6)

(Radius = 2.702 ft.)

X, ft.	Convex Y, ft.	Concave Y, ft.
.02819	.03646	-.00167
.05638	.05303	.00265
.08458	.05997	.00266
.11277	.05916	-.00175
.14097	.05178	-.00983
.17220	.03589	-.02302
.20334	.01097	-.04113
.23466	-.02405	-.06411
.26589	-.06614	-.09327

Center of Leading Edge Circle; X = .007916 ft.,
Y = 0.0000

Radius of Leading Edge Circle = .007916 ft.

Center of Trailing Edge Circle; X = .29294 ft.,
Y = -.11682 ft.

Radius of Trailing Edge Circle = .004058 ft.

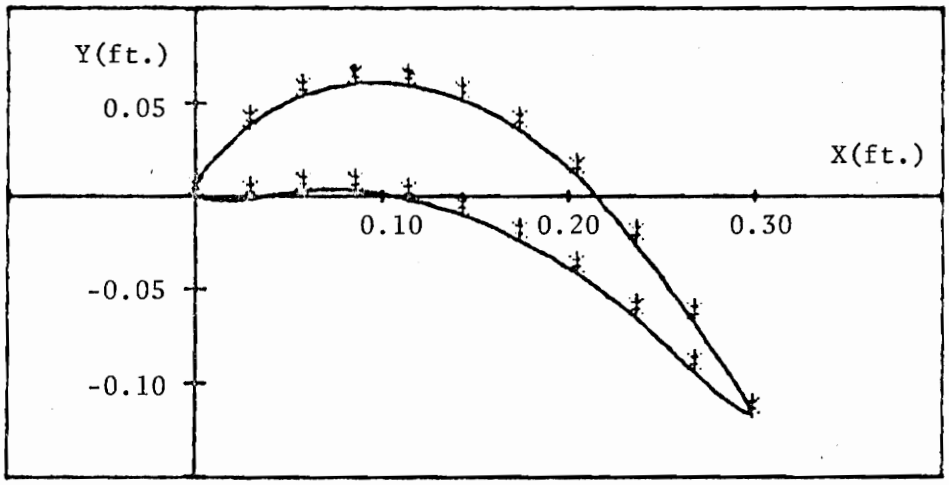

FIG. B-6. CROSS-SECTION OF BLADE 6

TABLE B-7.

COORDINATES OF FIRST STAGE STATOR BLADE SURFACES
THICK LEADING EDGE, SMALL TURNING ANGLE (BLADE 7)

(Radius = 2.718 ft.)

X, ft.	Convex Y, ft.	Concave Y, ft.
.04078	-.02416	.04999
.08157	-.02667	.05834
.12236	-.01916	.07504
.16314	-.00334	.10332
.20393	.02498	.13355
.24335	.06669	.16666
.28278	.11764	.20241
.32222	.19231	.25660
.36163	.26074	.30589

Center of Convex Leading Edge Circle; X = .018908 ft., Y = 0.0000

Radius of Convex Leading Edge Circle = .018908 ft.

Center of Concave Leading Edge Circle; X = .05105 ft., Y = 0.0000

Radius of Concave Leading Edge Circle = .05105 ft.

Center of Trailing Edge Circle; X = .394457 ft., Y = .35394 ft.

Radius of Trailing Edge Circle = .006583 ft.

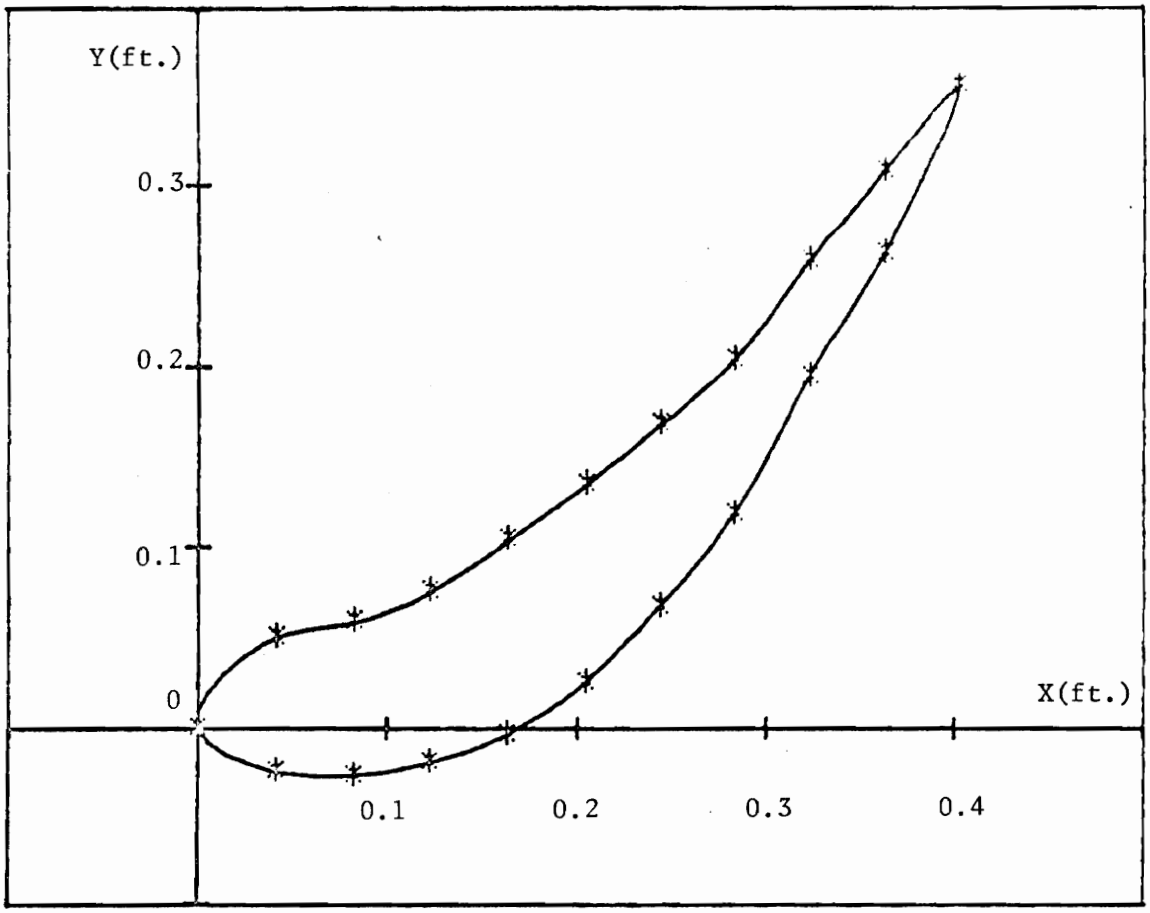

FIG. B-7. CROSS-SECTION OF BLADE 7

TABLE B-8.

COORDINATES OF FIRST STAGE STATOR BLADE SURFACES
MEDIUM THICKNESS LEADING EDGE, LOW TURNING ANGLE (BLADE 8)

(Radius = 2.718 ft.)

X, ft.	Convex Y, ft.	Concave Y, ft.
.04078	-.02416	.02500
.08157	-.02667	.04167
.12236	-.01916	.06503
.16314	-.00334	.09831
.20393	.02498	.13103
.24335	.06669	.17082
.28278	.11764	.20242
.32222	.19231	.25660
.36163	.26074	.30589

Center of Leading Edge Circle; X = .018908 ft.,
Y = 0.0000

Radius of Leading Edge Circle = .018908 ft.

Center of Trailing Edge Circle; X = .394457 ft.,
Y = .35394 ft.

Radius of Trailing Edge Circle = .006583 ft.

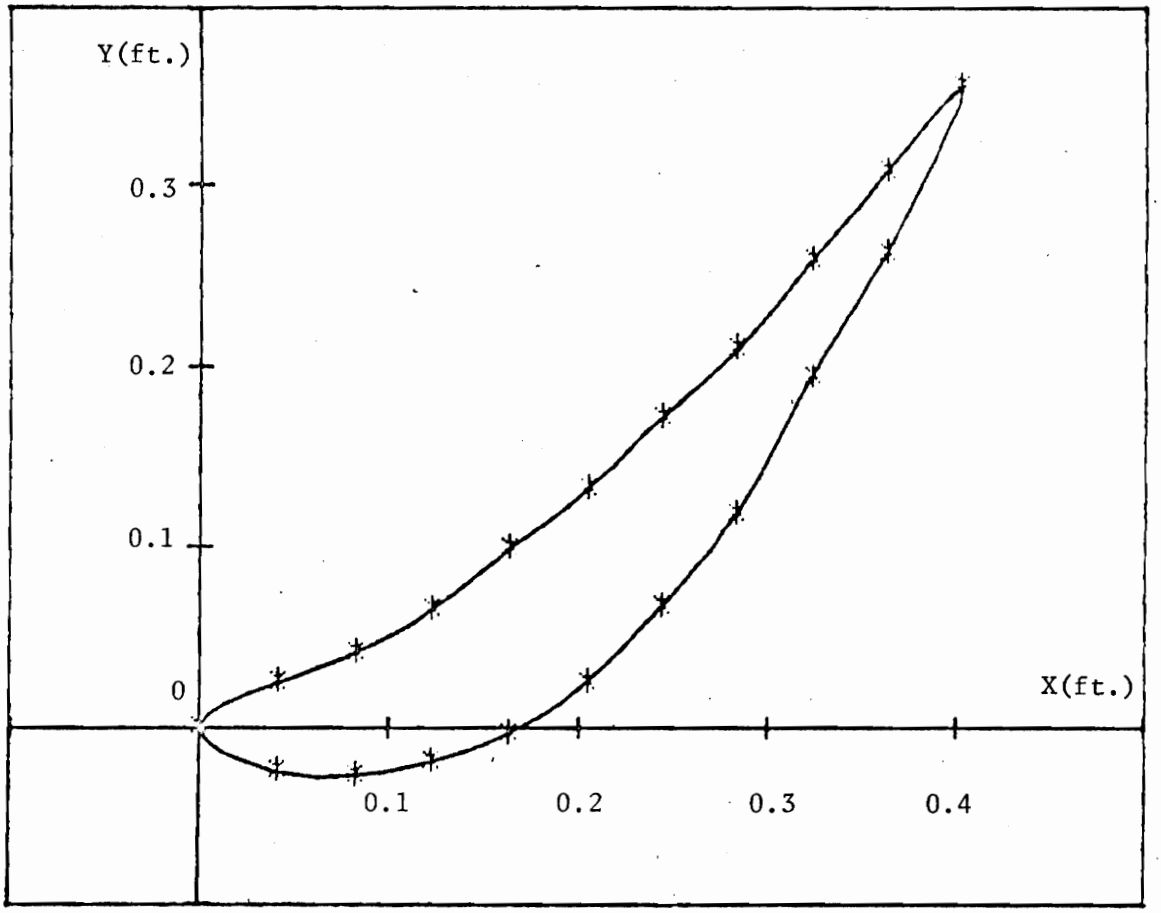

FIG. B-8. CROSS-SECTION OF BLADE 8

TABLE B-9

COORDINATES OF FIRST STAGE STATOR BLADE SURFACES
THIN LEADING EDGE, SMALL TURNING ANGLE (BLADE 9)

(Radius = 2.718 ft.)

X, ft.	Y, ft. Convex	Y, ft. Concave
.04078	-.02416	.01666
.08157	-.02667	.03082
.12236	-.01916	.06000
.16314	-.00334	.09583
.20393	.02498	.13019
.24335	.06669	.17082
.28278	.11764	.20241
.32222	.19231	.25660
.36163	.26074	.30589

Center of Convex Leading Edge Circle; X = .018908 ft., Y = 0.0000

Radius of Convex Leading Edge Circle = .018908 ft.

Center of Concave Leading Edge Circle; X = .008334 ft., Y = 0.0000

Radius of Concave Leading Edge Circle = .008334 ft.

Center of Trailing Edge Circle; X = .394457 ft., Y = .35394 ft.

Radius of Trailing Edge Circle = .006583 ft.

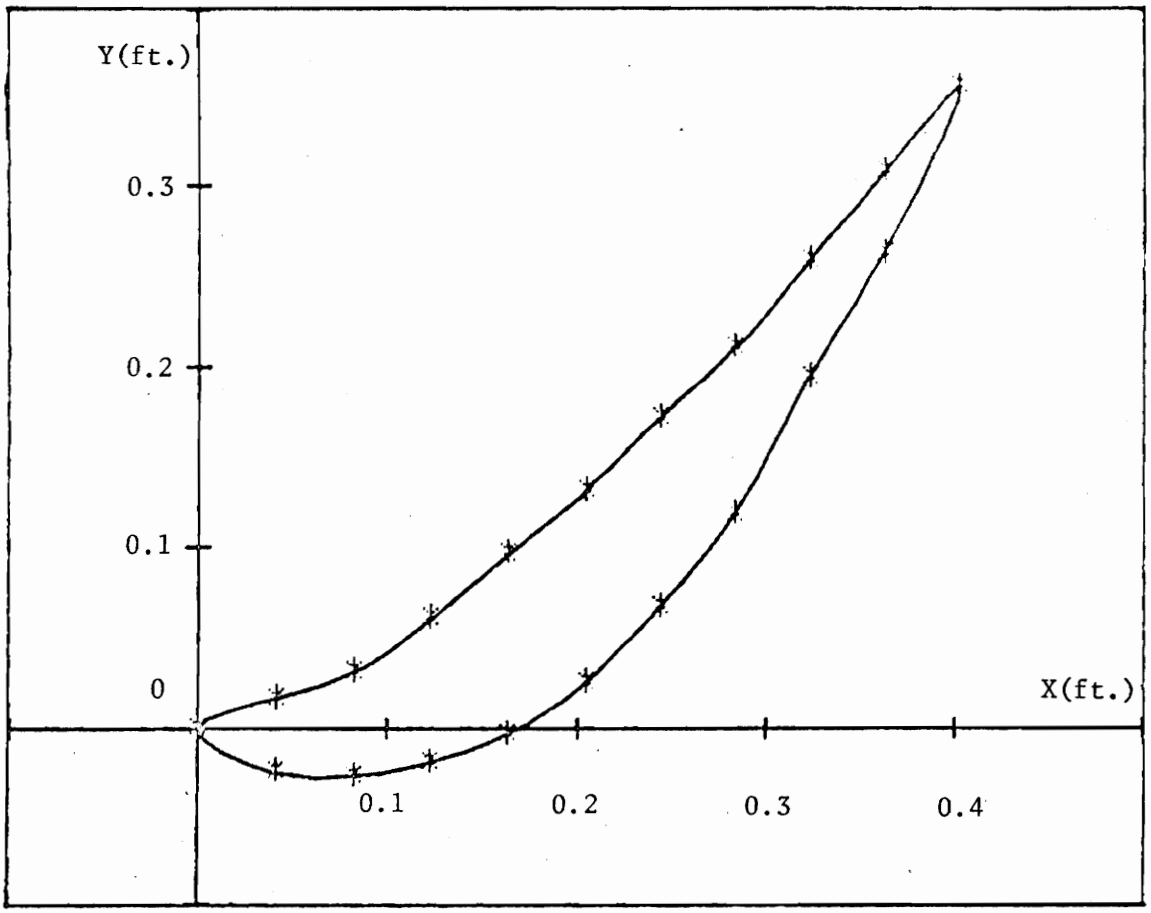

FIG. B-9. CROSS-SECTION OF BLADE 9

TABLE B-10.

COORDINATES OF FIRST STAGE ROTOR BLADE SURFACES
THICK LEADING EDGE, SMALL TURNING ANGLE (BLADE 10)

(Radius = 2.702 ft.)

X, ft.	Convex Y, ft.	Concave Y, ft.
.02819	.03646	-.00292
.05638	.05303	.00254
.08458	.05998	.00253
.11277	.05916	.00251
.14097	.05192	-.00424
.17220	.03592	-.01416
.20334	.01667	-.03167
.23466	-.00417	-.04835
.26589	-.04167	-------

Center of Leading Edge Circle; X = .007916 ft.,
Y = 0.0000

Radius of Leading Edge Circle = .007916 ft.

Center of Trailing Edge Circle; X = .29294 ft.,
Y = -.10001 ft.

Radius of Trailing Edge Circle = .004058 ft.

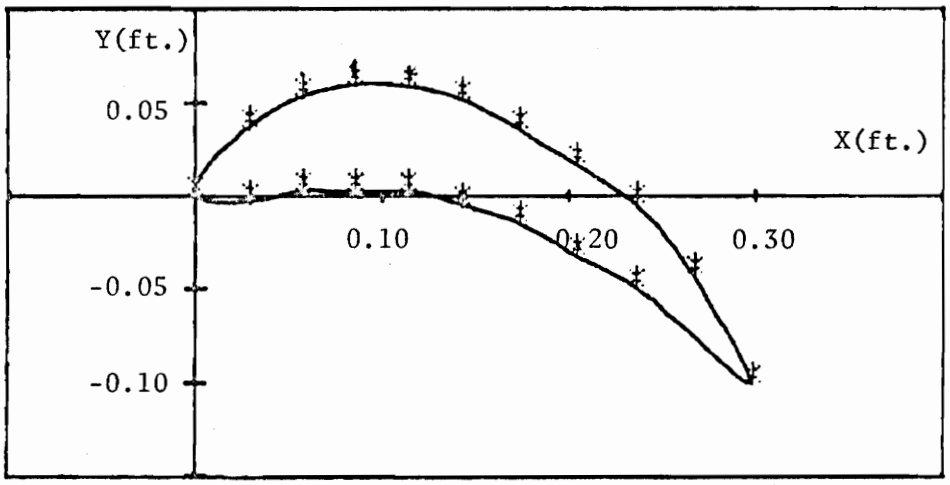

FIG. B-10. CROSS-SECTION OF BLADE 10

TABLE B-11.

COORDINATES OF FIRST STAGE ROTOR BLADE SURFACES
MEDIUM THICKNESS LEADING EDGE, SMALL TURNING ANGLE (BLADE 11)

(Radius = 2.702 ft.)

X, ft.	Convex Y, ft.	Concave Y, ft.
.02819	.03646	-.00217
.05638	.05303	.00259
.08458	.05998	.00264
.11277	.05916	.00268
.14097	.05192	-.00416
.17220	.03592	-.01584
.20334	.01667	-.03167
.23466	-.00417	-.04835
.26589	-.04167	-------

Center of Leading Edge Circle; X = .007916 ft.,
Y = 0.0000

Radius of Leading Edge Circle = .007916 ft.

Center of Trailing Edge Circle; X = .29794 ft.,
Y = -.10001 ft.

Radius of Trailing Edge Circle = .004058 ft.

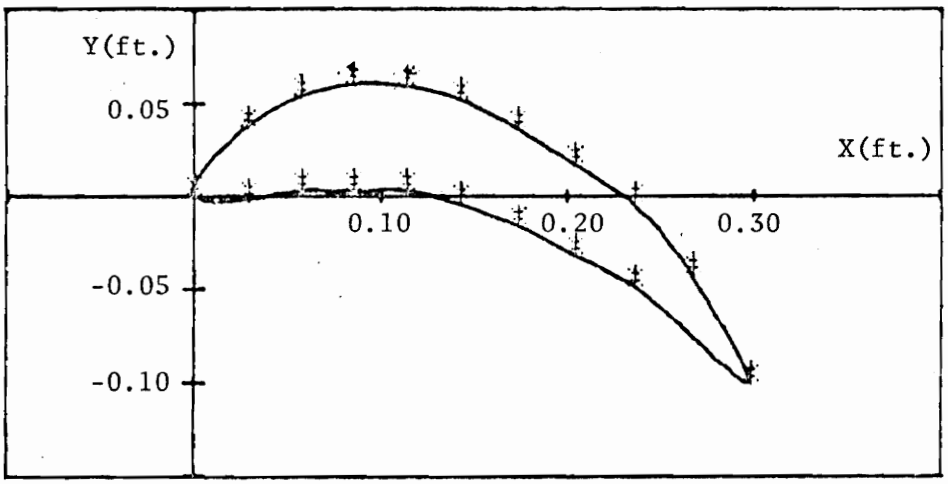

FIG. B-11. CROSS-SECTION OF BLADE 11

TABLE B-12.

COORDINATES OF FIRST STAGE ROTOR BLADE SURFACES
THIN LEADING EDGE, SMALL TURNING ANGLE (BLADE 12)

(Radius = 2.702 ft.)

X, ft.	Convex Y, ft.	Concave Y, ft.
.02819	.03646	-.00166
.05638	.05303	.00265
.08458	.05998	.00275
.11277	.05916	.00275
.14097	.05192	-.00408
.17220	.03592	-.01584
.20334	.01667	-.03167
.23466	-.00417	-.04835
.26589	-.04167	-------

Center of Leading Edge Circle; X = .007916 ft.,
Y = 0.0000

Radius of Leading Edge Circle = .007916 ft.

Center of Trailing Edge Circle; X = .29244 ft.,
Y = -.10001 ft.

Radius of Trailing Edge Circle = .004058 ft.

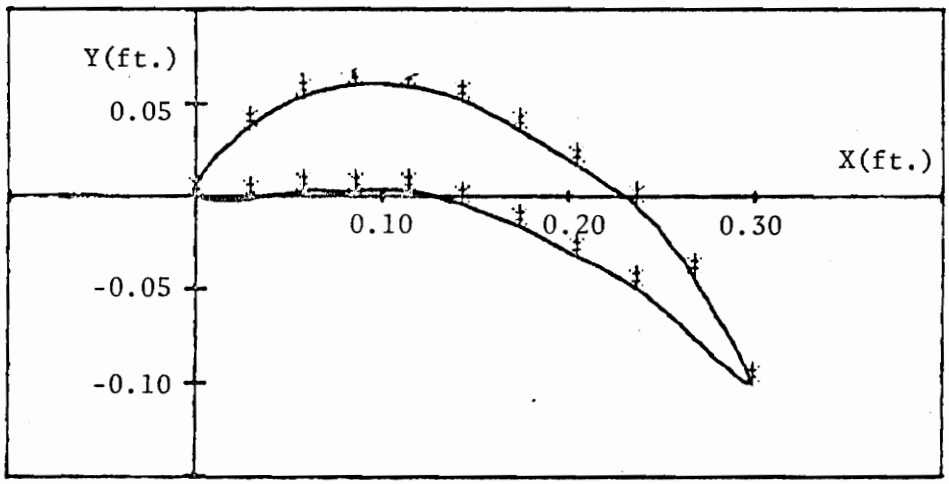

FIG. B-12. CROSS-SECTION OF BLADE 12

APPENDIX C. PARTICLE TRAJECTORY PLOTS

The following trajectory plots are selected examples of the output generated by the single-row particle trajectory program and the single-stage particle trajectory program as part of the parameter investigation. During all of the investigation, only half of the particle trajectories were actually plotted. This was done to avoid cluttering of the trajectories, especially for the rotor blades. Tables 1-4 denote which trajectories were actually plotted.

The particle trajectory plots can be divided into three major sections, corresponding to the three main parameters investigated: blade profile variation, temperature and mass flow variation and particle size and density variation.

Figures C-1 through C-12 represent the particle trajectories for Blades 1 through 12 at standard conditions (T_{o_3} = 2465°R, d_p = 10μ, ρ_p = 1.5 gm/cc) generated by the single row particle trajectory program.

Figures C-13 through C-22 represent the particle trajectory plots generated by the single-row particle trajectory program as part of the turbine inlet temperature variation with varying mass flow investigation. Note that trajectory plots for Blade 2 at d_p = 10μ, T_{o_3} = 2465° and Blade 5 at d_p = 10μ, T_{o_3} = 2465°R are not included in this set since they are previously found in Figures C-2 and C-5, respectively. The plots for constant mass flow were omitted because of similarity to those presented.

Figures C-23 through C-28 are the particle size and density variation investigation trajectories. Figures C-23 through C-26 were

generated by the single-stage particle trajectory program. Figures C-27 and C-28 were generated by the single-row particle trajectory program. Again, Blades 2 and 5 at standard conditions are not included in this section because they are found in Figures C-2 and C-5, respectively.

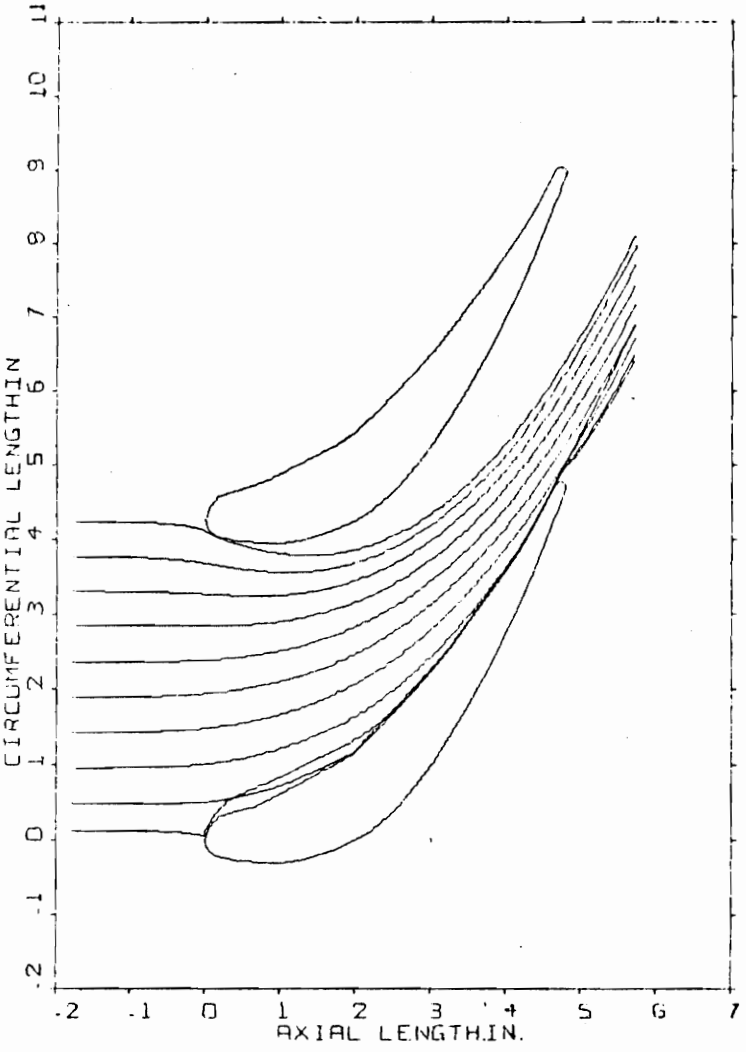

FIG. C-1. BLADE 1 PARTICLE TRAJECTORIES

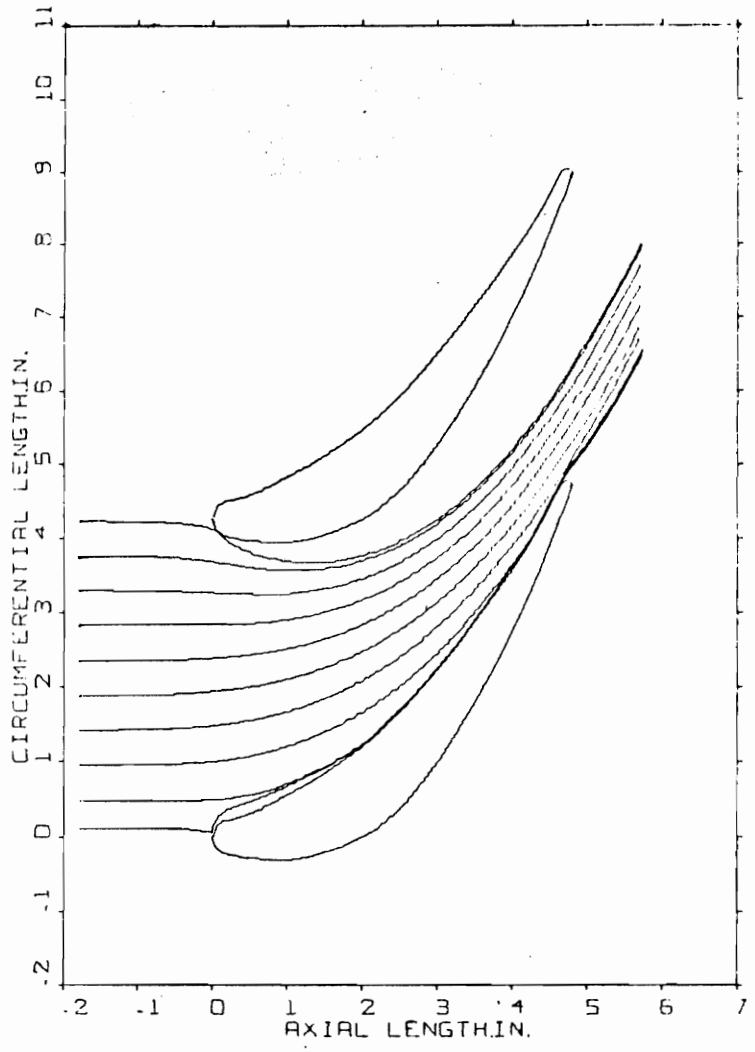

FIG. C-2. BLADE 2 PARTICLE TRAJECTORIES

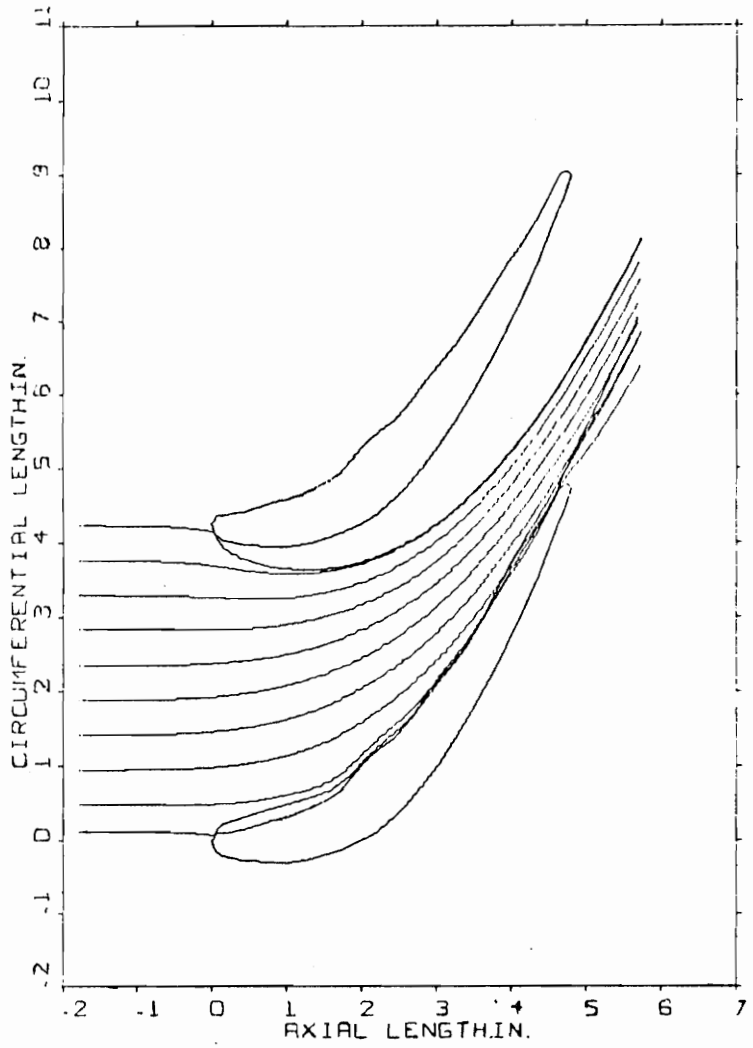

FIG. C-3. BLADE 3 PARTICLE TRAJECTORIES

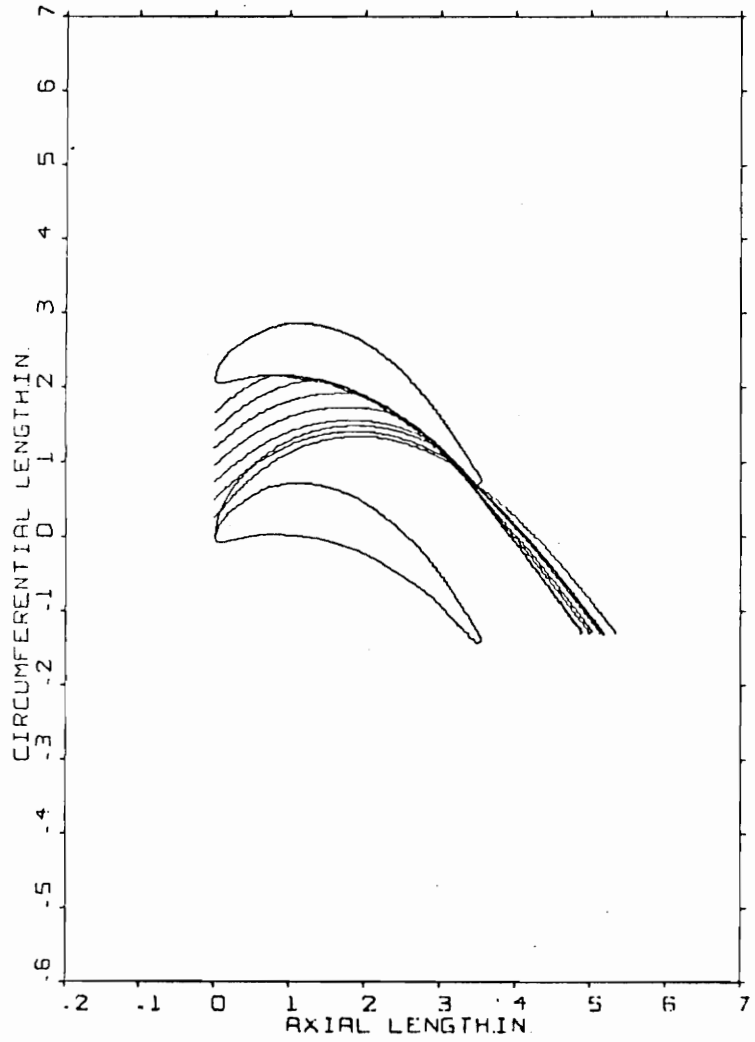

FIG. C-4. BLADE 4 PARTICLE TRAJECTORIES

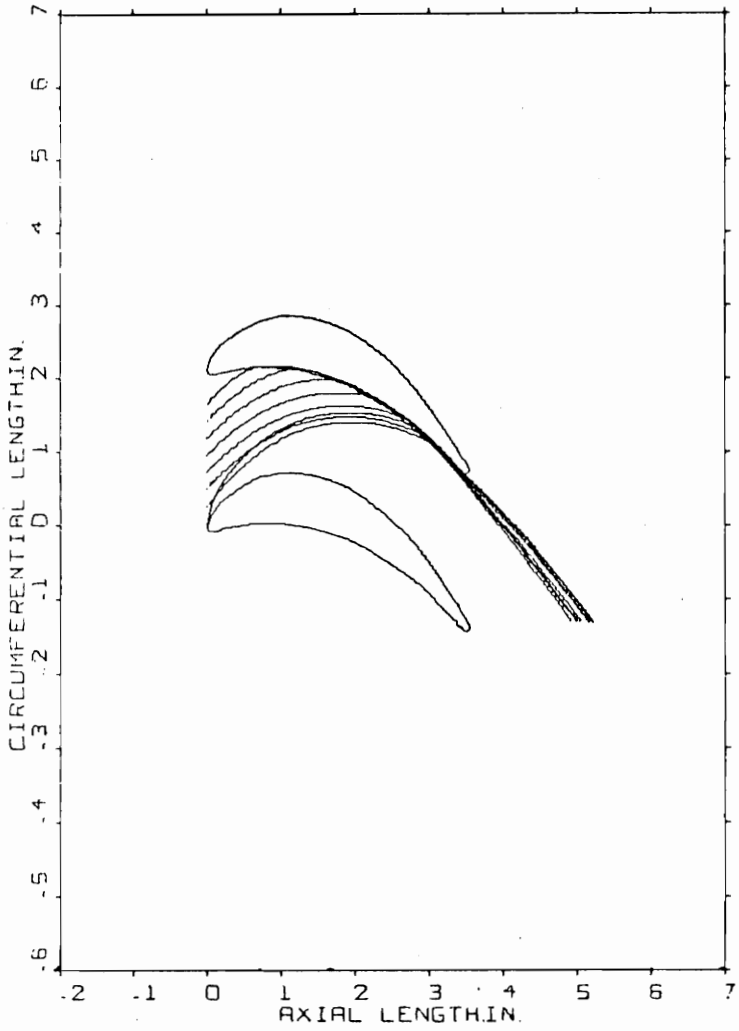

FIG. C-5. BLADE 5 PARTICLE TRAJECTORIES

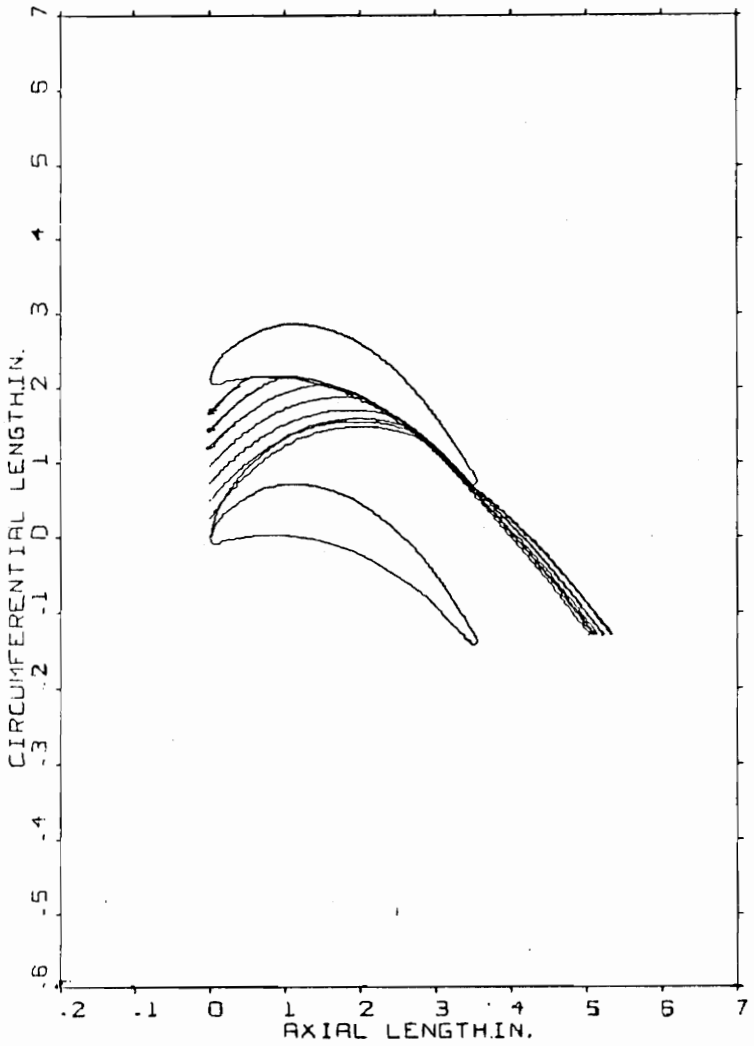

FIG. C-6. BLADE 6 PARTICLE TRAJECTORIES

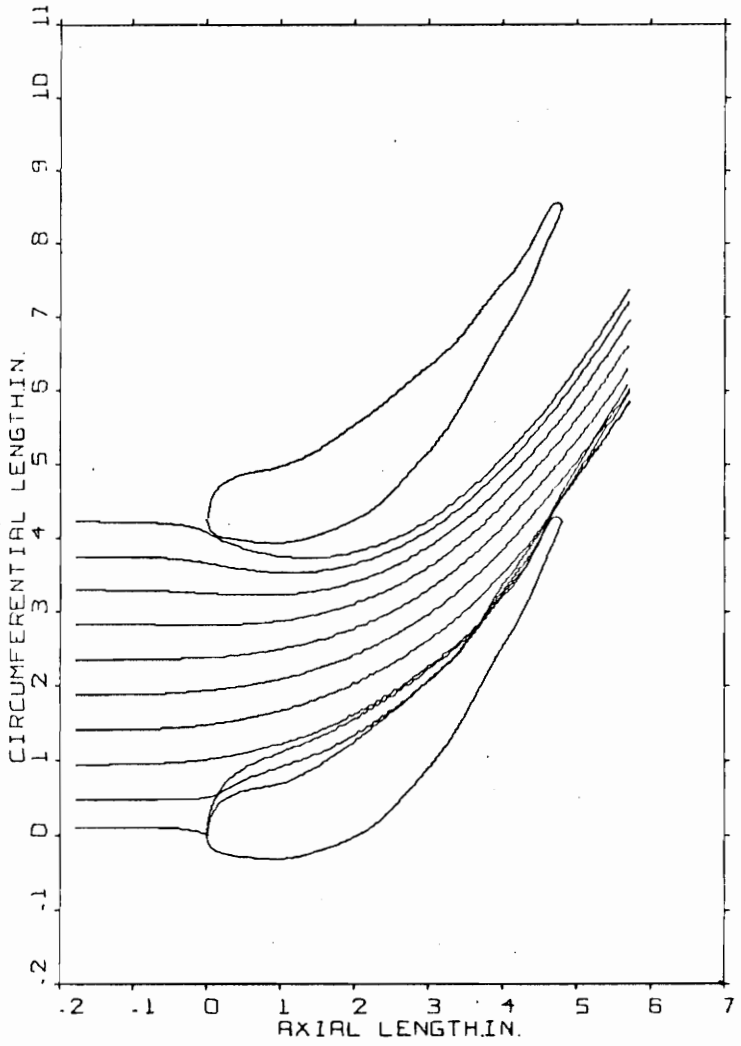

FIG. C-7. BLADE 7 PARTICLE TRAJECTORIES

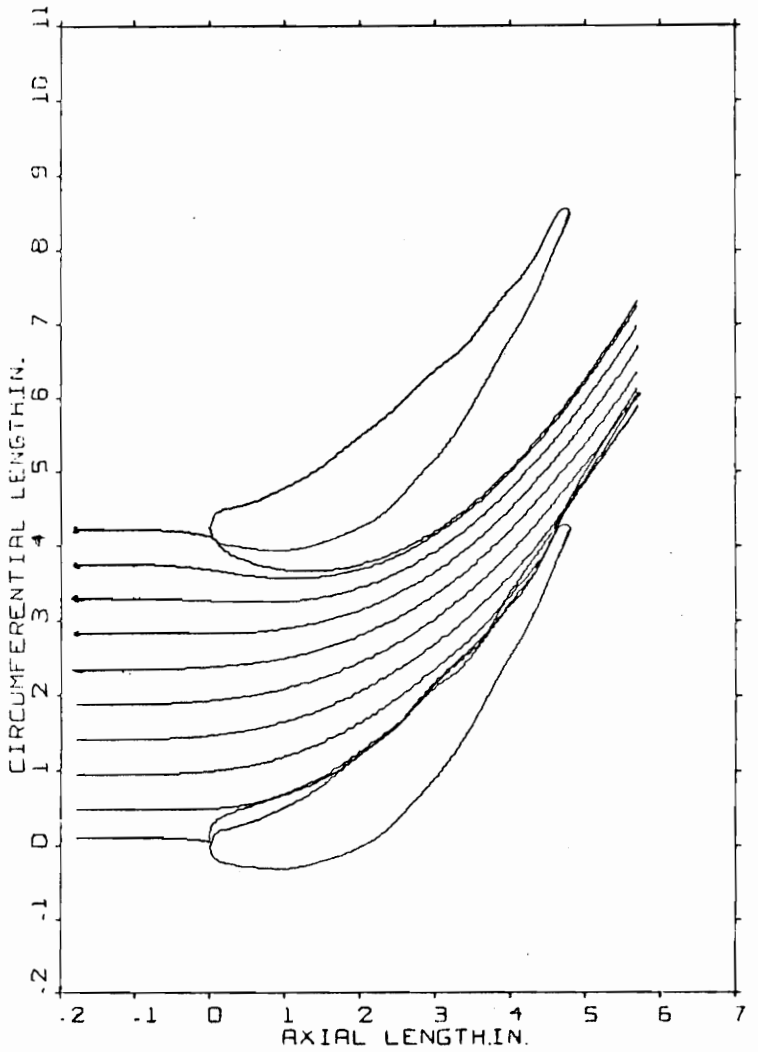

FIG. C-8. BLADE 8 PARTICLE TRAJECTORIES

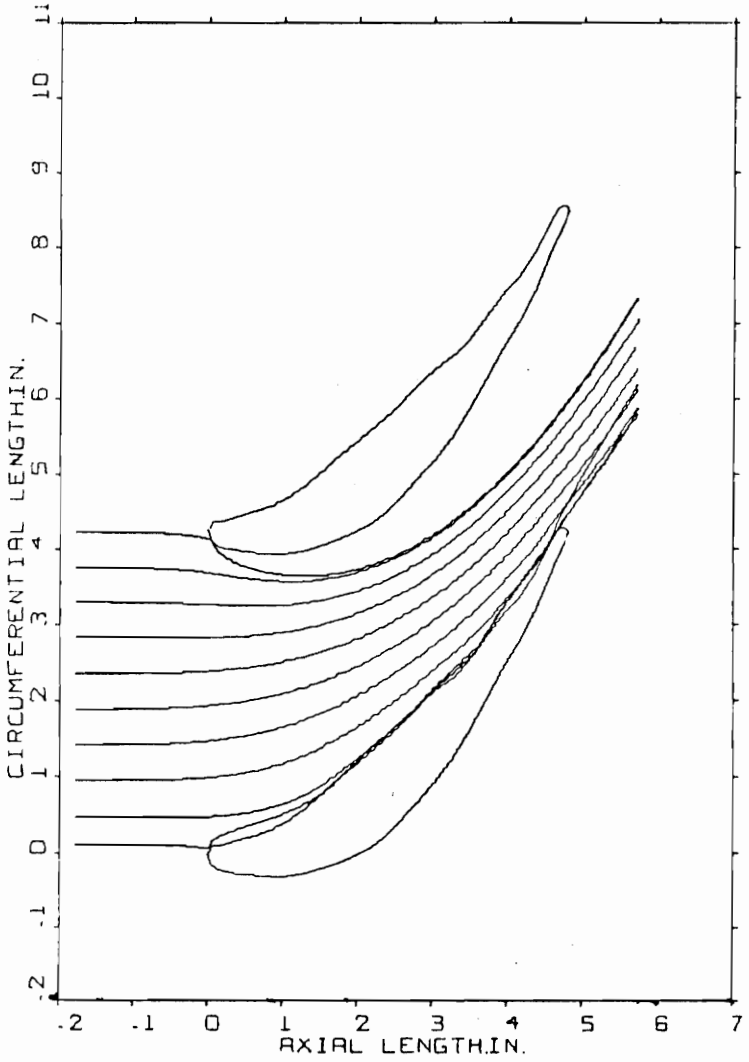

FIG. C-9. BLADE 9 PARTICLE TRAJECTORIES

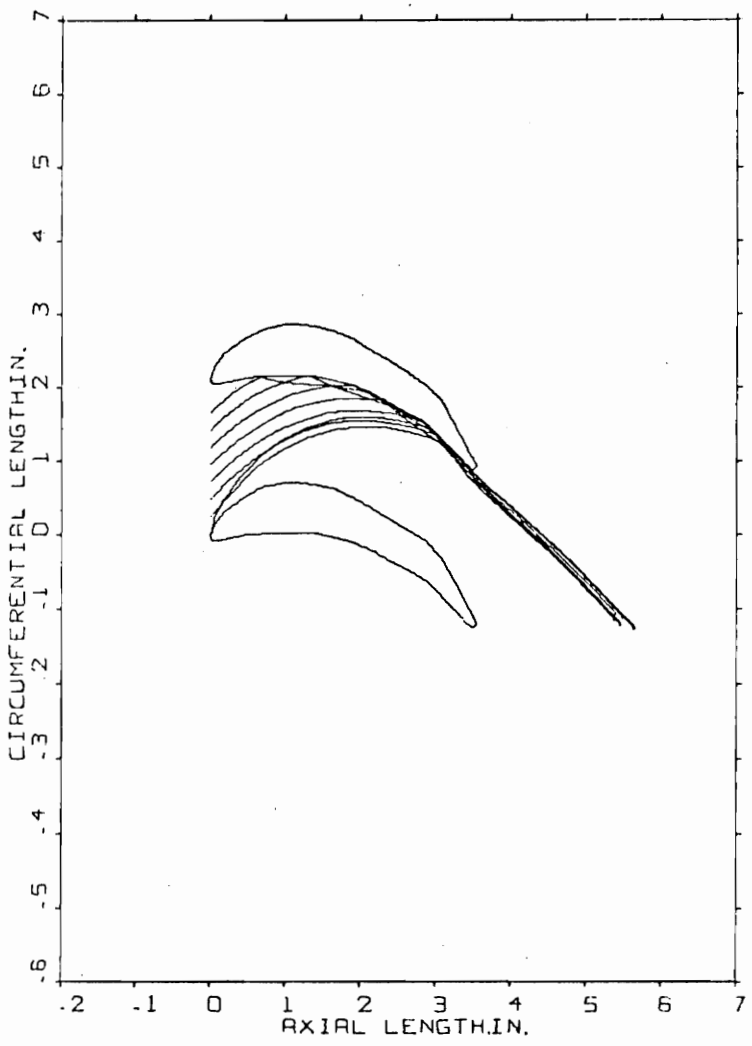

FIG. C-10. BLADE 10 PARTICLE TRAJECTORIES

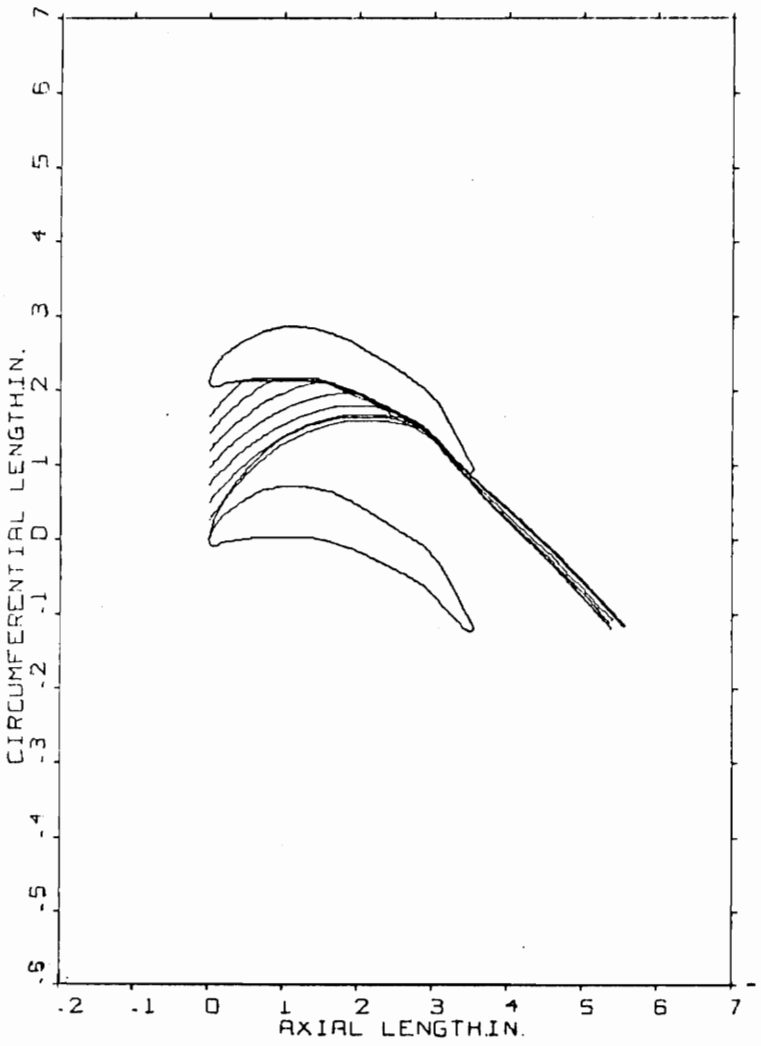

FIG. C-11. BLADE 11 PARTICLE TRAJECTORIES

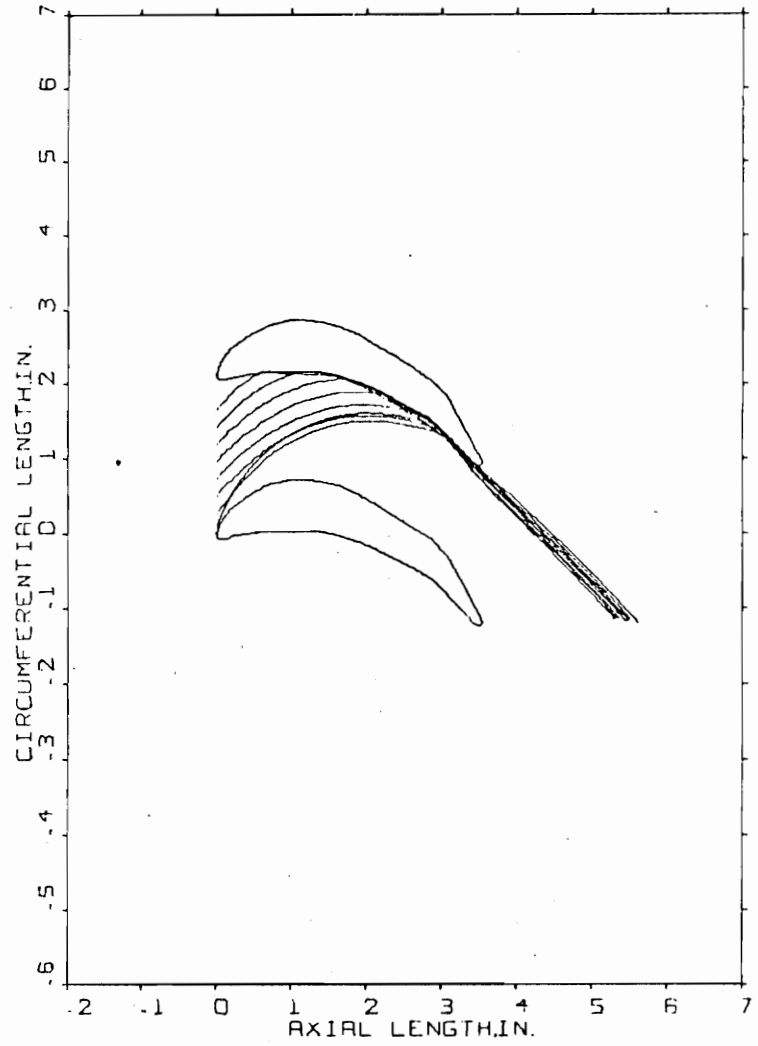

FIG. C-12. BLADE 12 PARTICLE TRAJECTORIES

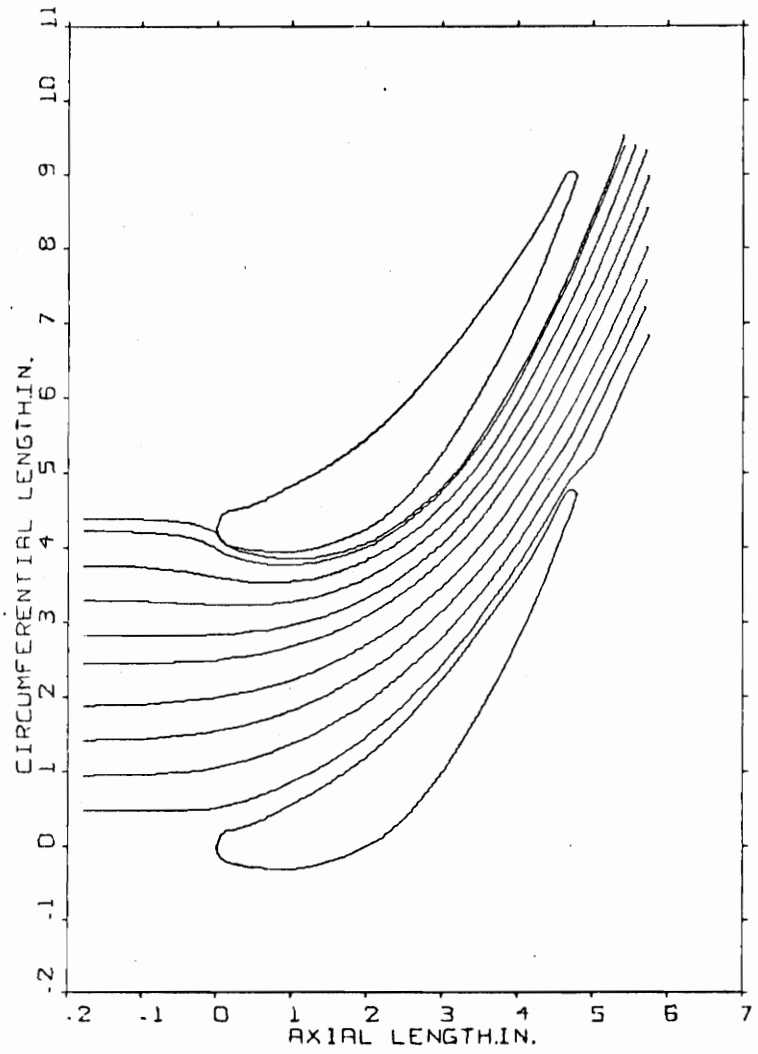

FIG. C-13. BLADE 2 PARTICLE TRAJECTORIES, T_{o_3} = 2365°R, d_p = 1μ

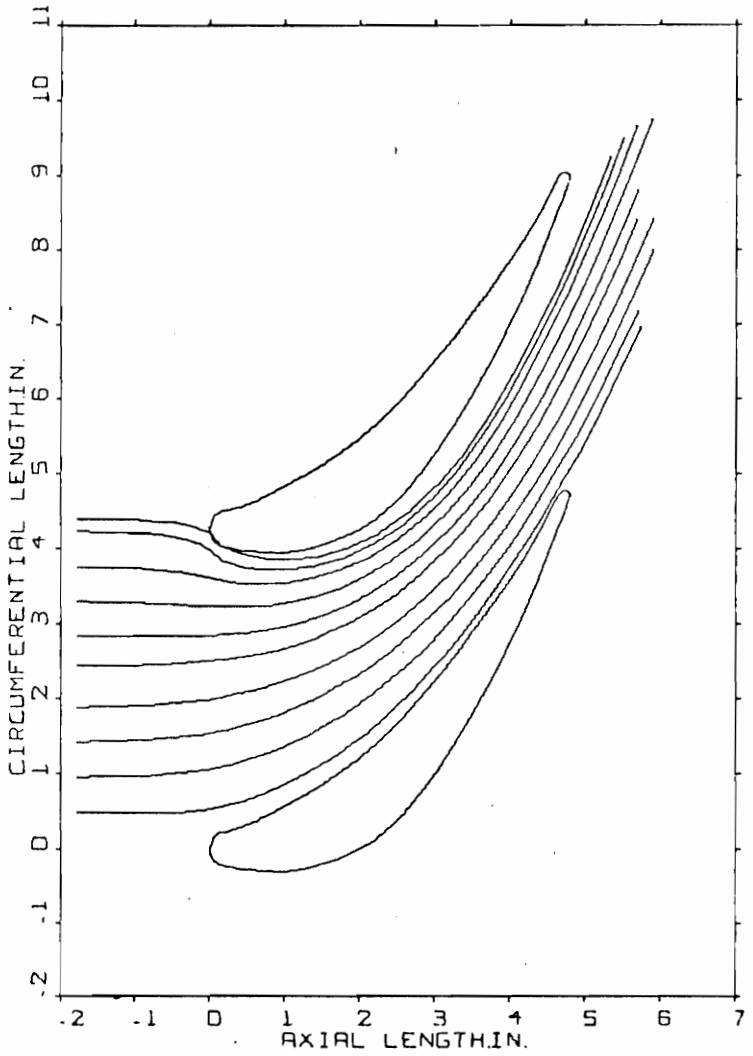

FIG. C-14. BLADE 2 PARTICLE TRAJECTORIES, T_{o_3} = 2465°R, d_p = 1μ

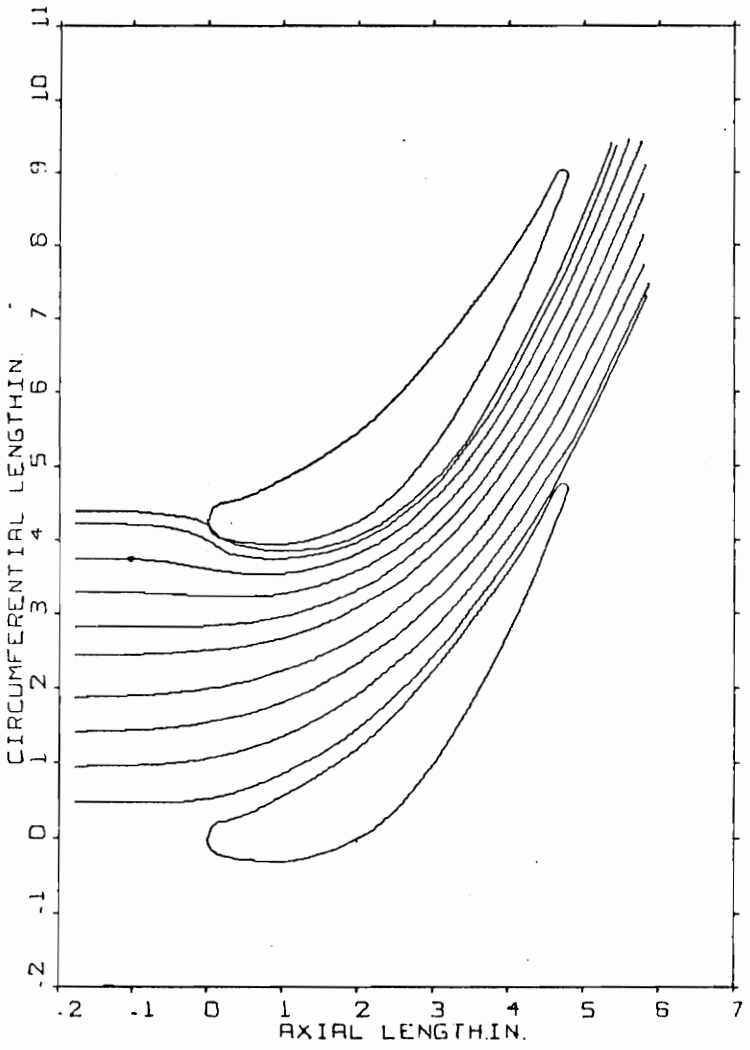

FIG. C-15. BLADE 2 PARTICLE TRAJECTORIES, T_{o_3} = 2565°R, d_p = 1μ

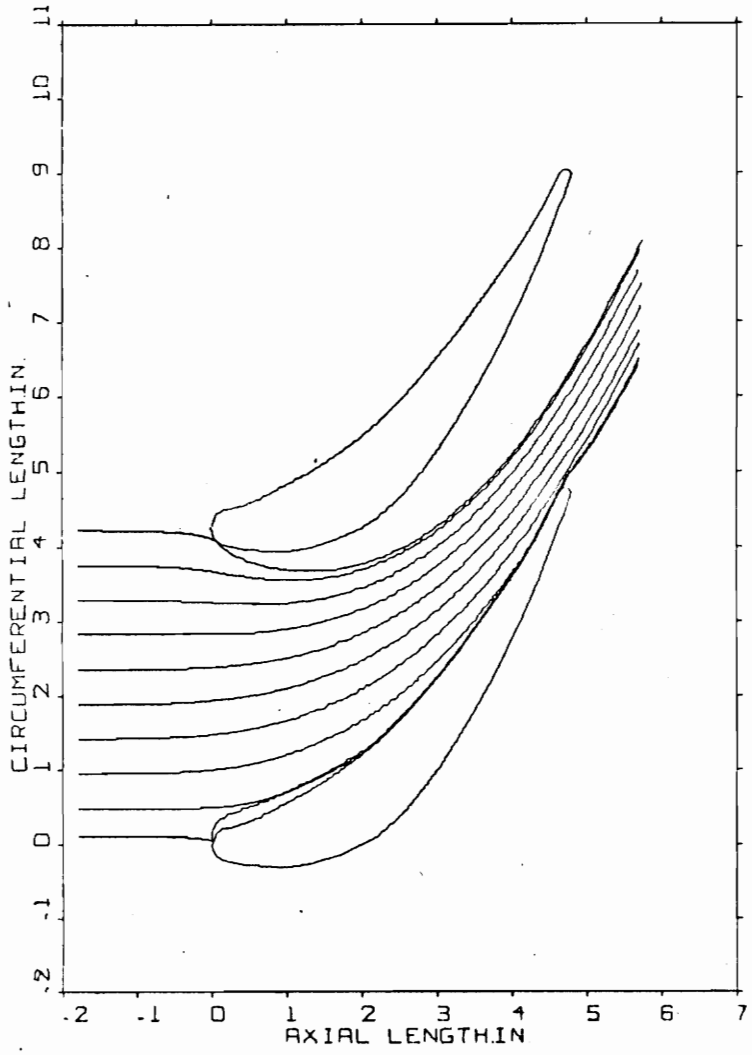

FIG. C-16. BLADE 2 PARTICLE TRAJECTORIES, T_{o_3} = 2365°R, d_p = 10μ

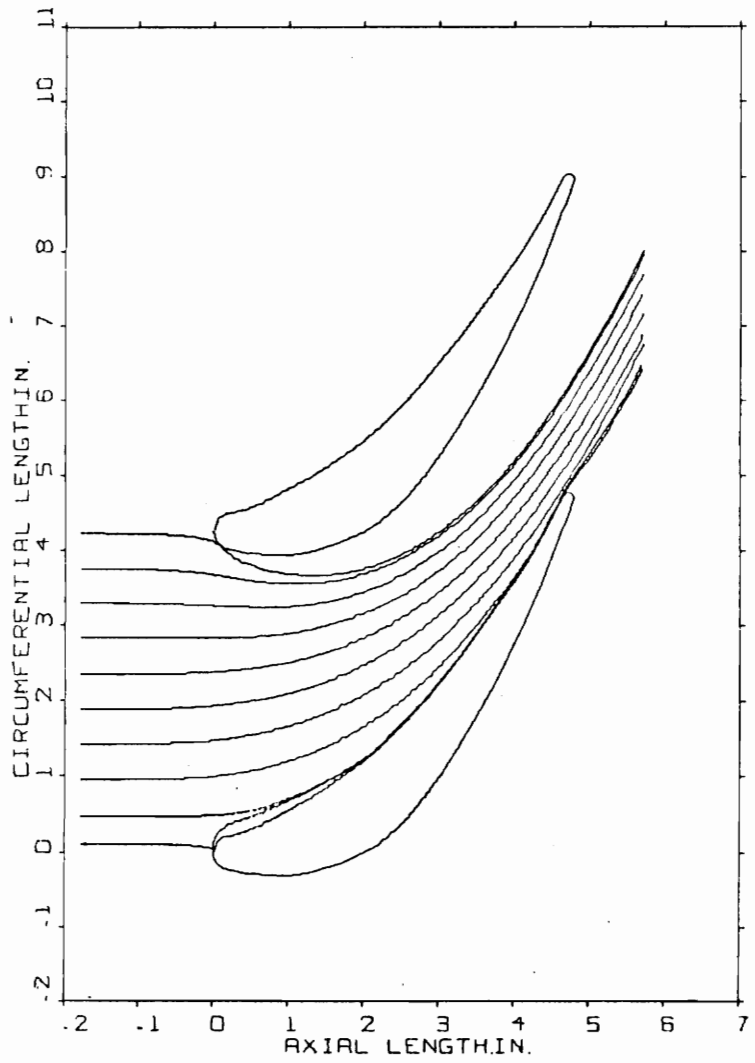

FIG. C-17. BLADE 2 PARTICLE TRAJECTORIES, T_{o_3} = 2565°R, d_p = 10μ

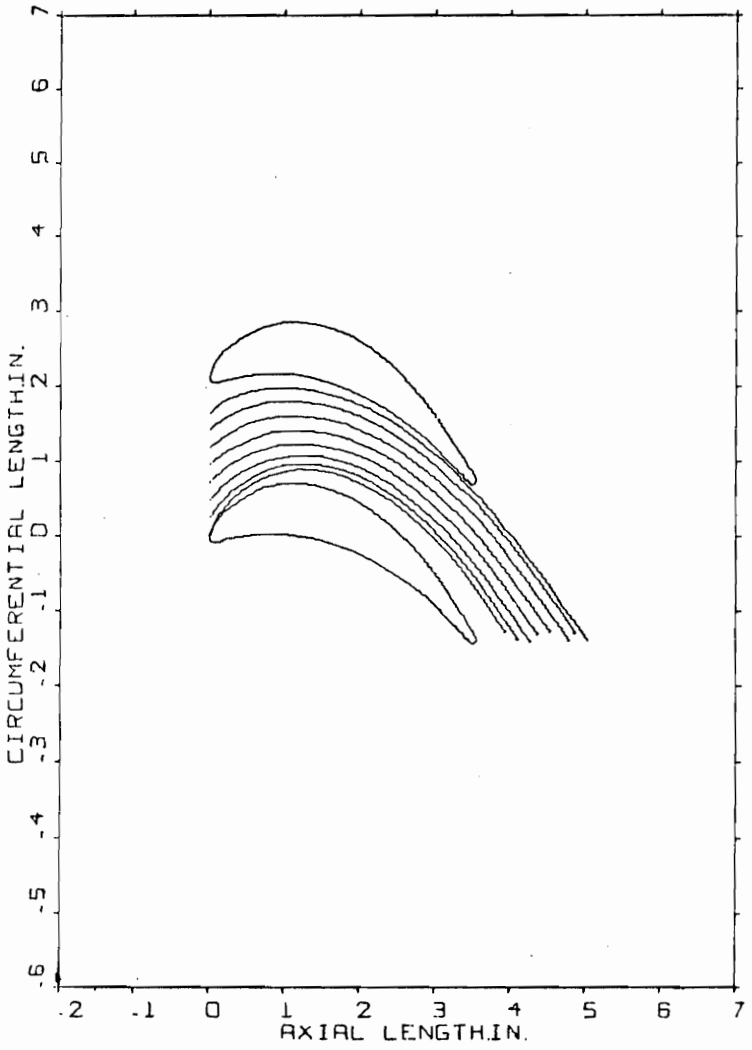

FIG. C-18. BLADE 5 PARTICLE TRAJECTORIES, T_{o_3} = 2365°R, d_p = 1μ

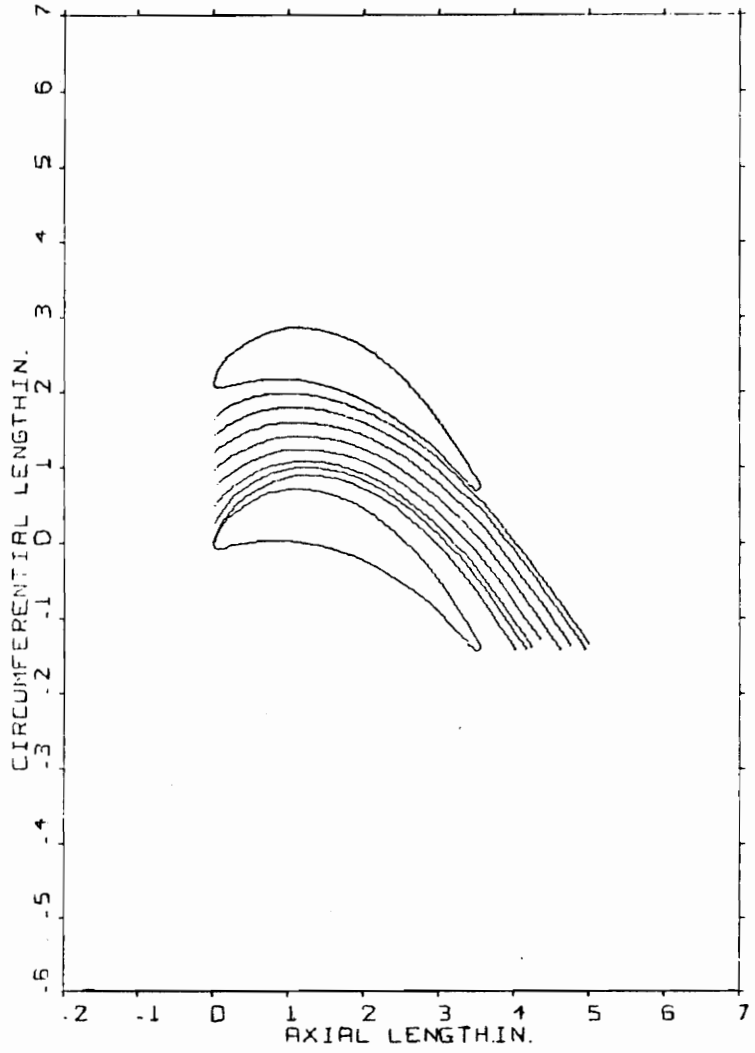

FIG. C-19. BLADE 5 PARTICLE TRAJECTORIES, T_{o_3} = 2465°R, d_p = 1μ

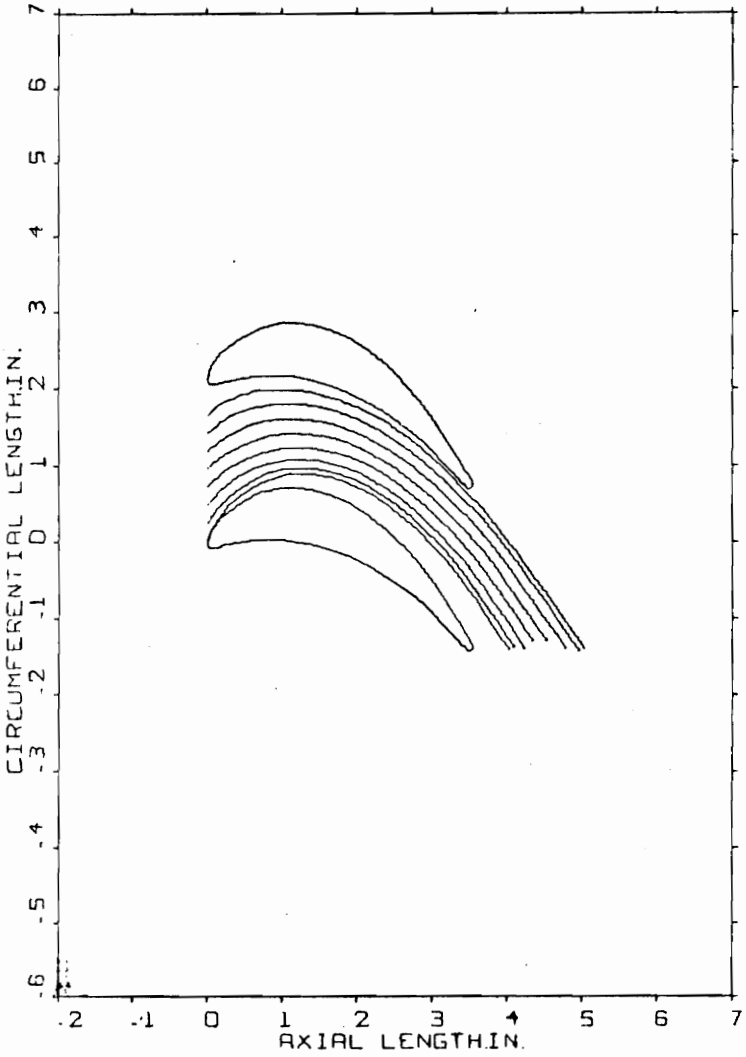

FIG. C-20. BLADE 5 PARTICLE TRAJECTORIES, T_{o_3} = 2565°R, d_p = 1μ

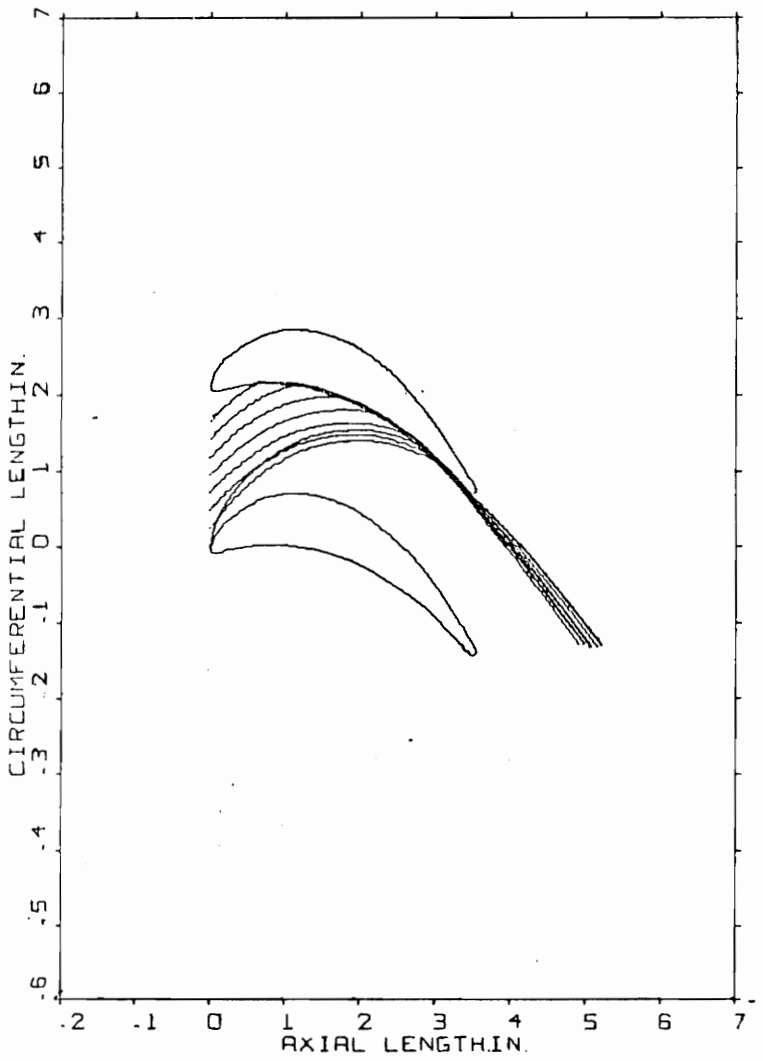

FIG. C-21. BLADE 5 PARTICLE TRAJECTORIES, T_{o_3} = 2365°R, d_p = 10μ

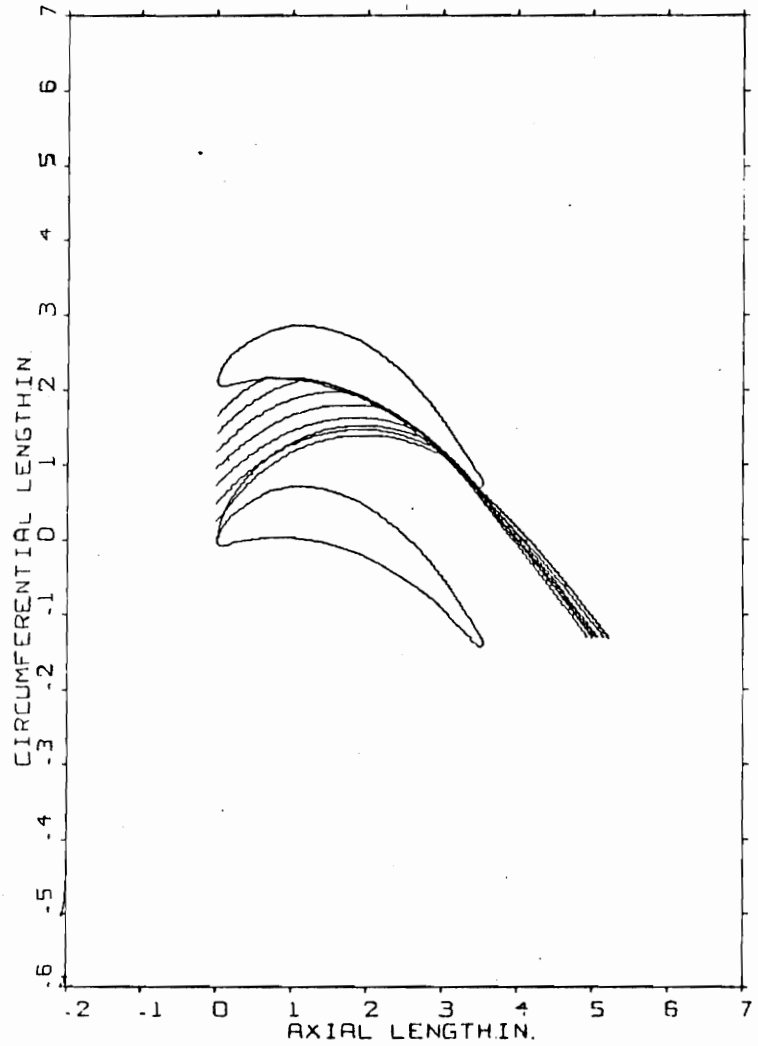

FIG. C-22. BLADE 5 PARTICLE TRAJECTORIES, T_{o_3} = 2565°R, d_p = 10μ

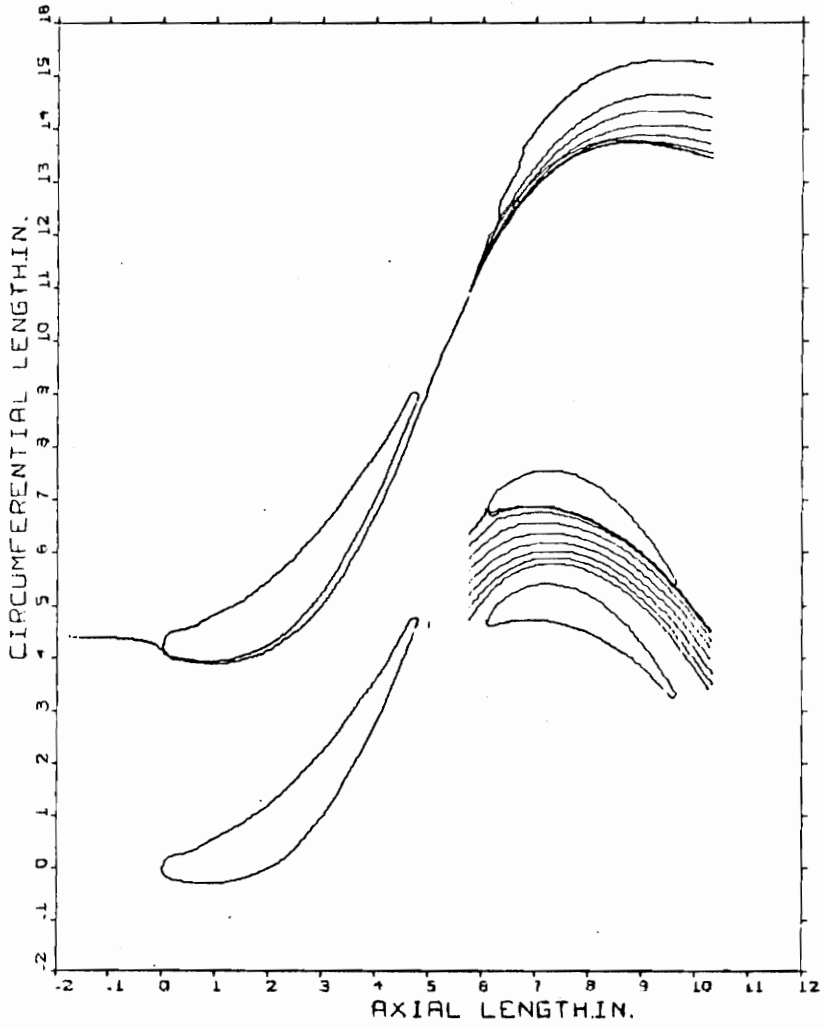

FIG. C-23. BLADES 2 AND 5 ABSOLUTE AND RELATIVE PARTICLE TRAJECTORIES, $d_p = 1\mu$, $\rho_p = 1.5$ gm/cc (Relative trajectories are shown within the rotor blade passage)

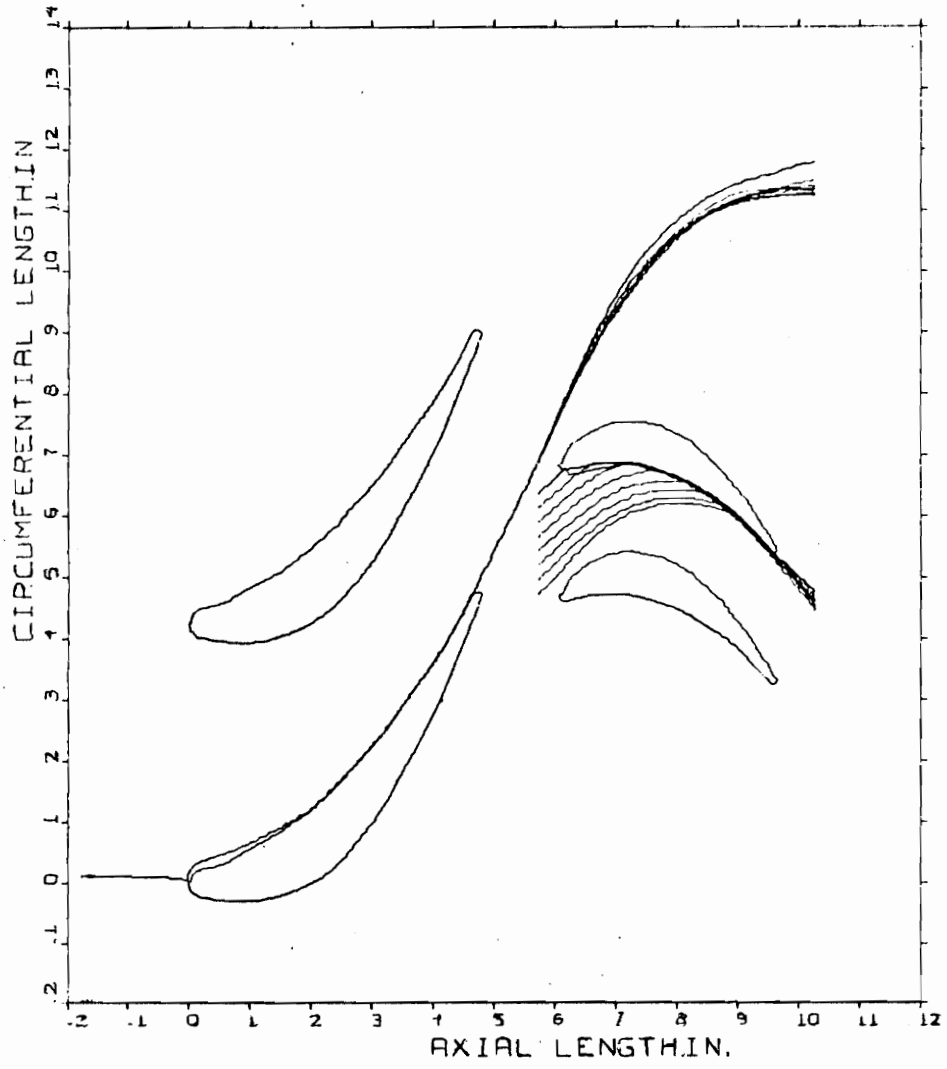

FIG. C-24. BLADES 2 AND 5 ABSOLUTE AND RELATIVE PARTICLE TRAJECTORIES, d_p = 1μ, ρ_p = 2.5 gm/cc (Relative trajectories are shown within the rotor blade passage)

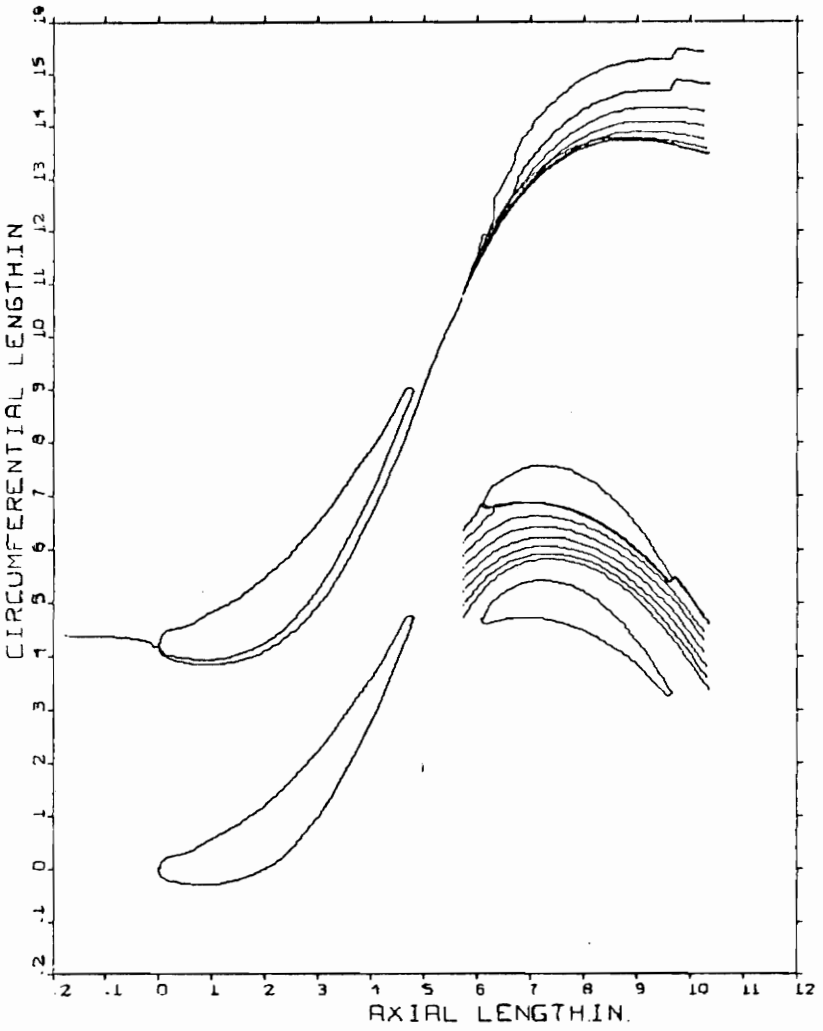

FIG. C-25. BLADES 2 AND 5 ABSOLUTE AND RELATIVE PARTICLE TRAJECTORIES, d_p = 10μ, ρ_p = 1.5 gm/cc (Relative trajectories are shown within the rotor blade passage)

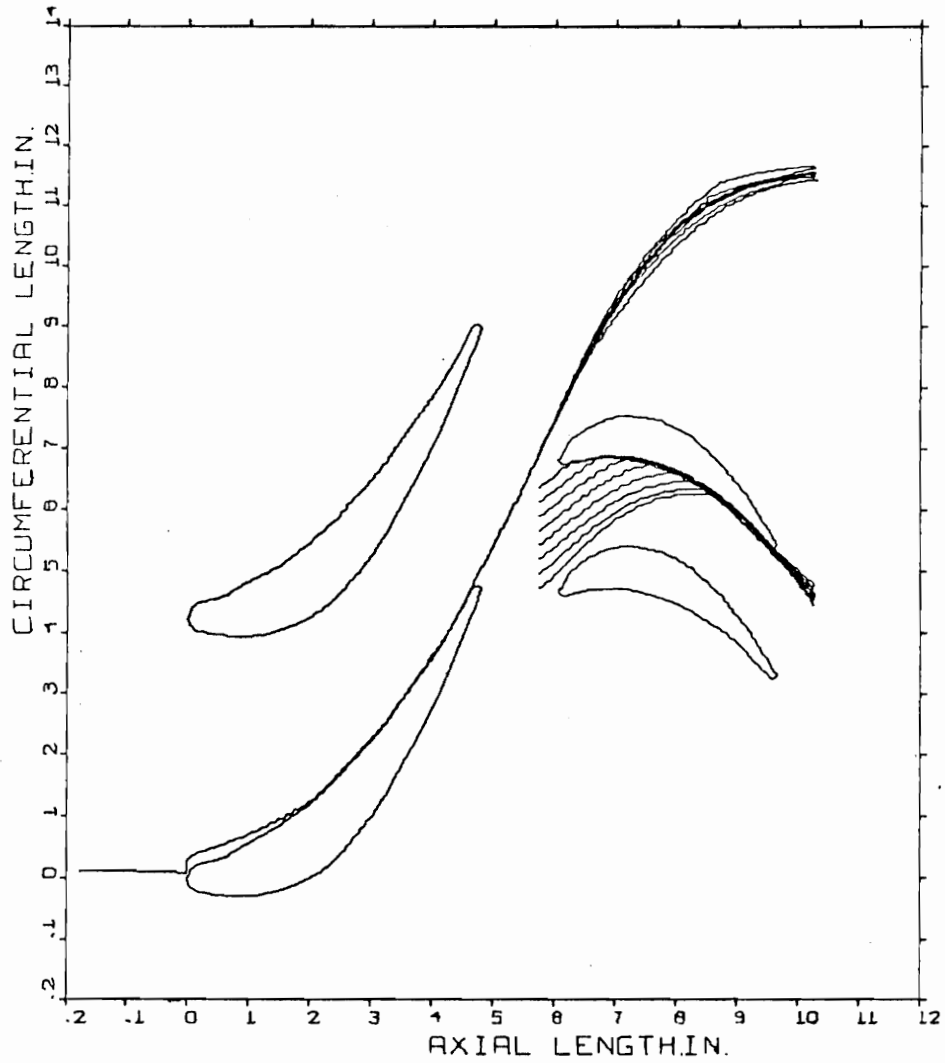

FIG. C-26. BLADES 2 AND 5 ABSOLUTE AND RELATIVE PARTICLE TRAJECTORIES, $d_p = 10\mu$, $\rho_p = 2.5$ gm/cc (Relative trajectories are shown within the rotor blade passage)

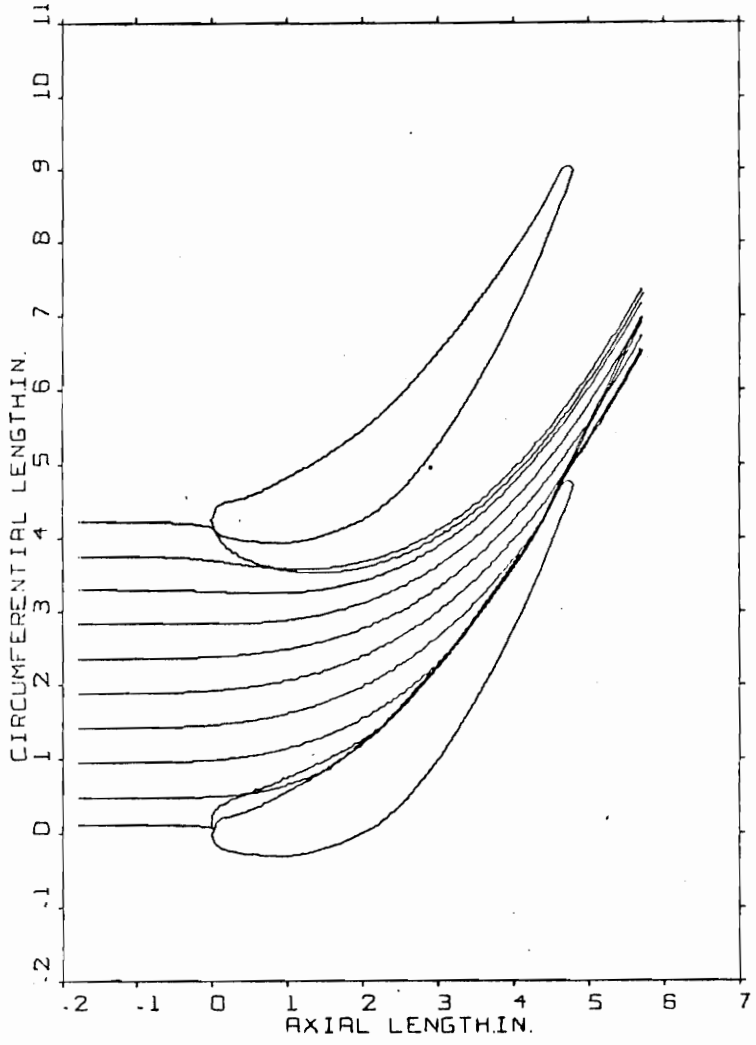

FIG. C-27. BLADE 2 PARTICLE TRAJECTORIES, ρ_p = 2.5 gm/cc, d_p = 10μ

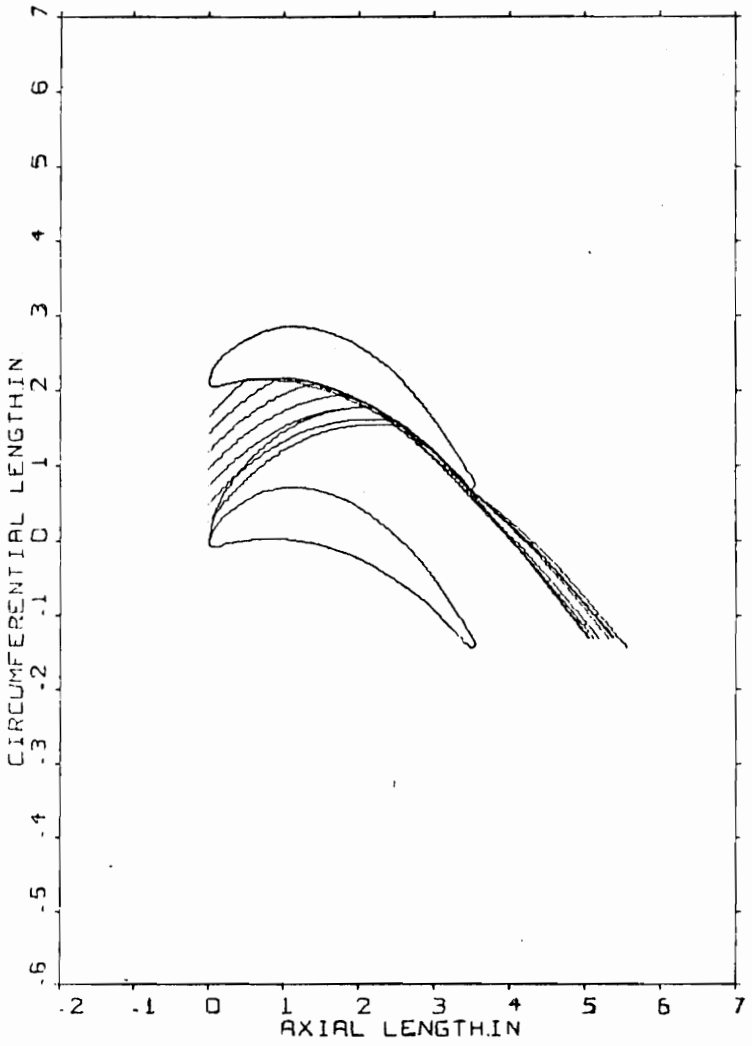

FIG. C-28. BLADE 5 PARTICLE TRAJECTORIES, ρ_p = 2.5 gm/cc, d_p = 10μ

XVII. VITA

The author, Dennis John Dubberley, was born in Brooklyn, New York, October 23, 1955.

In September 1973, he entered Virginia Polytechnic Institute and State University, majoring in Aerospace and Ocean Engineering. During his undergraduate career, he became a member of Sigma Gamma Tau Honorary Fraternity. In June 1976, he graduated with distinction, receiving the Bachelor of Science Degree in Aerospace and Ocean Engineering.

He received a Domestic Mining and Mineral and Fuel Conservation Fellowship from the U. S. Department of Health, Education and Welfare and began his graduate program in the Mechanical Engineering Department at Virginia Polytechnic Institute and State University in September 1976. In addition, he received a part-time Graduate Teaching Assistantship for two quarters.

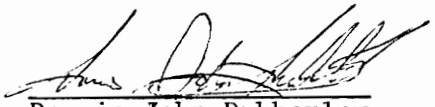

Dennis John Dubberley

AN ANALYTICAL PARAMETER STUDY ON THE EROSION OF TURBINE BLADES SUBJECTED TO FLOW CONTAINING PARTICULATES

by

Dennis John Dubberley

(ABSTRACT)

The erosion damage to stator and rotor blades associated with flow containing particulates in turbines is investigated. The main parameters studied are blade leading edge thickness, blade turning angle, turbine inlet temperature, particle size,and particle densities. The computer programs used in the investigation are based on inviscid flow theory. Flow velocities relative to blades ranged up to sonic values. Results predict that decreasing flow turning angles and increasing blade leading edge thicknesses are the most effective ways to reduce erosion damage caused by impacting particles. Decreasing particle sizes and densities can also significantly reduce erosion rates.

The erosion model uses the brittle and ductile mode response exhibited by materials subjected to particle impacts to predict the total erosion damage. The accuracy for small (1 micron) particles is questionable since some of these particles will have long residence times in the boundary layers, causing deposition rather than erosion.